ICETI

ENGINEERING TECHNOLOGY INNOVATION

4TH INTERNATIONAL CONFERENCE ON ENGINEERING TECHNOLOGY AND INNOVATION

BOOK OF PROCEEDINGS

www.iceti.org

November 04, 2020 Online

Western Michigan University · University of Cincinnati · IUS · Turkish Airlines · CNR Group

IV INTERNATIONAL CONFERENCE ON ENGINEERING TECHNOLOGY AND INNOVATION

ISBN 978-605-67955-9-6

ISSN 2687-2323

PROCEEDINGS OF THE
IV INTERNATIONAL CONFERENCE ON ENGINEERING TECHNOLOGY AND INNOVATION
November 04-08, 2020, Skopje

Edited by
Prof. Dr. Özer Çınar

Published, 2020

info@iceti.org
www.iceti.org

info@iceti.org

ISBN 978-605-67955-9-6
ISSN 2687-2323

SCIENTIFIC COMMITTEE

1. Prof. Dr. Adisa Parić - University of Sarajevo - Bosnia and Herzegovina
2. Prof. Dr. Aleksandar Dimitrov - Ss. Cyril and Methodius University - Macedonia
3. Prof. Dr. Anita Grozdanov - Ss. Cyril and Methodius University - Macedonia
4. Prof. Dr. Asif Šabanović – International University of Sarajevo - Bosnia and Herzegovina
5. Prof. Dr. Christos Douligeris - University of Erlangen-Nurnberg - Germany
6. Prof. Dr. Dragutin T. Mihailović - University of Novi Sad - Serbia
7. Prof. Dr. Erkan Şahinkaya – İstanbul Medeniyet University - Turkey
8. Prof. Dr. Falko Dressler - University of Paderborn - Germany
9. Prof. Dr. Harry Miller – International University of Sarajevo - Bosnia and Herzegovina
10. Prof. Dr. Houssam Toutanji – Western Michigan University - USA
11. Prof. Dr. Ian F. Akyıldız – Georgia Institute of Technology - USA
12. Prof. Dr. İsmail Usta - Marmara University - Turkey
13. Prof. Dr. Liljana Gavrilovska - Ss Cyril and Methodius University - Macedonia
14. Prof. Dr. Lukman Thalib - Qatar University - Qatar
15. Prof. Dr. M. Asghar Fazel – University of Environment - Iran
16. Prof. Dr. Mehmet Akalin - Marmara University - Turkey
17. Prof. Dr. Mehmet Kitiş – Süleyman Demirel University - Turkey
18. Prof. Dr. Muammer Koç - Hamad bin Khalifa University - Qatar
19. Prof. Dr. Özer Çınar – Yıldız Technical University - Turkey
20. Prof. Dr. Perica Paunovik - Ss. Cyril and Methodius University - Macedonia
21. Prof. Dr. Rifat Škrijelj – University of Sarajevo - Bosnia and Herzegovina
22. Prof. Dr. Samir Đug - University of Sarajevo - Bosnia and Herzegovina
23. Prof. Dr. Tanju Karanfil – Clemson University - USA
24. Prof. Dr. Tibor Biro - National University of Public Service, Budapest - Hungary
25. Prof. Dr. Ümit Alver – Karadeniz Technical University - Turkey
26. Prof. Dr. Wolfgang Gerstacker - University of Erlangen-Nurnberg - Germany
27. Prof. Dr. Yılmaz Yıldırım - Bülent Ecevit University - Turkey
28. Prof. Dr. Yousef Haik - Hamad bin Khalifa University - Qatar
29. Assoc. Prof. Dr. Alaa Al Hawari - Qatar University - Qatar
30. Assoc. Prof. Dr. Izudin Dzafic - International University of Sarajevo - Bosnia and Herzegovina
31. Assoc. Prof. Dr. Muhamed Hadziabdic - International University of Sarajevo - Bosnia and Herzegovina
32. Assoc. Prof. Dr. Nusret Drešković - University of Sarajevo - Bosnia and Herzegovina
33. Assist. Prof. Dr. Faruk Berat Akçeşme - University of Health Sciences - Turkey
34. Assist. Prof. Dr. Fouzi Tabet - German Biomass Research Center - Germany
35. Assist. Prof. Dr. Haris Gavranovic - International University of Sarajevo - Bosnia and Herzegovina
36. Assist. Prof. Dr. Murat Karakaya - Atılım University - Turkey
37. Assist. Prof. Dr. Sasan Rabieh - Shahid Beheshti University - Iran
38. Assist. Prof. Dr. Ševkija Okerić - University of Sarajevo - Bosnia and Herzegovina
39. Assist. Prof. Dr. Ivana Plazonić - University of Zagreb - Croatia
40. Assist. Prof. Dr. J. Amudhavel - VIT Bhopal University - India
41. Dr. Hasan Bora Usluer - Galatasaray University - Turkey
42. Dr. Muhammet Uzun - RWTH Aachen University - Germany
43. Dr. Zsolt Hetesi - National University of Public Service, Budapest - Hungary
44. Dr. Zsolt T. Németh - National University of Public Service, Budapest - Hungary

ORGANIZATION COMMITTEE

Chairman of the Conference

Prof. Dr. Özer Çınar – Yıldız Technical University - Turkey

Members of the Committee

Prof. Dr. M. Asghar Fazel – University of Environment - Iran

Prof. Dr. Ümit Alver - Karadeniz Technial University - Turkey

Assoc.Prof.Dr. Agim Mamuti - Mother Teresa University - North Macedonia

Assoc. Prof. Dr. Lukman Thalib - Qatar University - Qatar

Assoc. Prof. Dr. Nusret Drešković - University of Sarajevo - Bosnia and Herzegovina

Assist. Prof. Dr. Sasan Rabieh - Shahid Beheshti University - Iran

Alma Ligata - Zenith Group - Bosnia and Herzegovina

Ismet Uzun - Zenith Group - Bosnia and Herzegovina

Musa Kose - Zenith Group - Bosnia and Herzegovina

WELCOME TO ICETI 2020

On behalf of the organizing committee, we are pleased to announce that the International Conference On Engineering Technology And Innovation is held from on November 04-08 in Skopje, North Macedonia. ICETI 2020 provides an ideal academic platform for researchers to present the latest research findings and describe emerging technologies, and directions in Engineering Technology And Innovation. The conference seeks to contribute to presenting novel research results in all aspects of Engineering Technology And Innovation.

The conference aims to bring together leading academic scientists, researchers and research scholars to exchange and share their experiences and research results about all aspects of Engineering Technology And Innovation. It also provides the premier interdisciplinary forum for scientists, engineers, and practitioners to present their latest research results, ideas, developments, and applications in al lareas of Engineering Technology And Innovation. The conference will bring together leading academic scientists, researchers and scholars in the domain of interest from around the world. ICETI 2020 is the oncoming event of the successful conference series focusing on Engineering Technology And Innovation.

The International Conference on Engineering Technology and Innovation (ICETI 2020) aims to bring together leading academic scientists, researchers and research scholars to exchange and share their experiences and research results about all aspects of Engineering Technology and Innovation. It also provides the premier interdisciplinary forum for scientists, engineers, and practitioners to present their latest research results, ideas, developments, and applications in all areas of Engineering Technology and Innovation. The conference will bring together leading academic scientists, researchers and scholars in the domain of interest from around the world. The conference's goals are to provide a scientific forum for all international prestige scholars around the world and enable the interactive exchange of state-of-the-art knowledge. The conference will focus on evidence-based benefits proven in technology and innovation and engineering experiments.

Best regards,

Prof. Dr.Özer ÇINAR

Investigation of the Microstructure and Mechanical Properties of Gas Metal Arc Welded AISI 304 Austenitic Stainless Steel Butt Joints

Mehmet Ali Ezer[1], Gurel Cam[2]

Abstract

Austenitic stainless steels exhibit very good properties such as very good formability even at low temperatures, good mechanical properties and high corrosion resistance. Austenitic steels are the grades which are produced most in quantity among all stainless steels and AISI 304 is the most widely used grade among the austenitic steels. They are used widely in several industries such as chemistry and petro-chemistry industries, food processing industry, medical and dental equipments and kitchenware. However, several difficulties such as carbide precipitation in heat affected zone, and hot cracking and formation of brittle sigma phase in the fusion zone may be encountered in fusion joining of these steels. High heat inputs involved in arc welding may even increase the occurrence of these problems. Thus, successful joining of these alloys using conventional fusion welding methods is rather important. This study aims at investigating the influence of heat input on microstructural evolution in the weld region and the mechanical properties of the welded joints in gas metal arc welding of AISI 304 austenitic steel plates. For this purpose, 5 mm thick AISI 304 plates were joined using different heat input values. Detailed optical microscopy and micro-hardness measurements in addition to tensile and bending tests were carried out to study the microstructural and mechanical properties of the welded plates produced. Furthermore, it was also attempted to determine the effect of heat input on the performance of gas metal arc welded AISI304 joints.

Keywords: Austenitic stainless steel, AISI 304, heat input, carbide precipitation, weld performance.

1. INTRODUCTION

Austenitic stainless steels (ASS) exhibit good corrosion resistance and superior mechanical properties such as high good formability. Thus, they are widely used in a wide spectrum of applications ranging from kitchen utilities and implants to power plants and from steel bridges to petroleum, oil and gas, nuclear and marine industries [1-5]. The major problem encountered in fusion joining of stainless steels (SS) is the formation of chromium-depleted zones (i.e., carbide precipitation along the grain boundaries in heat affected zone - HAZ). Hot cracking and formation of brittle sigma phase may also be encountered in the fusion zone (FZ) of these steels. Somervuori et al. [6] clearly demonstrated that the Cr-depleted regions in the FZ deteriorated the corrosion behaviour. Kim et al. [7] investigated the influence of Cr_{eq}/Ni_{eq} ratio on the microstructural changes and mechanical behaviour of 316L SS joints. They observed that higher Cr_{eq}/Ni_{eq} ratios significantly affected the

[1] *Iskenderun Technical University, Institute of Engineering and Sciences, Department of Mechanical Engineering, 31200 Iskenderun-Hatay, Turkey.*

[2] *Corresponding author: Iskenderun Technical University, Faculty of Engineering and Natural Sciences, Department of Mechanical Engineering, 31200 Iskenderun-Hatay, Turkey. gurel.cam@iste.edu.tr*

microstructure of AISI 316L joints. Shojaati and Beidokhti [8] also studied how different filler metals (ER 310, ER 316L, duplex ER 2209 and Ni-based Nichrome 80/20 filler metals) influenced the microstructural and mechanical characteristics of dissimilar AISI 304/AISI 409 SS joints. They reported that austenite with different morphologies of ferrite such as lathy, acicular and vermicular were observed in the case of 310 and 316L austenitic filler metals. A mixture of austenite and ferrite phases was seen in the microstructure obtained with the duplex filler metal. Ferrite and Widmanstätten austenite were higher in the regions next to the weld interface owing to the faster cooling here and, thus, the incomplete transformation. The joint obtained using the Ni-based weld metal displayed a microstructure consisting of a Ni-Cr-Fe matrix and Fe-based precipitates in the FZ. Furthermore, the formation of a thin layer of martensite in this joint resulted in the fusion line cracking. It was also reported that the high content of δ-ferrite in the microstructure of FZ increased the hardness and tensile strength values.

As already mentioned hot cracking may also occur in welding of fully ASSs. In general, it is recommended that the delta-ferrite (δ-ferrite) content in the FZ should be kept in the range of 3-20% to prevent hot cracking problem [5]. But, higher amounts of delta ferrite make the FZ more sensitive to high temperatures because of the phase transformation [5,9]. Dadfar et al. [10] studied the corrosion behavior of autogenous Gas Tungsten Arc (GTA) welded AISI 316L joints and observed that the solution heat treatment enhances the corrosion resistance of the as-welded AISI 316L joint. Muthupandi et al. [11] studied the welding of super duplex stainless steels. They concluded that the heat input used should be kept as low as possible. Moreover, they claimed that higher heat inputs might also lead to the precipitation of undesirable brittle phases such as σ (sigma) or X (chi).

Heat input is of great importance in joining of austenitic stainless steels as already pointed out in the preceding paragraph. The solid state friction stir welding technique, which is originally developed for difficult-to-fusion join low melting temperature Al-alloys [12-17] as well as Cu-alloys [18-20] and Pb [21], offers a potential to join steels including stainless steels [22,23]. Additionally, low heat input CMT arc welding method [13,24] or power beam welding techniques such as laser beam welding [25-28] may also be used in joining of these steels. Due to this fact, numerous studies have been conducted on FSW of steels including stainless steels in last 30 years [23,24,29-36]. However, wear of the stirring tool is still a problem to overcome in FSW of steels since the peak temperature involved may reach over 1000 ^{o}C, and even the tools made of high temperature resistant materials may wear slowly over the time.

In this study, the influence of heat input applied to the AISI 304 plates on the microstructural evolution in the joint area and on joint properties were investigated. For this purpose, AISI 304 plates with a thickness of 5 mm were joined by gas metal arc welding (GMAW) using a filler wire of 308 with a diameter of 1.2 mm. Detailed microstructural investigations were conducted for microstructural characterization of the joints. Extensive microhardness measurements in addition to the mechanical testing were conducted to determine the joint properties. Moreover, the effect of heat input on the microstructural changes taking place in the weld region and thus on the joint performance was evaluated.

2. MATERIALS AND METHOD

The material used in this study is AISI 304 grade austenitic stainless steel plates of 5 mm thick. It was supplied in the form of large plate with the sizes of 1500x1000x5 mm^3. Its chemical composition is given in Table 1.
The as-received 304 large plate was cut into the rectangular pieces of 250x190 mm and welding grooves were machined as shown schematically in Fig. 1, for welding trials. The surfaces to be welded were cleaned mechanically using a stainless steel metal brush prior to joining. The plates were welded by GMAW process with the use of an ER308LSi filler wire of 1,2 mm in diameter (the chemical composition of which is given in Table 1), the feeding rate was 17,5 mm/s, in two passes. The weld parameters employed in welding trials were given in Table 2. Two different heat inputs were employed in order to determine the effect of heat input on joint quality.

Following the welding trials, a metallography specimen, two bend specimens and four tensile specimens were prepared for each joint to investigate the microstructural evolutions in the weld regions of the joints and their mechanical properties. Four tensile specimens were also extracted from the base plate for comparison purpose. The metallography specimens were first ground and then polished prior to etching procedure in which the

specimens were immersed in an etchant comprising of 50 ml HCl and 150 ml HNO_3 for about 15 seconds. A detailed microstructural investigations were conducted on these metallography specimens as well as microhardness measurements. Microhardness measurements were conducted on each joint along three lines across the weld region, one being almost in the center, the other two lines lying 1 mm from the surface and root of the joints, using a load of 500 g, as schematically illustrated in Fig. 2.

Table 1. Chemical composition of AISI 304 grade austenitic steel plates used in this study.

Chemical Composition (wt. %)										
Material	C	Si	Mn	P	S	Cr	Ni	N	Mo	Cu
Base Material (AISI 304)	0,019	0,42	1,56	0,035	0,002	18,2	8,1	0,053	--	--
Filler Material (ER308LSi)	0,025	0,804	1,95	0,010	0,023	20,016	9,966	0,035	0,181	0,287

Table 2. The weld parameters employed in welding trials (the same weld parameters were used in each pass in both welding trials).

Weld Trial	**Current (A)**	**Voltage (V)**	**Weld speed (mm/s)**	**Wire feed rate (mm/s)**	**Shielding gas**
Low Heat Input	ave. 385	28	4,5	17,5	Argon (99,95%)
High Heat Input	ave. 465	27	4,0	17,5	Argon (99,95%)

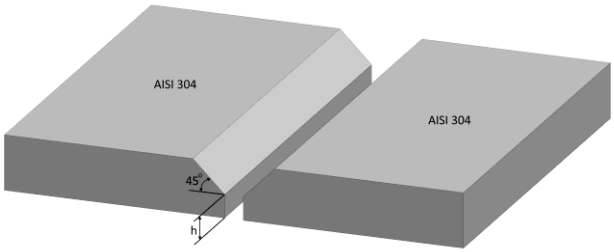

Figure 1. Preparation of the plates for welding trials.

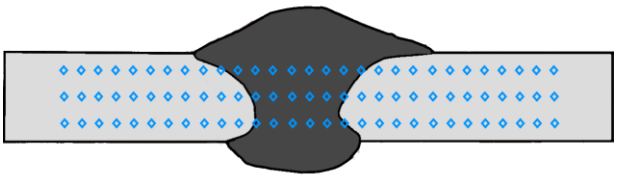

Figure 2. Schematic showing the conduction of microhardness measurements on each joint along three lines across the weld region, one being almost in the center, the other two lines lying 1 mm from the surface and root of the joints.

Transverse tensile specimens of the BM and the joints were also tested with a loading rate of 15 $mm.min^{-1}$ to evaluate the joint performance values and the weld qualities. In addition, the two bend specimens extracted from each joint for bend testing (180 degrees). One of them was bent in the condition of surface bend and the other in

the root bend configuration and the weld center in the middle position in order to determine whether cracking occurs in the weld region or not. Furthermore, an attempt was made to determine the effect of heat input on the microstructural evolution in the HAZ and thus on weld quality and performance.

3. RESULTS AND DISCUSSION

The results obtained from this study will be discussed in two subsections, namely microstructural aspects and mechanical properties, below.

3.1. Microstructural Aspects

The macrographs illustrating the weld cross-sections of the joints produced using low and high heat inputs, respectively, are given in Figure 3. Figure 4 shows micrographs illustrating the base plate microstructure and the microstructures evolved in the FZs and HAZs of the joints produced. As seen from the micrographs, the AISI 304 grade austenitic base plate has a single phase microstructure consisting of austenite grains. Both joints showed a similar microstructural evolution within the weld region. A fine dendritic structure is observed in the FZ of both joints (Fig. 4b and c), which is very usual for this steel. No visible difference was observed between the FZ structures of both joints. Thus, there is no clear effect of heat input difference used.

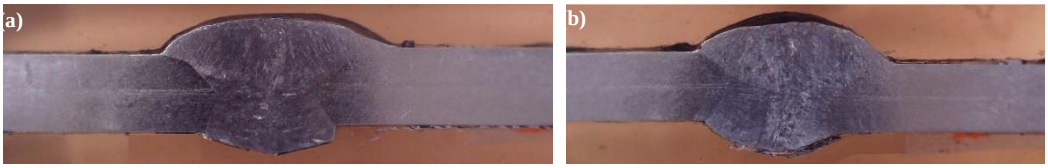

Figure 3. The macrographs illustrating the weld cross-sections of the joints produced: (a) the lower heat input joint and (b) the higher heat input joint.

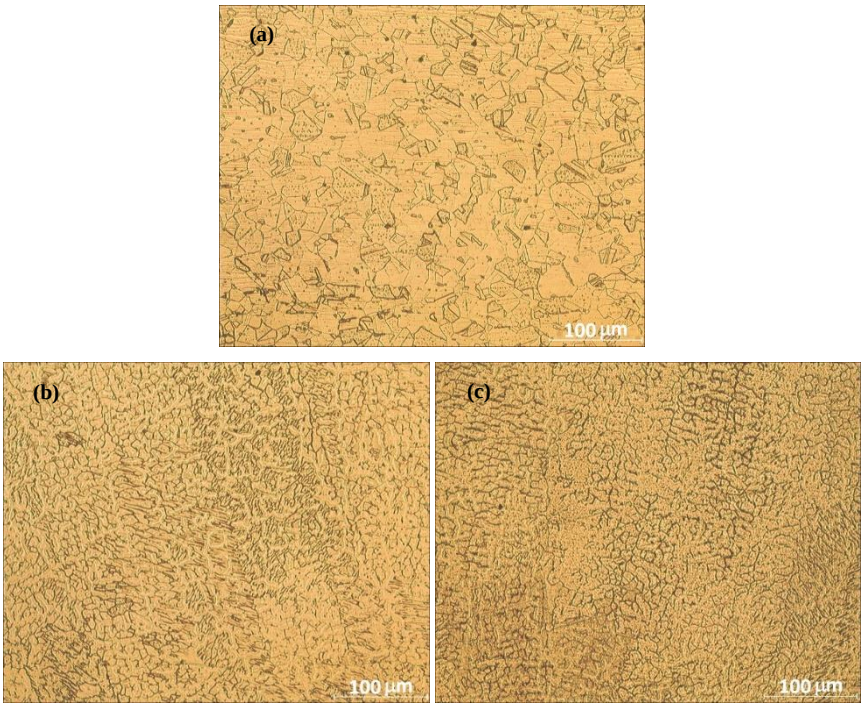

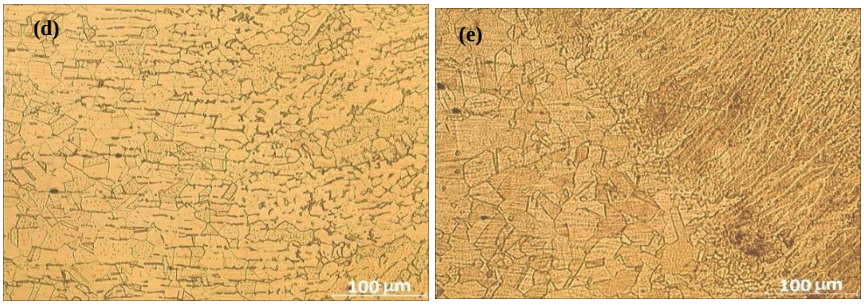

Figure 4. The micrographs illustrating the microstructures of: (a) base plate, (b) FZ of the lower heat input joint, (c) FZ of the higher heat input joint, (d) HAZ of the lower heat input joint and (e) HAZ of the higher heat input joint.

However, there is a clear difference between the microstructures evolving in the HAZs of two joints produced using different heat inputs. As seen from Figure 4(e), larger recrystallized grains of austenite phase were formed in the HAZ of the higher heat input joint. On the other hand, austenite grain size in the HAZ of the lower heat input joint is similar to that of the BM and finer compared to that of HAZ of the higher heat input joint. There are also some precipitates within the HAZ of the low heat input joint elongated in the cold rolling direction (Fig. 4d), indicating that a complete recrystallization did not occur due to lower input involved. Moreover, the fusion interface is more visible in the high heat input joint as a result of grain growth to a larger extent taking place in this joint due to the recrystallization occurring at higher temperatures compared to the lower heat input joint. In addition, there is no indication of chromium carbide precipitation within the HAZ of the higher heat input joint in contrast to the lower heat input joint as seen from Fig. 4(e).

3.2. Mechanical Properties

Figure 5 gives the hardness profiles obtained from the microhardness measurements conducted along three lines across the joints produced using low and high heat inputs. These hardness profiles show the hardness variations across the joints. As clearly seen from these profiles both joints exhibited similar hardness values across the weld region. The hardness profiles clearly show that there is neither a hardness increase (strength overmatching) nor hardness decrease (strength undermatching) in the weld region for both joints. Thus, both joints display a typical hardness profile of strength evenmatching joints. Furthermore, no significant hardness variation was observed across the weld area for both joints, indicating that the heat input variation used has no significant effect on hardness although a grain growth was detected in the high heat input joint. This implies that the slight grain growth in the HAZ of the high heat input joint does not significantly vary the hardness of this region.

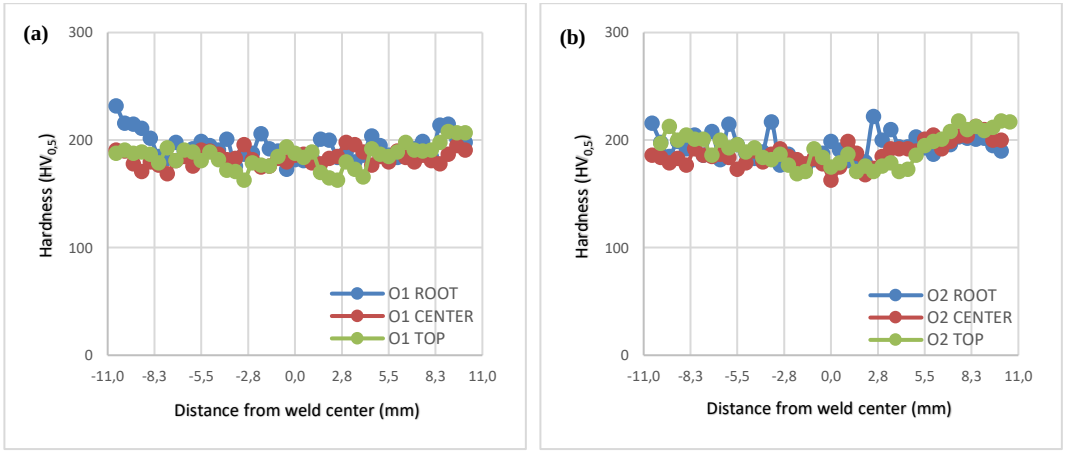

Figure 5. Hardness profiles showing the hardness variation across the joints: (a) lower and (b) the higher heat input joints.

Tensile test results obtained from the specimens prepared from the BM and the joints produced using low and high heat inputs are summarized in Table 3 and Figures 6 and 7. The AISI 304 base plate used in this study displayed a yield stress, tensile strength and elongation of 361 MPa, 636 MPa and about 48%, respectively. As clearly seen from the Table and Figures, both joints exhibited similar tensile properties to those of the BM, indicating that the performance of both joints are reasonably good. Indeed, the both joints exhibited similar tensile strength performance and ductility performance values of about 102% and 80%, respectively, indicating that the heat input variation employed in the current study does not have a significant influence on the joint performance. This results are quite reasonable since the joints did not display any weld defect and the hardness is more or less homogeneous across the joints. Figure 8 shows the fracture locations in all the tensile test specimens extracted from both lower and higher heat inputs joints after testing. As seen from this figure, all the specimens fractured in the base plate far away from the FZ. This clearly demonstrates that the weld quality, thus the joint performance, of both joints is quite good in tensile test condition.

Similar to the case in tensile testing, the heat input variation employed in this study did not have a significant effect on the joint behavior in bend testing. No cracking occurred in both surface and root bend specimens extracted from both joints (namely the lower and heat input joints) as shown in Figure 9. These results indicate that the heat input difference used in this study apparently did not have any diminishing effect on the weld performance in bending condition despite the presence of some carbide precipitates in the HAZ region next to the fusion line of the joint obtained using lower heat input (Fig. 4d).

Table 3. Tensile test results.

Specimen	**$R_{P0.2}$** (MPa)	**R_m** (MPa)	**Elongation** (%)	**Strength Performance** (%)	**Ductility Performance** (%)	**Failure Location**
Base Plate	366, 358, 359 **(361)**	643,631,633 **(636)**	48, 48, 49 (**48**)	----	----	--
Low Heat Input Joint	357, 374, 376, 362 **(367)**	650, 653, 649, 652 **(651)**	39, 38, 40, 40 (**39**)	102	81	Base plate
High Heat Input Joint	349, 366, 353 **(356)**	631,648, 641 **(640)**	38, 38, 40 (**38**)	101	79	Base plate

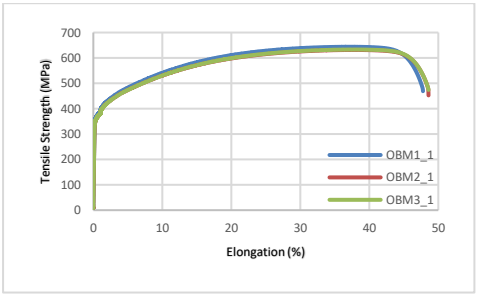

Figure 6. Stress-elongation (%) curve of the base plate AISI 304 steel used.

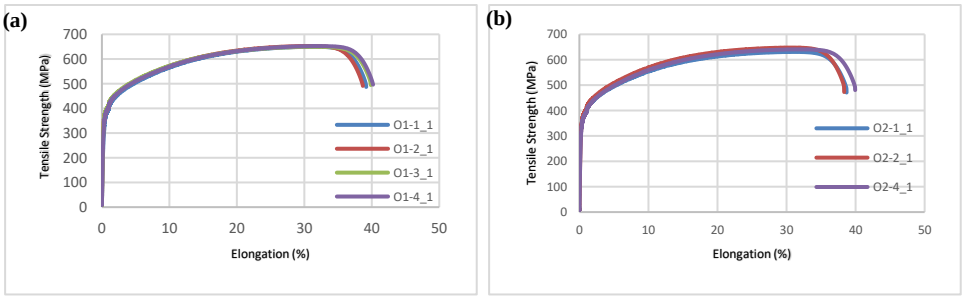

Figure 7. Stress-elongation (%) curves of the joints: (a) lower and (b) higher heat input joints.

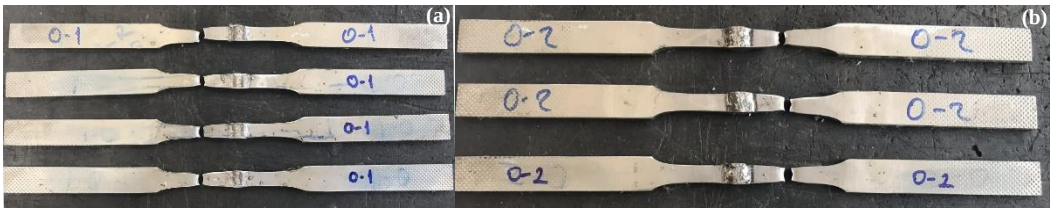

Figure 8. Macrographs showing the fracture locations in the tensile test specimens extracted from: (a) lower and (b) higher heat input joints.

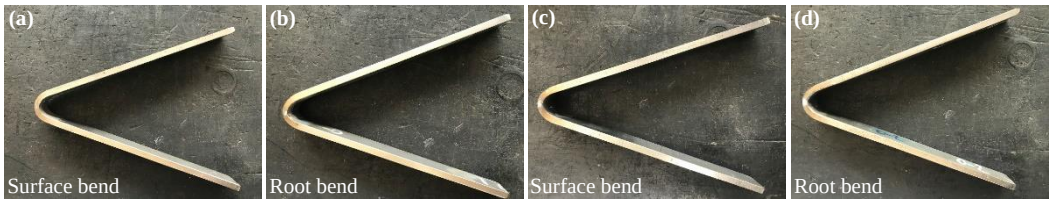

Figure 9. Macrographs showing the surface and root bend specimens, respectively, extracted from: (a) and (b) lower; and (c) and (d) higher heat input joints. Note that no cracking occurred in any of the specimens.

4. CONCLUSIONS

The influence of heat input experienced by the plates during welding on the microstructural evolution in the joint area and on joint properties were investigated for GMAW welded 5 mm thick AISI 304 plates using a filler wire of ER308 with a diameter of 1.2 mm. The following conclusions were withdrawn from this study:

- AISI 304 plates were defect-free welded in two passes by the GMAW process.
- A fine dendritic microstructure was obtained in the FZs of both joints.
- Some precipitates within the HAZ of the low heat input joint elongated in the cold rolling direction were observed while in the HAZ of the higher heat input joint larger recrystallized grains of austenite phase were formed but no carbide precipitates were observed.
- All the tensile test specimens prepared from both joints fractured in the BM far away from the FZ.
- Both joints exhibited similar mechanical properties (strength and ductility) to those of the base plate. Indeed, both joints displayed high tensile strength performance and ductility performance values of over 100% and about 80%, respectively.
- Both surface and root bend specimens extracted from both joints did not crack in bending test, indicating that the heat input variation employed in the current study does not have a significant influence on the joint performance.

ACKNOWLEDGEMENT

We would like to thank Mr. Tugrul YAZGAN from NOKSEL Celik Boru Sanayi A.S. (Noksel Steel Pipe Inc.), Iskenderun-Hatay, Turkey, for his help in conduction of the metallography and mechanical tests. The authors also thank Hikmet Gizem SARSILMAZ from Kahraman-Sarsilmaz Machinery, Iskenderun, for conducting welds.

REFERENCES

[1]. B. Weiss and R. Stickler, “Phase instabilities during high temperature exposure of 316 austenitic stainless steel”, Metall. Trans., vol. 3, pp. 851-866, 1972.
[2]. C. Balaji, S.V.A. Kumar, S.A. Kumar, and R. Satish, “Evaluation of mechanical properties of SS 316 L weldments using tungsten inert gas welding”, Int. J. Eng. Sci. Technol., vol. 4, pp. 2053-2057, 2012.
[3]. L.P. Karjalainen, T. Taulavuori, M. Sellman, and A. Kyröläinen, “Some strengthening methods for austenitic stainless steels”, Steel Research International, vol. 79, pp. 404-412, 2008.
[4]. K. Devendranath Ramkumar, A.Singh, S. Raghuvanshi, A. Bajpai, T. Solanki, M. Arivarasu, N. Arivazhagan, and S. Narayanan, “Metallurgical and mechanical characterization of dissimilar welds of austenitic stainless steel and super-duplex stainless steel - A comparative study”, Journal of Manufacturing Processes, vol. 19, pp. 212-232, 2015.
[5]. J.C. Lippold and D.J. Kotecki, *Welding Metallurgy and Weldability of Stainless Steels*. 1st ed., Hoboken: John Wiley & Sons Inc.; 2005.
[6]. M.E. Somervuori, L.S. Johansson, M.H. Heinonen, D.H.D. van Hoecke, N. Akdut, and H.E. Hänninen, “Characterisation and corrosion of spot welds of austenitic stainless steels”, Mater. Corros., vol. 55, pp. 421-436, 2004.
[7]. Y.H. Kim, D.J. Lee, J.C. Byun, K.H. Jung, J.I. Kim, H.J. Lee, Y.T. Shin, S.H. Kim, and H.W. Lee, “The effect of sigma phases formation depending on Cr/Ni equivalent ratio in AISI 316L weldments”, Mater. Des., vol. 32, pp. 330-336, 2011.
[8]. M. Shojaati and B. Beidokhti, “Characterization of AISI 304/AISI 409 stainless steel joints using different filler materials”, Construction and Building Materials, vol. 147, pp. 608-615, 2017.
[9]. J. Barcik, “Mechanism of σ-phase precipitation in Cr-Ni austenitic steels”. Mater Sci Technol., vol. 4, pp. 5-15, 1988.
[10]. M. Dadfar, M.H. Fathi, F. Karimzadeh, M. R. Dadfar, and A. Saatchi, “Effect of TIG welding on corrosion behavior of 316L stainless steel”. Mater Lett., vol. 61, pp. 2343-2346, 2007.
[11]. V. Muthupandi, P. Bala Srinivasan , S. K. Seshadri, and S. Sundaresan, “Effect of weld metal chemistry and heat input on the structure and properties of duplex stainless steel welds”, Mater. Sci. Eng. A, vol. 358, pp. 9-16, 2003.
[12]. N. Kashaev, V. Ventzke, and G. Cam, “Prospects of laser beam welding and friction stir welding processes for aluminum airframe structural applications”, Journal of Manufacturing Processes, vol. 36, pp. 571-600, 2018.

[13]. G. Cam and G. Ipekoglu, "Recent developments in joining of aluminium alloys", Int. J. Adv. Manuf. Technol., vol. 91(5-8), pp. 1851-1866, 2017.
[14]. G. Cam, "Friction stir welding (FSW) - A novel welding technology developed for Al-Alloys", Muhendis ve Makina, vol. 46 (541), pp. 30-39, Feb. 2005. (in Turkish).
[15]. A. Von Strombeck, G. Cam, J.F. Dos Santos, V. Ventzke, and M. Kocak, "A comparison between microstructure, properties, and toughness behavior of power beam and friction stir welds in Al-alloys", in Proc. of the TMS 2001 Annual Meeting Aluminum, Automotive and Joining (New Orleans, Louisiana, USA, February 12-14, 2001), eds: S.K. Das, J.G. Kaufman, and T.J. Lienert, pub.: TMS, Warrendale, PA, USA, pp. 249-264, 2001.
[16]. G. Cam, "New welding techniques developed for Al-alloys, in Proc. of TMMOB Makina Muhendisleri Odasi, Kaynak Teknolojisi III. Ulusal Kongresi, 19-20 October 2001, Istanbul, pp. 267-277, 2001. (in Turkish).
[17]. G. Ipekoglu, B. Goren Kiral, S. Erim, and G. Cam, "Investigation of the effect of temper condition friction stir weldability of AA7075 Al-alloy plates", Mater. Tehnol., vol. 46 (6), pp. 627-632, 2012.
[18]. T. Kucukomeroglu, E. Senturk, L. Kara, G. Ipekoglu, and G. Cam, "Microstructural and mechanical properties of friction stir welded nickel-aluminum bronze (NAB) alloy", Journal of Materials Engineering and Performance (JMEPEG), vol. 25 (1), pp. 320-326, 2016.
[19]. G. Cam, S. Mistikoglu, and M. Pakdil, 'Microstructural and mechanical characterization of friction stir butt joint welded 63%Cu-37%Zn brass plate', Weld. J., vol. 88 (11), pp. 225s-232s, 2009.
[20]. G. Cam, H.T. Serindag, A. Cakan, S. Mistikoglu, and H. Yavuz, 'The effect of weld parameters on friction stir welding of brass plates', Mat.-wiss. u. Werkstofftech., vol. 39 (6), pp. 394-399, 2008.
[21]. A. Gunen, E. Kanca, M. Demir, F. Cavdar, S. Mistikoglu, and G. Cam, "Microstructural and mechanical properties of friction stir welded pure lead", Indian Journal of Engineering & Materials Sciences (IJEMS), vol. 25 (1), pp. 26-32, 2018.
[22]. G. Cam, "Friction stir welded structural materials: Beyond Al-alloys", Int. Mater. Rev., vol. 56 (1), pp. 1-48, 2011.
[23]. G. Cam, G. Ipekoglu, T. Kucukomeroglu, and S.M. Aktarer, "Applicability of friction stir welding to steels", Journal of Achievements in Materials and Manufacturing Engineering (JAMME), vol. 80(2), pp. 65-85, 2017.
[24]. S. Selvi, A. Vishvaksenan, and E. Rajasekar, "Cold metal transfer (CMT) technology - An overview", Cold metal transfer (CMT) technology - An overview, Defence Technology, vol. 14, pp. 28-44, 2018.
[25]. G. Cam, C. Yeni, S. Erim, V. Ventzke, and M. Kocak, "Investigation into properties of laser welded similar and dissimilar steel joints", Sci. Technol. Weld. Join., vol. 3 (4), pp. 177-189, 1998.
[26]. J. dos Santos, G. Cam, F. Torster, A. Insfran, S. Riekehr, V. Ventzke, and M. Kocak, "Properties of power beam welded steels, Al- and Ti-alloys: Significance of strength mismatch", Welding in the World, vol. 44 (6), pp. 42-64, 2000.
[27]. G. Cam, M. Kocak, and J.F. dos Santos, "Developments in laser welding of metallic materials and characterization of the joints", Welding in the World, vol. 43 (2), pp. 13-26, 1999.
[28]. G. Cam, V. Ventzke, J.F. dos Santos, M. Kocak, G. Jennequin, P. Gonthier-Maurin, M. Penasa, and C. Rivezla: "Characterization of laser and electron beam welded Al-alloys", Prakt. Metallogr., vol. 36 (2), pp. 59-89, 1999.
[29]. T. Kucukomeroglu, S.M. Aktarer, G. Ipekoglu, and G. Cam, "Investigation of mechanical and microstructural properties of friction stir welded dual phase (DP) steel", The 2nd International Conference on Material Strength and Applied Mechanics (MSAM 2019), IOP Conf. Series: Materials Science and Engineering, vol. 629, Paper No: 012010, 2019.
[30]. G. Ipekoglu, T. Kucukomeroglu, S.M. Aktarer, D.M. Sekban, and G. Cam, "Investigation of microstructure and mechanical properties of friction stir welded dissimilar St37/St52 joints", Materials Research Express, vol. 6 (4), Article Number: 046537, 2019.
[31]. T. Kucukomeroglu, S.M. Aktarer, G. Ipekoglu, and G. Cam, "Mechanical properties of friction stir welded St 37 and St 44 steel joints", Materials Testing, vol. 60 (12), pp. 1163-1170, 2018.
[32]. T. Kucukomeroglu, S.M. Aktarer, G. Ipekoglu, and G. Cam, "Microstructure and mechanical properties of friction stir welded St52 steel joints", International Journal of Minerals, Metallurgy and Materials, vol. 25 (12), pp. 1457-1464, 2018.
[33]. L. Cui, H. Fujii, N. Tsuji, and K. Nogi, "Friction stir welding of a high carbon steel", Scripta Mater., vol. 56, pp. 637-40, 2007.
[34]. P. Chansoria, P. Solanki, and M.S. Dasgupta, "Parametric study of transient temperature distribution in FSW of 304L stainless steel", Int. J. Adv. Manuf. Technol., vol. 80, pp. 1223-1239, 2015.
[35]. H. Kokawa, S.H.C. Park, Y.S. Sato, K. Okamoto, S. Hirano, and M. Inagaka, "Microstructures in friction stir welded 304 austenitic stainless steel", Welding in The World, vol. 49, pp. 34-40, 2005.
[36]. A.P. Reynolds, W. Tang, T. Gnaupel-Herold, and H. Prask, "Structure, properties, and residual stress of 304L stainless steel friction stir welds", Scripta Mater., vol. 48 (9), pp. 1289-1294, 2003.

Biography: *Gurel Cam is currently a full professor at the Department of Mechanical Engineering of Iskenderun Technical University, Iskenderun-Hatay, Turkey. He earned his PhD degree in Materials Science from Imperial College of Science, Technology, and Medicine, University of London, U.K., in 1990. He has authored or coauthored 77 journal articles, 73 proceeding papers, 7 keynote presentations (invited lectures) and one book chapter. His publications have been cited more than 3560 times in Google Scholar, h-index = 33 (2526 citations in Scopus; h index: 30; more than 2300 citations in WOS; h-index: 28). He is the writer of a book entitled 'Science and Technology of Welding' (in Turkish). His research interests include welding technologies including friction stir welding, diffusion bonding, electron beam welding and laser beam welding, characterization of welded joints, and low transformation temperature (LTT) filler materials. He is a member of AWS (American Welding Society), USA, and DVS (Deutsche Verband fur Schweisstechnik), Germany. He is also a member of the General Board, Institute of Turkish Welding Technologies, Istanbul, Turkey, since January 2009, and MUDEK Programme Evaluator, Turkey (Mechanical Engineering and Metallurgy-Materials Engineering) since May 2018.*

Microstructural and Mechanical Characterization of Gas Metal Arc Welded AISI 430 Ferritic Stainless Steel Joints

Mustafa Senol[1], Gurel Cam[2]

Abstract

Ferritic stainless steels contain Cr as the main alloying element and display very good corrosion resistance even at high temperatures. These steels are widely used in manufacturing of products such as hot water storage units, car chassis components, exhaust systems and kitchenware. The most characteristic difficulty in fusion joining of this type of stainless steels is the grain growth in the HAZ. Furthermore, martensite formation or carbide precipitation along the grain boundaries in the HAZ may also be observed if the heat input used is extremely high or C content of the steel and/or filler wire high. Thus, it is required that the heat input should be kept low or filler wires with low C should be used to successfully join these steels by conventional fusion welding methods. The determination of the effect of heat input on microstructural evolution in the weld region and the mechanical properties of the joints in gas metal arc welding of AISI 430 ferritic steel plates is aimed in this study. To that end, AISI 430 ferritic steel plates with a thickness of 5 mm were joined using different heat input values. The microstructures in the weld region and mechanical properties of the welded joints were determined by extensive optical microscopy investigations, microhardness measurements, tensile and bending tests. Moreover, the heat input effect on the joint performance was also studied.

Keywords: *Ferritic stainless steel, AISI 430, heat input, martensite formation, weld performance.*

1. INTRODUCTION

AISI 430 grade ferritic stainless steel (FSS) possesses high strength and corrosion resistance coupled with relatively low cost. In addition, ferritic stainless steels have more resistance to chloride stress corrosion cracking than austenitic stainless steels (ASS). Thus, it is widely used in a wide range of applications ranging from household utensils, vehicle exhausts, road and rail vehicles to other applications in several industries such as oil, gas, petrochemical, nuclear and power industries [1-10]. They are the second largest selling type of stainless steels behind austenitic grades.

The major problem encountered in welding of FSSs is the reduced ductility (toughness) in the heat affected zone (HAZ) which limits their application [2]. This problem is caused by the evolution of large grains in the HAZ of fusion welds. The temperature in this region reaches a critical temperature (955 ^{o}C) and causes rapid growth of the ferrite grains [3]. Moreover, although the carbon content of FSSs is very small, on rapid cooling the formation of intergranular martensite and/or chromium-depleted zones may take place along the grain

[1] *Iskenderun Technical University, Institute of Engineering and Sciences, Department of Mechanical Engineering, 31200 Iskenderun-Hatay, Turkey.*

[2] *Corresponding author: Iskenderun Technical University, Faculty of Engineering and Natural Sciences, Department of Mechanical Engineering, 31200 Iskenderun-Hatay, Turkey. gurel.cam@iste.edu.tr*

boundaries in HAZ. Formation of martensite in the HAZ even in small amounts results in a loss of ductility in addition to grain coarsening. Carbide precipitation can make the steel sensitive to inter-crystalline corrosion.

For instance, Aguilar et al. [6] investigated the metallurgical transformations occurring during the submerged arc welding (SMAW) of AISI 430 FSS with AISI 316L ASS using two different filler wires, namely E309L and E2209. They clearly demonstrated that both grain growth and martensite formation at the ferrite grain boundaries took place in the HAZ of 430 steel next to the fusion line in both joints. They also reported that a refined grain zone was present following the coarse grain zone in the BM side of the HAZ of 430 steel. Similarly, Antunes et al [8] investigated the effect of the weld metal on the microstructure and mechanical behaviour of FSS AISI 444 welded joints employing two types of filler metal of ASS, namely E309L and E316L. The microstructural examinations conducted showed that a grain coarsening occurred in the HAZ of both welded joints. A recent study indicated that duplex SS consumables such as E2204 can be used to obtain defect-free welds of FSS. Duplex SS consumables can also yield higher strength than ASS consumables [9]. Moreover, Zhou et al [7] studied the influence of heat input on microstructural and mechanical characteristics of AISI 430 FSS joints produced by cold metal transfer GMA welding using E308L filler wire. They observed that the carbide precipitation and the formation of intergranular martensites as well as the coarsening of ferrite grains occurred in the coarse-grained zone of HAZ. They also reported that increasing heat input also caused an increase in the amount of intergranular martensite and carbide precipitation.

Heat input is a very important weld parameter in joining of FSSs. Thus, a low heat input solid state welding technique, namely friction stir welding, which was originally developed for low melting temperature Al-alloys [11-16] as well as Cu-alloys [17-19] and Pb [20], has a potential to join steels including stainless steels [21,22]. Similarly, low heat input CMT arc welding method [12,23] or power beam welding techniques [24-27] also offers a potential to join these steels. As a result, several studies have been conducted on FSW of steels including SSs in last 30 years [22,23,28-35]. However, it was observed that wear of the stirring tool takes place in FSW of steels since a peak temperature may reach over 1000 ^{o}C. Thus, even the tools made of high temperature resistant materials may wear slowly over the time. Furthermore, extra low C, Ti or Nb containing FSS grades have been developed in recent years to overcome carbide precipitation and martensite formation along the ferrite grain boundaries within the HAZ. However, it is usually required to keep the heat input as low as possible to avoid grain growth within the HAZ next to the fusion line. Thus, the use of a low heat input (1kj/mm) and an interpass temperature of maximum 100-120°C is recommended in welding of these steels. Moreover, preheat is not advisable although it may be helpful when welding sections over 10mm thick, where excessive grain growth and welding restraint may result in cracking of the joint. Although preheating will lead to grain growth, it will reduce the cooling rate experienced in the HAZ. Thus, this will keep the FZ temperature above the ductile-brittle transition point and may reduce residual stresses. Preheat temperatures should be, however, kept between 50-250 °C depending on the composition of the steel.

In this study, the weldability of FSS, namely AISI 430, and the influence of heat input applied to the plates on the microstructural evolution in the joint area and thus on joint properties were investigated. Thus, 5 mm thick AISI 430 plates were welded by gas metal arc welding (GMAW) using a filler wire of ER307 with a diameter of 1.2 mm. Detailed microstructural investigations were conducted for microstructural characterization of the joints and detailed microhardness measurements were carried out in addition to the mechanical tests to determine the joint properties. Moreover, the influence of heat input on the microstructure in the joint area and thus on the joint performance was evaluated.

2. MATERIALS AND METHOD

In this study, AISI 430 grade FSS plates with a thickness of 5 mm was used. It was received in the form of large plate with the sizes of 1500x1000x5 mm^3. Its composition is illustrated in Table 1.
Rectangular pieces with the sizes of 250x190 mm were extracted from the as-received large plate and welding grooves were machined as illustrated in Fig. 1, prior to welding. The surfaces to be joined were cleaned mechanically using a stainless steel metal brush prior to the joining process. GMAW welding was carried out in two passes using an ER307 filler wire of 1.2 mm in diameter, the feeding rate was 17,5 mm/s. The weld parameters employed in welding trials were given in Table 2. As seen from this table, the welding trials were conducted using two different heat inputs in order to determine how the joint performance is influenced by heat input.

One metallography specimen, two bend specimens and four tensile specimens were extracted from each joint in order to investigate the microstructural evolutions in the weld regions of the joints produced and to evaluate its influence on the mechanical properties. For comparison purposes and to evaluate the joint performance, four tensile specimens were also extracted from the base plate. The metallography specimens were first ground and polished prior to etching in which the specimens were immersed in a solution comprising of 50 ml HCl and 150 ml HNO_3 for about 17 seconds. A detailed microstructural investigations were carried out on these specimens as well as microhardness measurements. Microhardness measurements were done on each joint along three lines across the weld region, using a load of 500 g, as schematically illustrated in Fig. 2.

Table 1. Composition of AISI 430 grade austenitic steel plates used in this study.

Chemical Composition (wt. %)										
Material	C	Si	Mn	P	S	Cr	Ni	N	Mo	Cu
Base Material (AISI 430)	0,037	0,38	0,50	0,031	0,002	16,16	0,27	0,033	0,01	0,20
Filler Material (ER307)	0,075	0,790	7,10	0,009	0,020	19,075	9,010	----	0,005	0,070

Table 2. The process parameters employed in welding.

Weld Trial	**Current (A)**	**Voltage (V)**	**Weld speed (mm/s)**	**Feeding rate of filler wire (mm/s)**	**Shielding gas**
Low Heat Input	ave. 385	28	4,5	17,5	Argon (99,95%)
High Heat Input	ave. 465	27	4,0	17,5	Argon (99,95%)

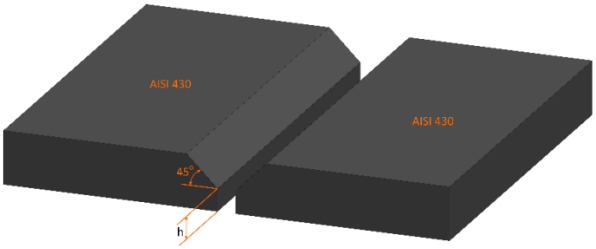

Figure 1. Preparation of the plates for welding trials.

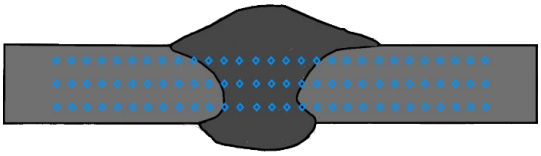

Figure 2. Schematic showing the conduction of microhardness measurements on each joint along three lines across the weld region.

Moreover, tensile test specimens of both the BM and the joints were tested with a loading rate of 15 mm/s to evaluate the mechanical properties, joint performance values and the weld qualities. Two bend specimens were also extracted from each joint in order to determine whether cracking occurs in the weld region of the joints produced using different heat input values. One of them was bent in the condition of surface bend and the other in the root bend configuration. The specimens were bent about 180 degrees and the weld center in the middle position. Furthermore, the influence of heat input on the microstructural evolution in the HAZ and thus on mechanical behavior of the joints was also determined.

3. RESULTS AND DISCUSSION

The results obtained from this study will be discussed below in two subsections.

3.1. Microstructural Aspects

Figure 4 (a) shows the microstructure of the BM used in this study. The BM microstructure consists of a fully ferritic microstructure containing carbides, which are evenly distributed within the grains as well as along the grain boundaries. Figure 3 and 4 give macrograph and micrographs illustrating the weld cross-sections of the joints and the microstructures observed in the HAZ and FZ of the joints produced using low and high heat inputs, respectively. As seen from the micrographs, a fine dendritic structure was observed in the FZ of both joints. However, the grain size of dendritic structure is slightly coarser in the high heat input joint (Fig. 4c). This is not unexpected since high heat input applied during welding results in grain growth in the FZ.

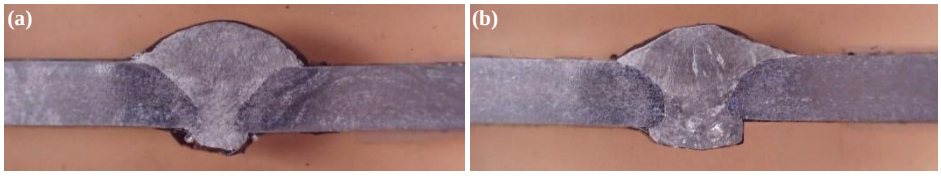

Figure 3. The macrographs illustrating the weld cross-sections of the welds produced: (a) the lower and (b) the higher heat input joint.

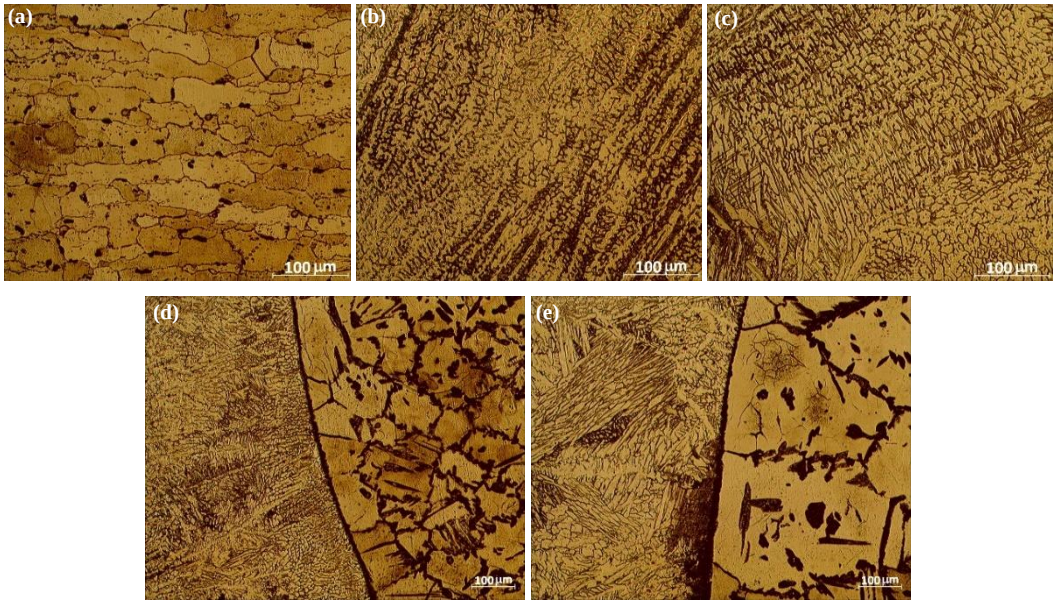

Figure 4. The micrographs illustrating the microstructures of: (a) BM, (b) and (c) FZ of the lower and higher heat input joint, respectively, and (d) and (e) HAZ of the lower and higher heat input joints, respectively.

Furthermore, it was observed that the BM microstructure was affected by solid state phase transformations induced by the weld thermal cycle in the HAZ of both joints. Thus, two distinct HAZ regions were formed in both joints, namely high temperature HAZ (so-called coarse grained HAZ, i.e. FGHAZ) and low temperature HAZ (often referred to fine grained HAZ, i.e FGHAZ) which is on the base metal (BM) side. Although both joints did exhibit CGHAZ next to the fusion boundary (FB), the extent of grain growth is much higher in the high heat input joint as clearly seen from Figs. 4(d) and (e). Martensite formation along the grain boundaries of ferrite phase and the growth of ferrite grains were detected in the HAZ region. Moreover, carbide precipitation along the fusion boundary was also observed in both joints. The grains were clearly much finer in

the FGHAZ, and the grain size was almost the same as that of the BM, in contrast to CGHAZ where the grains are much coarser. Moreover, the evolution of intergranular martensites were also observed in the FGHAZ. However, compared with CGHAZ, the amount of martensite was significantly less, and the martensite distributed discretely at the grain boundaries and no longer formed within the grains. The reason for this is the fact that the fine grain zone is far away from the FZ and the temperature is low. Thus, the formation of high-temperature austenite is suppressed, which inhibits martensite formation. The content of intergranular martensite and carbide precipitates along the fusion boundaries increases with an increase in heat input. Thus, the width of the HAZ also increases slightly with increasing heat input. According to Khorrami et al [36], the martensite formation in the HAZ of medium-Cr FSS joint is a well-known phenomenon. Van Warmelo et al [37] also proposed that the precipitates of carbides, nitrides or carbonitrides were usually formed in the HAZ of FSS. Moreover, Zou et al [7] reported that the dominant precipitate was Cr-rich carbide, i.e., M23C6 in which 'M' mostly stands for Cr and Fe. However, there is no clear indication of these precipitations in the HAZ of 430 FSS joints in the current study.

3.2. Mechanical Properties

Figure 5(a) and 5(b) gives the hardness profiles obtained from the joints produced using low and high heat inputs. These hardness profiles show the hardness variations across the joints. As clearly seen from these profiles, both joints displayed similar hardness variations across the weld region. The hardness profiles clearly show that there is a hardness increase (strength overmatching) in the weld region for both joints, particularly in the HAZ region. Thus, both joints display a typical hardness profile of strength overmatching joints. This hardness increase in the weld region of both joints is due to the formation of fine dendritic microstructure in the fusion zone (FZ) and the formation of intergranular martensite and growth of ferrite grains in the HAZ. Furthermore, the width of the HAZ in which hardness variation took place is wider in the higher heat input joint, indicating that the higher heat input has a significant effect on microstructure and thus on hardness across the weld region.

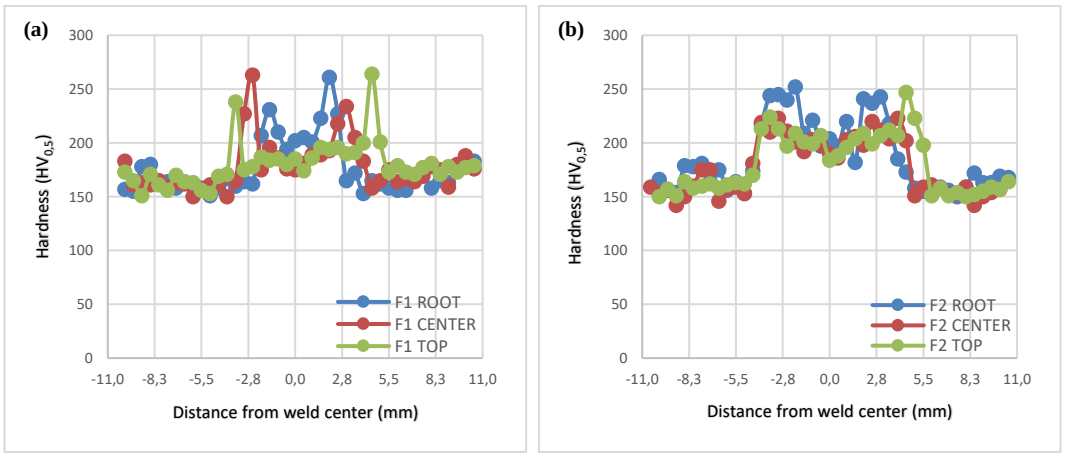

Figure 5. Hardness variation across the joints: (a) the lower heat input joint and (b) the higher heat input joint.

The results of tensile tests performed on the specimens of the BM and the joints produced using different heat input values are summarized in Table 3 and shown in Figure 6-7. Both welded joints showed good tensile strength and the failure took place at the BM away from the FZ for all samples. The tensile strength of both joints were very similar to that of the BM, Fig. 7. Thus, the tensile strength performance of both joints was found to be as high as 99%. On the other hand, both joints displayed lower ductility; i.e. about 15%, than that of the BM, i.e. 23%. This is not surprising since there is a strength overmatching in both joints as clearly illustrated by the hardness profiles. Thus, the higher strength weld region stays in the elastic region and does not contribute to the total elongation. This confined plasticity occurring only in the base plate sides of the tensile test specimen results in decreasing of the percentage elongation value. Similar results were also reported inhomogeneous welded joints, namely strength overmatched laser beam welded steels [24,38], strength

undermatching Al-alloys joints [39-44] and bi-metallic joints showing confined plasticity [45,46]. Moreover, all the tensile specimens of the joints failed in the BM (in the region between fine grained HAZ and the base metal), as shown in Figure 8.

Table 3. Tensile test results.

Specimen	**$R_{P0.2}$** (MPa)	**R_m** (MPa)	**Elongation** (%)	**Strength Performance** (%)	**Ductility Performance** (%)	**Failure Location**
Base Plate	396, 392, 395 **(394)**	506,501,504 **(504)**	21, 25, 22 **(23)**	----	----	--
Low Heat Input Joint	358, 364, 348, 354 **(356)**	498, 496, 495, 499 **(497)**	14, 15, 15, 15 **(15)**	99	65	Base plate
High Heat Input Joint	352, 300, 342, 341 **(335)**	497,496, 498, 503 **(499)**	15, 16, 14, 15 **(15)**	99	65	Base plate

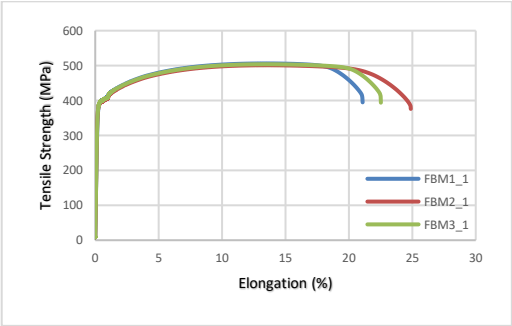

Figure 6. Stress-elongation (%) curve of the base plate AISI 304 steel used.

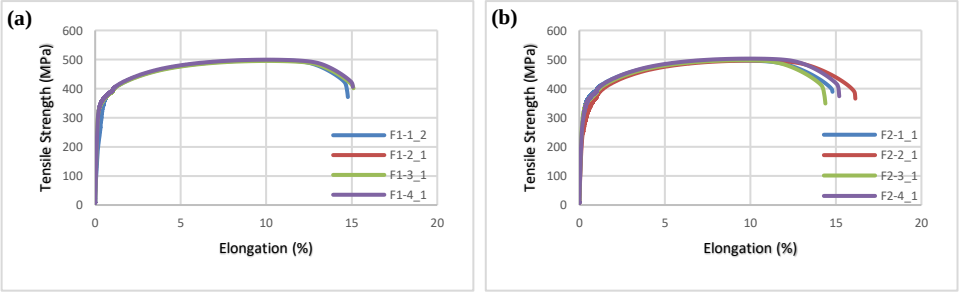

Figure 7. Stress-elongation (%) curves of: (a) lower heat input joint, and (b) higher heat input joint.

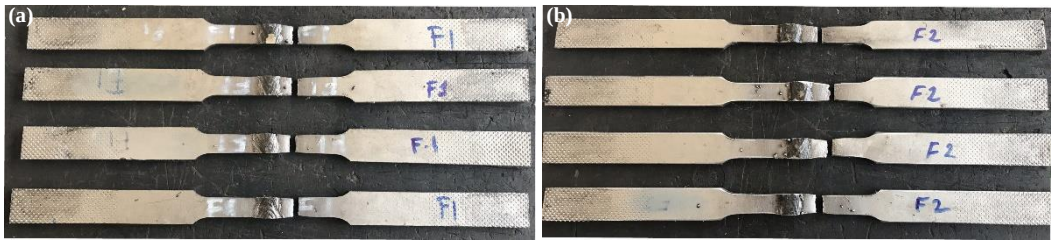

Figure 8. Macrographs showing the fracture locations in the tensile test specimens extracted from: (a) lower heat input joint and (b) higher heat input joint.

Figure 9. Macrographs showing the surface and root bend specimens extracted from: (a) lower heat input joint and (b) higher heat input joint. Note that no cracking occurred in any of the specimens.

Figure 10. Macrograph showing the failure location in root bend specimens extracted from the higher heat input joint. Note that failure takes place in the coarse grained HAZ (CGHAZ) region.

4. CONCLUSIONS

The weldability of AISI 430 plates with a thickness of 5 mm by GMAW welded using a filler wire of 307 with a diameter of 1.2 mm and the influence of heat input on the microstructural evolution in the joint area and thus on joint properties were investigated. The following conclusions were withdrawn from this study:

- AISI 430 plates with a thickness of 5 mm was defect-free welded in two passes by GMAW process.
- A fine dendritic microstructure was evolved in the fusion zone of both joints, although the grain size of the dendrites was slightly coarser in the higher heat input joint.
- Two distinct HAZ regions were formed in both joints namely coarse grained HAZ (CGHAZ) and fine grained HAZ (FGHAZ) regions.
- It was observed that the martensite formation along ferrite grain boundaries (intergranular martensites) and the coarsening of ferrite grains took place in the CGHAZ. However, no martesite was observed along the grain boundaries in the CGHAZ next to the fusion boundary. On the contrary, carbide precipitation was observed along the fusion boundaries of both joints.
- Both joints displayed a hardness increase in the weld region.
- All the tensile test specimens failed in the base plate. Both joints showed similar strength values to that of the BM, the strength performance of the joints being about 99%. However, the ductility performance was lower, i.e. about 65%, due to confined plasticity resulting from strength overmatching weld region. No clear indication of the influence of the heat input on joint performance has been observed in tensile loading condition.
- Both surface and root bend specimens extracted from lower heat input joint did not crack in bending test while the surface bend specimen did not crack but root bend specimen failed in the case of higher heat input joint, indicating that the heat input variation did in fact affect the joint behavior in bending condition. The results also indicate that the strength overmatching weld region cannot shield the cracking in root bend condition in the case of higher heat input joint.

ACKNOWLEDGEMENT

We would like to thank Mr. Tuğrul YAZGAN from NOKSEL Çelik Boru Sanayi A.Ş. (Noksel Steel Pipe Inc.), İskenderun-Hatay, Turkey, for his help in conduction of the metallography and mechanical tests.

REFERENCES

[1]. N. Ghosh, P.K. Pal, G. Nandi, "GMAW dissimilar welding of AISI 409 ferritic stainless steel to AISI 316L austenitic stainless steel by using AISI 308 filler wire", Engineering Science and Technology, an International Journal, vol. 20, pp. 1334–1341, 2017.
[2]. T. Mohandas, M.G. Reddy, M. Naveed, "A Comparative Evaluation of Gas Tungsten and Shielded Metal Arc Welds of a Ferritic Stainless Steel", J. Mater. Process. Technol., vol. 94, pp. 133-140, 1999.
[3]. J.C. Lippold and D.J. Kotecki, *Welding Metallurgy and Weldability of Stainless Steels*. 1st ed., Hoboken: John Wiley & Sons Inc.; 2005.
[4]. F.B. Pickering, "Physical Metallurgy of Stainless Steel Development", Int. Met. Rev., vol. 21, pp. 227-268, 1976.
[5]. R. Ghasemi, B. Beidokhti, M. Fazel-Najafabadi, "Effect of Delta Ferrite on The Mechanical Properties of Dissimilar Ferritic-Austenitic Stainless Steel Welds", Arch. Metall. Mater., vol. 63 (1), pp. 437-443, 2018.
[6]. S. Aguilar, R. Tabares, C. Serna, "Microstructural Transformations of Dissimilar Austenite-Ferrite Stainless Steels Welded Joints", Journal of Materials Physics and Chemistry,vol. 1 (4), pp. 65-68, 2013.
[7]. J. Zhou, J. Shen, S. Hu, G. Zhao, Q. Wang, "Microstructure and mechanical properties of AISI 430 ferritic stainless steel joints fabricated by cold metal transfer welding", Materials Research Express, vol. 6 (11), Article No: 116536, 2019.
[8]. P.D. Antunes, E.O. Correa, N.D. Barbedo, P. de Oliveira Souza, J.L. Gonçalves, and A.A. Diacenco, "Mechanical and Microstrutural Characterization of Weldments of Ferritic Stainless Steel AISI 444 Using Austenitic Stainless Steels Filler Metals". Journal of ASTM International, vol. 9 (2), pp. 1-9, 2012.
[9]. K. Shanmugam, A.K. Lakshminarayanan and V. Balasubramanian, "Tensile and Impact Properties of Shielded Metal Arc Welded AISI 409M Ferritic Stainless Steel Joints", J. Mater. Sci. Technol., vol. 25 (2), pp. 181-186, 2009.
[10]. A.K., Lakshminarayanan, "Effect of Welding Processes on Tensile and Impact Properties, Hardness and Microstructure of AISI 409M Ferritic Stainless Joints Fabricated by Duplex Stainless Steel Filler Metal", Journal of Iron and Steel Research, International, vol. 16., pp. 66-72, 2009.
[11]. N. Kashaev, V. Ventzke, and G. Çam, "Prospects of laser beam welding and friction stir welding processes for aluminum airframe structural applications", Journal of Manufacturing Processes, vol. 36, pp. 571-600, 2018.
[12]. G. Çam and G. İpekoğlu, "Recent developments in joining of aluminium alloys", Int. J. Adv. Manuf. Technol., vol. 91(5-8), pp. 1851-1866, 2017.
[13]. G. Çam, "Friction stir welding (FSW) - A novel welding technology developed for Al-Alloys", Mühendis ve Makina, vol. 46 (541), pp. 30-39, Feb. 2005. (in Turkish).
[14]. A. Von Strombeck, G. Çam, J.F. Dos Santos, V. Ventzke, and M. Koçak, "A comparison between microstructure, properties, and toughness behavior of power beam and friction stir welds in Al-alloys", in Proc. of the TMS 2001 Annual Meeting Aluminum, Automotive and Joining (New Orleans, Louisiana, USA, February 12-14, 2001), eds: S.K. Das, J.G. Kaufman, and T.J. Lienert, pub.: TMS, Warrendale, PA, USA, pp. 249-264, 2001.
[15]. G. Çam, "New welding techniques developed for Al-alloys, in Proc. of TMMOB Makina Mühendisleri Odası, Kaynak Teknolojisi III. Ulusal Kongresi, 19-20 October 2001, İstanbul, pp. 267-277, 2001. (in Turkish).
[16]. G. İpekoğlu, B. Gören Kıral, S. Erim, and G. Çam, "Investigation of the effect of temper condition friction stir weldability of AA7075 Al-alloy plates", Mater. Tehnol., vol. 46 (6), pp. 627-632, 2012.
[17]. T. Küçükömeroğlu, E. Şentürk, L. Kara, G. İpekoğlu, and G. Çam, "Microstructural and mechanical properties of friction stir welded nickel-aluminum bronze (NAB) alloy", Journal of Materials Engineering and Performance (JMEPEG), vol. 25 (1), pp. 320-326, 2016.
[18]. G. Çam, S. Mistikoglu, and M. Pakdil, 'Microstructural and mechanical characterization of friction stir butt joint welded 63%Cu-37%Zn brass plate', Weld. J., vol. 88 (11), pp. 225s-232s, 2009.
[19]. G. Çam, H.T. Serindağ, A. Çakan, S. Mıstıkoğlu, and H. Yavuz, 'The effect of weld parameters on friction stir welding of brass plates', Mat.-wiss. u. Werkstofftech., vol. 39 (6), pp. 394-399, 2008.
[20]. A. Günen, E. Kanca, M. Demir, F. Çavdar, S. Mistikoğlu, and G. Çam, "Microstructural and mechanical properties of friction stir welded pure lead", Indian Journal of Engineering & Materials Sciences (IJEMS), vol. 25 (1), pp. 26-32, 2018.
[21]. G. Çam, "Friction stir welded structural materials: Beyond Al-alloys", Int. Mater. Rev., vol. 56 (1), pp. 1-48, 2011.
[22]. G. Çam, G. İpekoğlu, T. Küçükömeroğlu, and S.M. Aktarer, "Applicability of friction stir welding to steels", Journal of Achievements in Materials and Manufacturing Engineering (JAMME), vol. 80(2), pp. 65-85, 2017.
[23]. S. Selvi, A. Vishvaksenan, and E. Rajasekar, "Cold metal transfer (CMT) technology - An overview", Cold metal transfer (CMT) technology - An overview, Defence Technology, vol. 14, pp. 28-44, 2018.
[24]. G. Çam, Ç. Yeni, S. Erim, V. Ventzke, and M. Koçak, "Investigation into properties of laser welded similar and dissimilar steel joints", Sci. Technol. Weld. Join., vol. 3 (4), pp. 177-189, 1998.
[25]. J. dos Santos, G. Çam, F. Torster, A. Insfran, S. Riekehr, V. Ventzke, and M. Koçak, "Properties of power beam welded steels, Al- and Ti-alloys: Significance of strength mismatch", Welding in the World, vol. 44 (6), pp. 42-64, 2000.
[26]. G. Çam, M. Koçak, and J.F. dos Santos, "Developments in laser welding of metallic materials and characterization of the joints", Welding in the World, vol. 43 (2), pp. 13-26, 1999.
[27]. G. Çam, V. Ventzke, J.F. dos Santos, M. Koçak, G. Jennequin, P. Gonthier-Maurin, M. Penasa, and C. Rivezla: "Characterization of laser and electron beam welded Al-alloys", Prakt. Metallogr., vol. 36 (2), pp. 59-89, 1999.

[28]. T. Küçükömeroğlu, S.M. Aktarer, G. İpekoğlu, and G. Çam, "Investigation of mechanical and microstructural properties of friction stir welded dual phase (DP) steel", The 2nd International Conference on Material Strength and Applied Mechanics (MSAM 2019), IOP Conf. Series: Materials Science and Engineering, vol. 629, Paper No: 012010, 2019.
[29]. G. İpekoğlu, T. Küçükömeroğlu, S.M. Aktarer, D.M. Sekban, and G. Çam, "Investigation of microstructure and mechanical properties of friction stir welded dissimilar St37/St52 joints", Materials Research Express, vol. 6 (4), Article Number: 046537, 2019.
[30]. T. Küçükömeroğlu, S.M. Aktarer, G. İpekoğlu, and G. Çam, "Mechanical properties of friction stir welded St 37 and St 44 steel joints", Materials Testing, vol. 60 (12), pp. 1163-1170, 2018.
[31]. T. Küçükömeroğlu, S.M. Aktarer, G. İpekoğlu, and G. Çam, "Microstructure and mechanical properties of friction stir welded St52 steel joints", International Journal of Minerals, Metallurgy and Materials, vol. 25 (12), pp. 1457-1464, 2018.
[32]. L. Cui, H. Fujii, N. Tsuji, and K. Nogi, "Friction stir welding of a high carbon steel", Scripta Mater., vol. 56, pp. 637-40, 2007.
[33]. Y. Azuma, Y. Kameno, and T. Takasugi, "Friction stir welding in stainless steel sheet of type 430 using Ni-based dual two-phase intermetallic alloy tool", Welding International, vol. 27 (12), pp. 929-935, 2013.
[34]. B.W. Ahn, D.H. Choi, D.J. Kim, and S.B. Jung, "Microstructures and properties of friction stir welded 409 L stainless steel using a Si3N4 tool", Mater. Sci. Eng. A, vol. 532, pp. 476-479, 2012.
[35]. A.K. Lakshminarayanan and V. Balasubramanian, "An assessment of microstructure, hardness, tensile and impact strength of friction stir welded ferritic stainless steel joints", Mater. Des., vol. 31, pp. 4592-4600, 2010.
[36]. M.S. Khorrami, M.A. Mostafaei, H. Pouraliakbar, and A.H. Kokabi, "Study on microstructure and mechanical characteristics of low-carbon steel and ferritic stainless steel joints", Materials Science & Engineering A, vol. 608, pp. 35-45, 2014.
[37]. M. van Warmelo, D. Nolan, and J. Norrish, "Mitigation of sensitisation effects in unstabilised 12%Cr ferritic stainless steel welds", Materials Science & Engineering A, vol. 464, pp. 157-169, 2007.
[38]. G. Çam, S. Erim, Ç. Yeni, and M. Koçak, 'Determination of mechanical and fracture properties of laser beam welded steel joints', Weld. J., vol. 78 (6), pp. 193s-201s, 1999.
[39]. G. Çam, V. Ventzke, J.F. dos Santos, M. Koçak, G. Jennequin, and P. Gonthier-Maurin, 'Characterisation of electron beam welded aluminium alloys', Sci. Technol. Weld. Join., vol. 4 (5), pp. 317-323, 1999.
[40]. G. İpekoğlu, S. Erim, B. Gören Kıral, and G. Çam, 'Investigation into the effect of temper condition on friction stir weldability of AA6061 Al-alloy plates', Kovove Mater., vol. 51 (3), pp. 155-163, 2013.
[41]. G. Çam, S. Güçlüer, A. Çakan, and H.T. Serindağ: 'Mechanical properties of friction stir butt-welded Al-5086 H32 plate', Mat.-wiss. u. Werkstofftech., vol. 40 (8), pp. 638-642, 2009.
[42]. M. Pakdil, G. Çam, M. Koçak, and S. Erim, 'Microstructural and mechanical characterization of laser beam welded AA6056 Al-alloy', Mater. Sci. Eng. A, vol. 528 (24), pp. 7350-7356, 2011.
[43]. G. İpekoğlu, S. Erim, and G. Çam, 'Investigation into the influence of post-weld heat treatment on the friction stir welded AA6061 Al-alloy plates with different temper conditions', Metall. Mater. Trans. A, vol. 45A (2), pp. 864-877, 2014.
[44]. G. İpekoğlu, S. Erim, and G. Çam: 'Effects of temper condition and post weld heat treatment on the microstructure and mechanical properties of friction stir butt welded AA7075 Al-alloy plates', Int. J. Adv. Manuf. Technol., vol. 70 (1), pp. 201-213, 2014.
[45]. M. Koçak, M. Pakdil, and G. Çam, 'Fracture behaviour of diffusion bonded Ti-alloys with strength mismatch', Sci. Technol. Weld. Join., vol. 7 (4), pp. 187-196, 2002.
[46]. G. Çam, M. Koçak, D. Dobi, L. Heikinheimo, and M. Siren, 'Fracture behaviour of diffusion bonded bimaterial Ti-Al joints', Sci. Technol. Weld. Join., vol. 2 (3), pp. 95-101, 1997.

Biography: *Gürel Çam is currently a full professor at the Department of Mechanical Engineering of Iskenderun Technical University, İskenderun-Hatay, Turkey. He earned his PhD degree in Materials Science from Imperial College of Science, Technology, and Medicine, University of London, U.K., in 1990. He has authored or coauthored 77 journal articles, 73 proceeding papers, 7 keynote presentations (invited lectures) and one book chapter. His publications have been cited more than 3560 times in Google Scholar, h-index = 33 (2526 citations in Scopus; h index: 30; more than 2300 citations in WOS; h-index: 28). He is the writer of a book entitled 'Science and Technology of Welding' (in Turkish). His research interests include welding technologies including friction stir welding, diffusion bonding, electron beam welding and laser beam welding, characterization of welded joints, and low transformation temperature (LTT) filler materials. He is a member of AWS (American Welding Society), USA, and DVS (Deutsche Verband für Schweisstechnik), Germany. He is also a member of the General Board, Institute of Turkish Welding Technologies, İstanbul, Turkey, since January 2009, and MUDEK Programme Evaluator, Turkey (Mechanical Engineering and Metallurgy-Materials Engineering) since May 2018.*

Classification of Live / Lifeless Assets from Long Distance with Laser Signals by Using Deep Learning Network

Nevzat Olgun[1], Ibrahim Turkoglu[2]

Abstract

In this study, it is aimed to classify targets as living/lifeless with low-power laser signals in cases of the fight against terrorism, chemical, biological or radioactive attack, urban warfare operations, natural disasters such as earthquakes, floods, storms, and in situations where people such as high- altitude falls are not directly reached. For this purpose, people as living samples and different types of lifeless materials at a certain distance were pointed with a low-powered laser light source and laser signals reflected from the targets were recorded with the receiving system. In the classification of Live / Lifeless, human vitality and other materials (non-living) in nature are compared. In the study, laser signal samples are taken from different points of the arm of 9 volunteer men for living assets and 17 materials frequently used by people for lifeless assets. For lifeless assets, often found in nature, aluminum, black, fabric, frosted glass, glass, pottery, iron, galvanize, granite, linden, magnet, mdf, marble, cardboard, polyethylene, polystyrene, PVC and artificial marble are selected. The laser signals obtained from the targets are classified as live/lifeless by undergoing training in Long-Short Term Memory networks (LSTM) after preprocessing and feature extraction steps. As a result of the study, a live / lifeless assets distinction are made with an accuracy rate of 99.1%.

Keywords: Laser, Laser Signs, Deep Learning, Artificial Intelligence, Live Detection, Target Detection

1. INTRODUCTION

In health institutions or in environments where health care professionals can reach patients, healthcare can be provided to people in some way, but this is not always the case. In the chemical, biological or radioactive attack situations, in the active combat environments, in the fight against terrorism, urban combat operations, earthquakes, floods, and natural disasters such as storms or where the paramedics such as falling from height cannot reach the person, it is very important to reach and intervene as soon as possible. In order to learn about the patient, wired and contact systems are often used [1]–[3]. The use of these techniques becomes impossible for the situations mentioned above.

In addition, the determination of the vitality of the elements on the enemy front line is also important in war environments. In some cases, mannequin and similar materials are used in the elements on the enemy line and if this can be detected remotely, significant gains can be achieved. In such cases, it is important to determine the presence of live / inanimate assets of the target from far distances with laser signals.

In the literature, many studies are conducted on viability detection. Some of these studies focus on radio frequency, while others focus on lasers. In the literature, there are studies on the localization of a person behind the wall with the wall radar and signs of life [4]–[7]. The focus of such studies is to take advantage of the micro-doppler characteristic caused by small vibrations in the body during human breathing. In such systems, a radio

[1] *Corresponding author: Zonguldak Bulent Ecevit University, Department of Computer Technologies, 67800, Devrek/Zonguldak, Turkey, nevzat.olgun@beun.edu.tr*

[2] *Author: Firat University, Department of Software Engineering, 23200, Merkez/Elazig, Turkey, iturkoglu@firat.edu.tr*

frequency signal is sent to the body, and when the signal reaches the body, small displacement information is returned as a phase shift signal due to breathing or heartbeat movement.

Laser beams can travel linearly and focus on a target determined with the help of optical devices. Lasers are divided into 4 classes according to their operating power levels [8]. Class II lasers, called low power lasers, emit visible wavelength (400-700 nm) and have an output power less than 1 mW. Diode lasers are generally used in low power lasers. Diode lasers are small in size and low cost, they can be produced at different output powers and different wavelengths. Because of these advantages, they are frequently used in chemical analysis, remote sensing, medical applications, defense technologies, telecommunications and industry [9].

Very small amounts of mechanical vibrations can be measured with laser interferometers [10]–[14]. With traditional Michelson interferometer-based laser vibration meters, it can measure heartbeats and skin changes during breathing at close range [15]–[17]. Such interferometers require stable optical setup and are not suitable for use outside the laboratory. Laser Doppler Vibrometers (LDV) are laser vibration meters that are widely used in measuring small vibrations and are also commercially available on the market [18]. In a study with LDV, vibrations in the chest wall as a result of beating of the heart were measured and the results were associated with ECG [19]. In another study, the vibrations of the skin surface in the neck are studied depending on the cardiac rate[20], [21]. Qu et al. have worked on the detection of human voice using pan-tilt-zoom (PTZ) camera and LDV. In this study, they focused on the detection of the moving person with the PTZ camera and the orientation of the LDV on the moving person for sound detection with LDV [22].

In the previous study carried out by our team, a single laser light source and receiver system are used to classify different types of lifeless materials at a distance [23].

In this study, when health teams such as earthquakes, floods, storms, war environments and falls from height cannot reach the patient directly, or when it is necessary to determine the viability of elements on the enemy front line in a combat environment, it is necessary to collect information with low power laser signs from the specified target and in the light of the information obtained, It is intended to be classified as life/lifeless. In the classification of Live / Lifeless, human vitality and other materials (non-living) in nature are compared. Within the scope of the study, laser signals are obtained from a certain distance from live and lifeless targets, the obtained signals are classified as live/lifeless by undergoing training in Long-Short Term Memory networks (LSTM) after preprocessing and feature extraction steps and the results are examined.

2. MATERIALS AND METHODS

2.1. Experimental Setup and Data Collection

Laser meter module that emits red light at 1 mW output power and 650 nm wavelength is used in the scope of the study. The firmware of the laser meter module is reprogrammed to take 3000 raw laser mark samples per measurement and transfer them to the computer via the serial port [23]. Different points of the live / lifeless targets in the laboratory environment are pointed with the laser light source on the cartesian robot arm in line with the coordinates coming from the computer program, and the laser signals reflected from the target are detected by the device and transferred to the computer system. The distance between the laser light source and the targets is chosen as 2 meters. In Figure 1, the sensor module consisting of the experimental study setup, laser light source and optical device are shown.

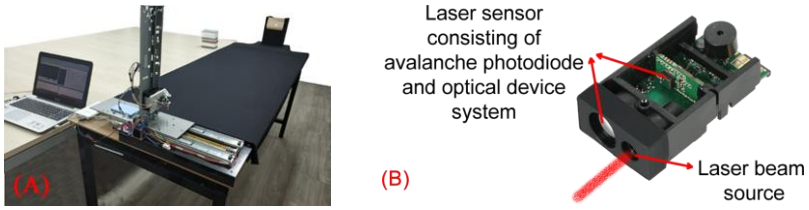

Figure 1. A) Experimental work setup. B) Laser light source and optical system.

In the study conducted during daylight hours, 130 laser signal samples are taken from different points of the arm of 9 volunteer men for live assets, and 69 laser signal samples from different points of 17 materials

frequently used by people for lifeless assets. Aluminum, black fabric, frosted glass, glass, pottery, iron, galvanize, granite, linden, magnet, mdf, marble, cardboard, polyethylene, polystyrene, pvc and artificial marble are selected for lifeless assets. In Figure 2, the visuals of the materials used in the study and the position of living and inanimate beings in the experimental setup are shown. In addition, before each measurement, measurements are made by turning off the laser light to detect white noise caused by the device and daylight. At the end of the data collection process, a total of 1170 laser signals are obtained from the arms of male subjects and a total of 1170 laser signals from lifeless assets.

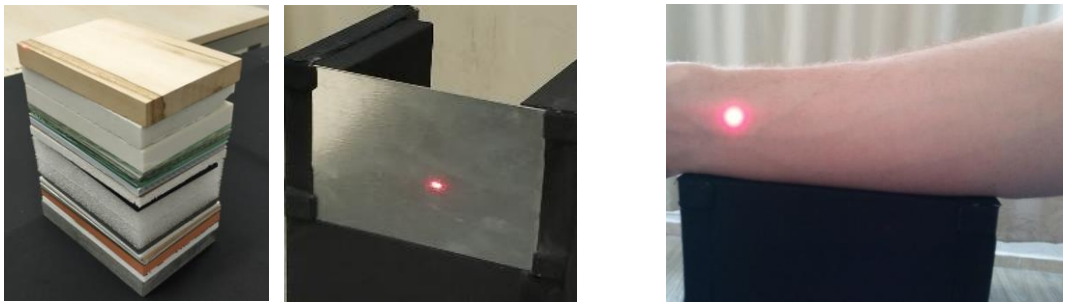

Figure 2. *Images of the materials used in the study and the position of live/lifeless assets in the experimental system.*

2.2. Signal Processing and Deep Learning

The study consists of steps for data collection, signal processing, feature extraction and classification. Figure 3 shows the block diagram of the study.

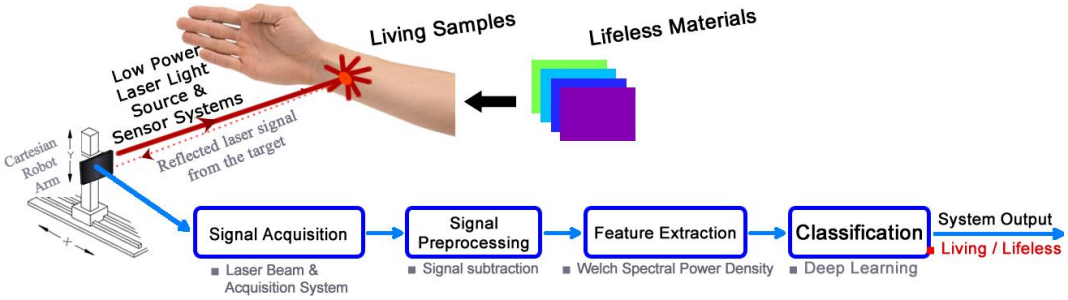

Figure 3. Block diagram of the study

In the preprocessing step of the study, the subtraction process defined in Equation 1 is performed to separate the white noises from the laser signals obtained from live and lifeless assets.

$$x(n) = s(n) - d(n) \quad (1)$$

In Equation 1, $x(n)$ refers to the noise-free laser signal, $x(n)$ refers to the noisy laser signal, and v refers to the white noise. In Figure 4, the raw laser signals of the male subject's arm, aluminum and galvanize are seen, their white noises are seen and the laser signals as a result of the subtraction process are seen.

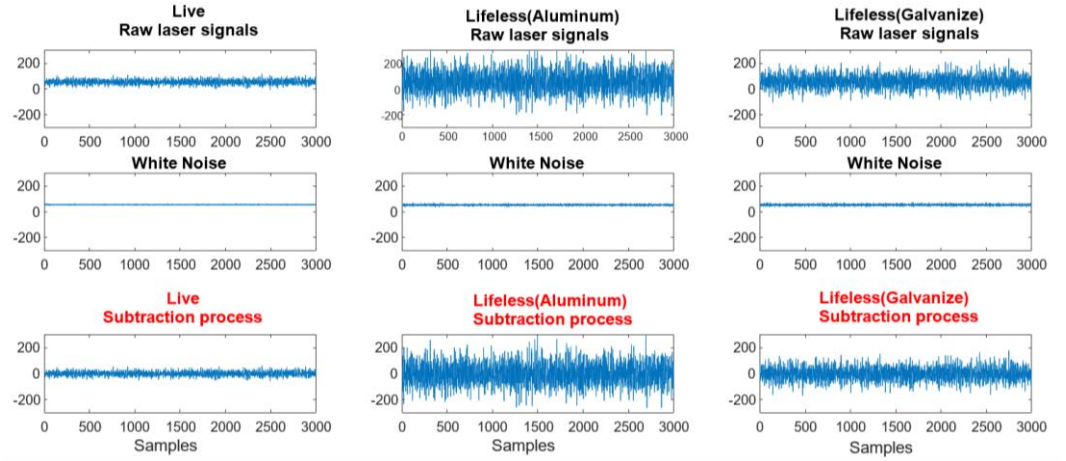

Figure 4. Raw laser signals of live, lifeless(aluminum), lifeless(galvanize) materials, white noises and the laser signals as a result of the subtraction process

The spectral power density is based on the process of estimating the power distribution in the frequency band of the signal. This process is based on the Fourier transform. Welch method is an advanced version of this method [18]. The Welch spectral power density is explained as in Equation 2.

$$P_w = \frac{1}{l}\sum_{i=0}^{l-1} \acute{S}_{xx}^{i}(f) \quad (2)$$

In Equation 2, P_w shows Welch spectral power density, $\acute{S}_{xx}^{i}(f)$ shows the i^{th} improved periodogram of spectral power density, and l shows the length of the signal. In the study, Welch spectral power density is applied to laser signals following subtraction process. Figure 5 shows the laser signals with subtraction process and laser signals with Welch spectral power density applied.

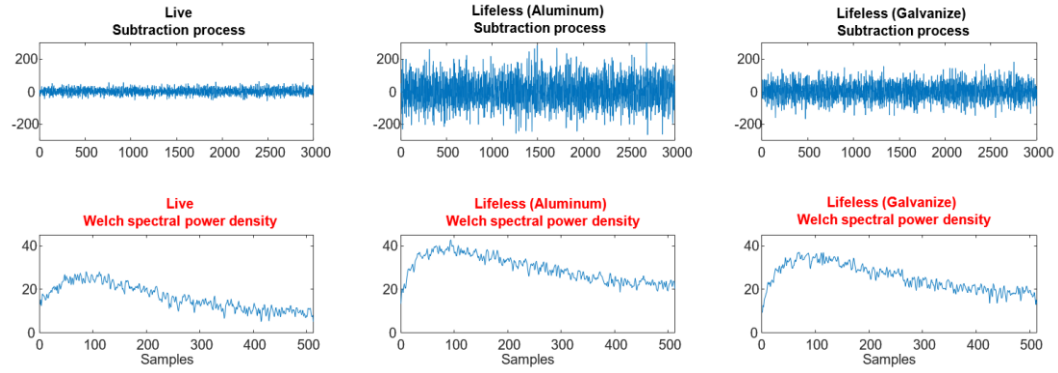

Figure 5. *Preprocessed laser signals for live, lifeless(aluminum), lifeless (galvanize) materials and laser signals with Welch spectral power density applied*

LSTM architecture used in deep learning networks is frequently used in natural language processing, time series and sign processing [24]. Due to its structure, LSTM can establish a relationship between its previous entries and its current entries, and because of this feature, it can produce successful results in signal processing and similar applications.

In the study, a bidirectional LSTM architecture consisting of 100 layers are used to classify laser signals from a total of 2340 live/lifeless assets obtained as a result of signal processing steps. K-fold cross validation is used as a data validation method and the LSTM network is trained by dividing the data set into 10 equal parts. Figure 6 shows the LSTM architecture used in the study.

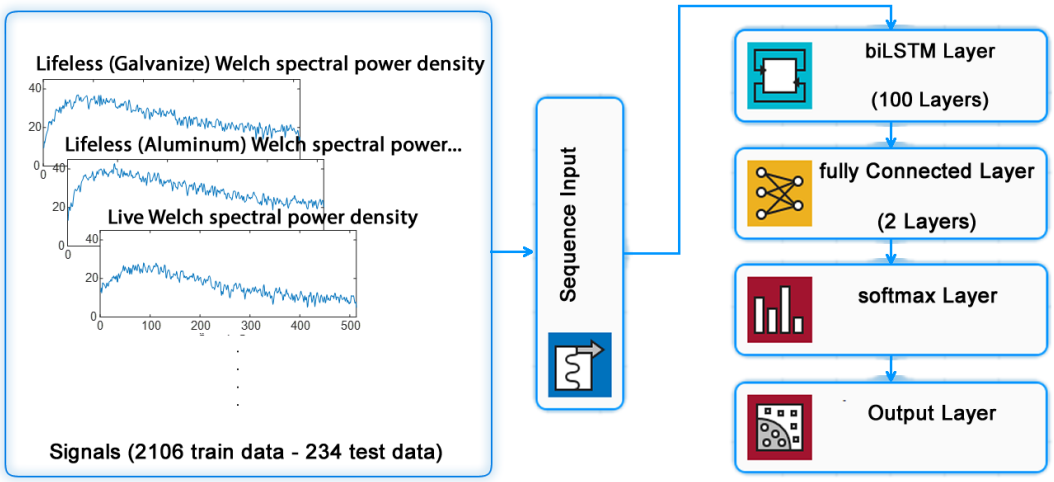

Figure 6. LSTM architecture used in the study

3. RESULTS AND DISCUSSION

In LSTM architecture, which is used for classification of live and lifeless assets, the data set is divided into 10 equal parts, and the remaining data is used for training at a time. After the training of the network, the classification performance in the test data is calculated as the lowest 98.3%, the highest 100% and the average performance is 99.1%. Figure 7 shows the confusion matrix of the highest training and test performance of the LSTM network.

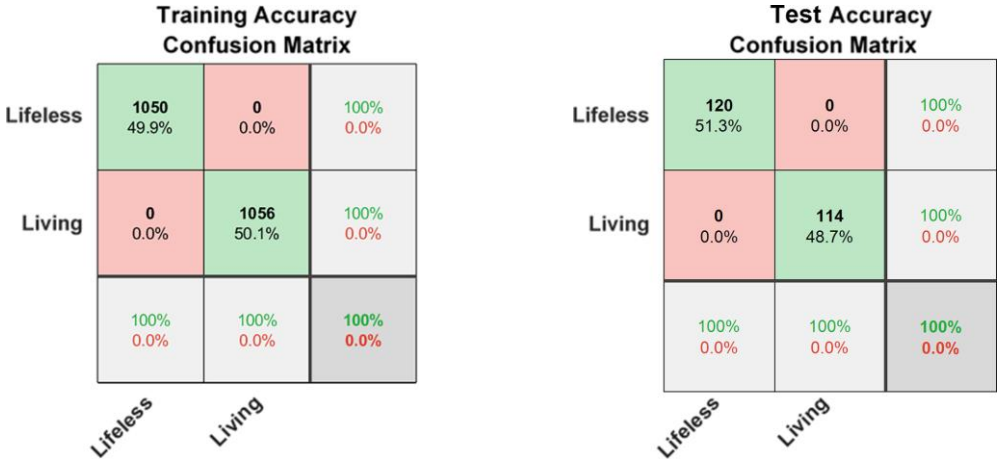

Figure 7. Confusion matrix showing the highest results in the classification performance of live and lifeless assets.

In this study, in cases where medical teams cannot reach the patient directly, such as earthquakes, floods, storms, battle environments and falling from heights, or when it is necessary to determine the viability of elements on the enemy front line in a combat environment, it is aimed to classify the target as live/lifeless with low power laser signals from a certain distance. For this purpose, laser signals are obtained from the arms of the volunteer subjects and 17 materials, the laser signals obtained are passed through the signal processing steps and they are trained and classified using the LSTM architecture used in deep learning networks. With the proposed system, a high performance of 99.1% has been achieved.

In later studies, the classification of the target from more distances and the effect of atmospheric conditions on the performance of the system can be examined.

REFERENCES

[1] D. Ibrahim and K. Buruncuk, "Heart Rate Measurement From The Finger Using A Low- Cost Microcontroller."

[2] J. Parkka, M. Ermes, and M. van Gils, "Automatic feature selection and classification of physical and mental load using data from wearable sensors," in *Proceedings of the 10th IEEE International Conference on Information Technology and Applications in Biomedicine*, 2010, pp. 1–5.

[3] J. L. Garvey, "ECG techniques and technologies," *Emergency Medicine Clinics of North America*, vol. 24, no. 1. pp. 209–225, 2006.

[4] S. B. C. Debnath, "TTW life sign detection by means of CW X-band radar, homeland security and rescue applications," in *2017 USNC-URSI Radio Science Meeting (Joint with AP-S Symposium), USNC-URSI 2017*, 2017, pp. 89–90.

[5] H. Zhang, L. Zhang, Q. Gao, Y. Xiao, H. Hong, and X. Zhu, "Body Movement Cancellation Based on Hybrid Radar-Webcam Sensing System," in *IEEE MTT-S 2019 International Microwave Biomedical Conference, IMBioC 2019 - Proceedings*, 2019.

[6] F. JalaliBidgoli, S. Moghadami, and S. Ardalan, "A Compact Portable Microwave Life-Detection Device for Finding Survivors," *IEEE Embed. Syst. Lett.*, vol. 8, no. 1, pp. 10–13, Mar. 2016.

[7] C. W. Wu and Z. Y. Huang, "Using the phase change of a reflected microwave to detect a human subject behind a barrier," *IEEE Trans. Biomed. Eng.*, vol. 55, no. 1, pp. 267–272, Jan. 2008.

[8] K. Schulmeister and M. Jean, "The risk of retinal injury from Class 2 and visible Class 3R lasers, including medical laser aiming beams," *Med. Laser Appl.*, 2010.

[9] H. Nasim and Y. Jamil, "Diode lasers: From laboratory to industry," *Optics and Laser Technology*, vol. 56. pp. 211–222, 2014.

[10] R. Schnabel, "Squeezed states of light and their applications in laser interferometers," *Physics Reports*, vol. 684. Elsevier B.V., pp. 1–51, 24-Apr-2017.

[11] T. Y. Yu, "Laser-based sensing for assessing and monitoring civil infrastructures," in *Sensor Technologies for Civil Infrastructures*, vol. 1, Elsevier Inc., 2014, pp. 327–356.

[12] P. Lutzmann, B. Gohler, F. van Putten, and C. A. Hill, "Laser vibration sensing: overview and applications," 2011, p. 818602.

[13] P. Lutzmann, B. Gohler, C. A. Hill, and F. van Putten, "Laser vibration sensing at Fraunhofer IOSB: review and applications," *Opt. Eng.*, vol. 56, no. 3, p. 031215, 2016.

[14] Z. Zalevsky *et al.*, "Simultaneous remote extraction of multiple speech sources and heart beats from secondary speckles pattern.," *Opt. Express*, vol. 17, no. 24, pp. 21566–21580, Nov. 2009.

[15] S. Yazdanfar, M. D. Kulkarni, and J. A. Izatt, "High resolution imaging of in vivo cardiac dynamics using color Doppler optical coherence tomography," *Opt. Express*, vol. 1, no. 13, p. 424, Dec. 1997.

[16] I. Cikajlo, S. Šprager, T. Erjavec, and D. Zazula, "Cardiac arrhythmia alarm from optical interferometric signals during resting or sleeping for early intervention," *Biocybern. Biomed. Eng.*, vol. 36, no. 1, pp. 267–275, 2016.

[17] S. Šprager and D. Zazula, "Detection of heartbeat and respiration from optical interferometric signal by using wavelet transform," *Comput. Methods Programs Biomed.*, vol. 111, no. 1, pp. 41–51, Jul. 2013.

[18] "Leader in Optical Measurement Equipment - Polytec." [Online]. Available: https://www.polytec.com/eu/. [Accessed: 06-Feb-2020].

[19] L. Scalise, U. Morbiducci, and M. De Melis, "A laser Doppler approach to cardiac motion monitoring: effects of surface and measurement position," in *SPIE Proceedings*, 2006, vol. 6345, pp. 63450D-63450D–11.

[20] L. Scalise and U. Morbiducci, "Non-contact cardiac monitoring from carotid artery using optical vibrocardiography.," *Med. Eng. Phys.*, vol. 30, no. 4, pp. 490–7, May 2008.

[21] M. De Melis, U. Morbiducci, and L. Scalise, "Identification of cardiac events by Optical Vibrocardiograpy: Comparison with Phonocardiography," in *Annual International Conference of the IEEE Engineering in Medicine and Biology - Proceedings*, 2007.

[22] Yufu Qu, Tao Wang, and Zhigang Zhu, "Remote audio/video acquisition for human signature detection," in *2009 IEEE Computer Society Conference on Computer Vision and Pattern Recognition Workshops*, 2009, pp. 66–71.
[23] N. Olgun and I. Turkoglu, "Lazer Isaretleri ile Otomatik Hedef Tanima," *Sak. Univ. J. Comput. Inf. Sci.*, vol. 1, no. 3, pp. 1–10, 2018.
[24] S. Hochreiter and J. Schmidhuber, "Long short-term memory," *Neural Comput.*, vol. 9, no. 8, pp. 1735–1780, 1997.

The use of Biomaterials in Furniture Design: Towards sustainable ecology

Teja Siva Srinivas Payapalle [1], Ece Ariburun Kirca L.N.[2]

Abstract

Recent proposals on London Design Fair, 2019, and many design awards since 2016 on the International stage have made it clear that our future, sustainable living belongs to bio-based materials inspired by nature. The abundant availability of resources and material studies in exploring and creating alternatives to existing synthetic materials suggest a promising future of sustainable living and environmental protection, which are important initiatives for human survival. This opens up a whole new world, and perspective of looking at materials and nature informed design. The importance of furniture design which provides for the welfare and well-being of individuals as well as society, socially, culturally, and influences the living quality directly has long been advocated based on the idea of human-oriented, human-centric, meets the needs of user form physiology and psychology. This idea of design and manufacturing which has such a huge impact on everyday life should include nature-based along with human-oriented in its premise. This can further help in creating sustainable ecology around us and instead of creating static forms of bio-inspired designs, we could actually be creating bio-informed designs that are more sustainable, biodegradable and have very little impact on the environment. While significant progress and research are being done over the years on a wide array of biomaterials, this idea needs to be widely accepted and implemented at a global scale, so that it does not remain as just another folly of the design world in search of new materials and actually is a significant step towards sustainable development. This paper aims at detailing investigation on the idea of using biomaterials in furniture design, and corresponding manufacturing processes by evaluating case studies based on factors contributing to sustainability and how biomaterials can help in creating sustainable ecology around us.

Keywords: Bioinformed design, Biomaterials, furniture design, human-centric, manufacturing processes, sustainability, Sustainable ecology

1. INTRODUCTION - BIOMATERIALS

" The future of design is a future where anything material in the environment — whether it's wearables, cars, buildings — can be designed with this variation of properties and relationship with the environment that can take part in the natural ecology. Hopefully, it points towards a shift that goes beyond the age of assembly into the age of a new kind of organism"[1].

Our view of Nature has been created for centuries by the dynamic relationship between biology and technology. It has also limited our capacity as designers to integrate external environmental forces with the buildings and products' inherent material behavior. However, while the biological world expresses functionality from the bottom up-through self-organization, cell differentiation, growth, remodeling, and regeneration-the design practice traditionally operates from the top-down, establishing constraints that inform or guide the generation and construction of designs.

A new understanding of the material is rapidly evolving in design. Designers no longer think of the physical world as distinct from the digital environment. Computation is being considered to be the main platform for

[1] *Teja Siva Srinivas Payapalle: Centre for Environmental Planning and Technology University (CEPT), Faculty of Design, 380009, Ahmedabad, Gujarat, India, tejasivasrinivas.pg191054@cept.ac.in*

[2] *Ece Ariburun Kirca L.N. : Istanbul Technical University (ITU), Department of Industrial Design, 34467, Sariyer/Istanbul, Turkey. ariburun@itu.edu.tr*

material discovery and vice versa. It reflects a major perceptional change in which design materiality is no longer seen as a fixed property and passive shape receptor, but is transformed into an active design driver and an adaptive design performance. Materialization is now starting to coexist with design as explorative robotic processes in sharp contrast to previous linear and mechanistic manufacturing types. This reflects a radical break from both the trite modernist focus on 'reality to materials' and the prior generation of digital architects rejecting materials.

Materials that followed the form, structure, and function of furniture were subordinate to design for centuries. Although manufacturing technologies and fabrication methods were improved, materials used in furniture design/ design remain traditionally rigid [2]. Advanced responsive materials offer radical changes in furniture design because of novel properties and functions [3]. Some of these materials have been shown to respond to different stimuli such as light and temperature and undergo structural changes [4]. While a number of material systems were investigated previously in architecture such as shape memory alloy for Blanket [5], most of them are not capable of interfacing with biological matters, since they do not contain water.

2. BIOMANUFACTURING IS THE FUTURE OF MATERIALS

"I think that as a designer nowadays we should not think we are all making the antiques of the future, We should create products that can be part of a circular system, and are designed considering what material goes into the product and what it leaves behind after use."

- Christien Meindertsma,

E. Tucker (2016, November 14) Christien Meindertsma designs a fully biodegradable chair using flax.https://www.dezeen.com/2016/11/14/christien-meindertsma-flax-chair-furniture-design-biodegradable-dutch-design-week-2016-awards/ [6].

The driver of this phenomenon is rapid development in the biomanufacturing market. This new trend in material science allows biobased products to be manufactured from very different raw materials. This involves cells, molecules, or extracellular matrices, some of which are actually extracted from human skin. Production can go far beyond natural materials known for millennia, such as natural textiles, leather, wood, and paper, all of which are derived from plants and animals.

Biomaterial science and cellular biology have been at work for a long time to make biomanufacturing technology widely available. The main field of interest is medicine, where technology is essential in studying and preventing rare diseases.

Furthermore, these technologies provide a valid alternative to synthetic materials that will be used by the biofuels industry to produce sustainable energy in the future. In addition, it's worth remembering that they're also useful in developing agricultural and food products that don't use animal parts or products, necessary given the expansion of veganism.

Figure 1. Biodesigner Jen Keane has developed an interesting "microbial weaving" process by manipulating the growth of k. rhaeticus, a type of bacteria typically found in kombucha tea. The resulting material, a synthetic fiber, is stronger than steel and more resistant than Kevlar © Vita Larvo, Retrieved from: https://www.lifegate.com/biomaterials-design-future [7].

Less in the spotlight is how biomanufacturing technologies are being employed to create biobased design materials with applications in Furniture design and in the overall thinking of what furniture is. We have had comprehensive studies in subjects related to construction, architecture, and industrial design.

3. CASE STUDIES: ONGOING PRACTICES IN FURNITURE DESIGN

All paragraphs must be justified, i.e. both left-justified and right-justified.

3.1. Yamanaka Chair, Designer: Phil Ross

Figure 2. Yamanaka Chair by Phil Ross, Exhibition at Espace Foundation (2012). Retrieved from http://thisisalive.com/yamanaka-furniture/ [8].

In the early 1990s, Phill Ross began growing a series of sculptural artworks using living fungus as a primary material. These artworks were created by infusing live fungal cells into a pulverized cellulose-based medium (sawdust).

The cellulose acts as both the food and the foundation for the organism to grow on, and this aggregate solidifies within a week as a result of the natural inclination of the fungi to tie together smaller parts of its tissue into a larger whole. The fungal tissue binds, solidifies and hardens into any form chosen, and becomes a lightweight, strong material once dried and processed. With this process, he can create simple modular bricks to build a shelter (see project 'Mycotecture'), or, as presented here, a range of chairs and tools.

Figure 3. Showing Stages of mycelium on cellulose and development of fungi, Exhibition at Espace Foundation. Retrieved from http://thisisalive.com/yamanaka-furniture/ (2012) [8].

The furniture is constructed of wooden frames, with glue and bolts fixed to the mycelium frame. Citrus oil and other essential oils sanitize and protect the surface while removing much of the odor.

3.2. Zostera Stool, Designer: Carolin Pertsch

Eelgrass is a type of seagrass that frequently washes up on beaches in the North Sea. Governments tend to clean the beaches and throw away the material, as they form unsightly brown carpets that are bad for tourism. Every year, thousands of tons are removed from German beaches alone and brought to landfills as special waste. However, German designer Carolin Pertsch does not consider eelgrass to be waste. Alternatively, she uses the material to build seats for stools, called the Zostera Stool.

Pertsch wanted to explore the material 's potential and began a series of experiments. Finally, with the help of a bio-resin made mainly from vegetable oil she developed a new biomaterial, which is a fiber-reinforced eco-plastic. This eco-making material is used for the development of a round seat for a simple stool, named after the Latin Zostera marina for the eelgrass. In Pertsch 's opinion, there is no better way of confronting people with new materials than through furniture, because the interaction between people and objects is always necessary. The design of the stool emphasizes the appearance of the material and its functionality with its minimalism.

Figure 4. Zostera Stool, and close up of the eelgrass, resin seating material. Carolin Pertsch (2017, January 27). Zostera Stool: Sitting on washed-up seagrass.Retrieved from https://materialdistrict.com/article/zostera-stool-sitting-washed-up-seagrass/ [9].

The eco-material is lightweight and stable at the same time and brings out the natural aesthetics of the eelgrass. The texture of the finished product feels very much like cork and still shows the embedded strands of eelgrass.

Figure 5. Zostera Stool, Figure showing seating material thickness 1cm. Carolin Pertsch (2017, January 27). Zostera Stool: Sitting on washed-up seagrass. Retrieved from https://materialdistrict.com/article/zostera-stool-sitting-washed-up-seagrass/ [9].

Pertsch has designed three four-legged stools for the range, each of which features a subtly different shade of material. The different shading is possible by sorting the different shades of the seagrass. The material is very stable, which is proven by the only one-centimeter thick seat.

3.3. Potato Stool, Designer: Jarrell Goh, FDA 2016 Finalist Entry

Figure 6. Potato Stool, FDA 2016, Finalist Entry
https://www.facebook.com/SingaPlural/photos/a.620365121436059.1073741903.172127376259838/620365241436047 [10].

Apart from making an eco-material, the project's aim was to show people new and creative ways for potential materials. This project imagined an unusual and creative way of using perishable waste material. Starchy vegetables were blended, dehydrated, and used as the casting material, for example, potatoes. The dry aggregate was bonded with flour glue, allowed to dry, then finished with a homemade sealant based on milk. A much more hard, durable, and robust material was the outcome that proved more than a point or two, Biomaterial but manufactured at home and is accessible by everyone.

3.4. Flax Chair 2015, Designer: Christien Meindertsma, Commissioned By: Label/Breed, Special Credits: Stijn Roodnat, Havivank, Cato

Figure 7. Flax chair Imagery. Retrieved from, Emma Tucker (2016, November 14)
Christien Meindertsma designs fully biodegradable chair using flax. Retrieved from https://www.dezeen.com/2016/11/14/christien-meindertsma-flax-chair-furniture-design-biodegradable-dutch-design-week-2016-awards/ [6].

Christien Meindertsma's Flax chair has won two Dutch Design Awards for its innovative use of flax fiber.

The Flax chair was a collaborative project launched by Label / Breed with natural fiber specialist Enkev. The new composite material was created using four layers of an existing woven flax textile and five layers of a newly developed dry-needle felted flax. The woven linen and textile PLA (a biodegradable plastic) use long

flax fibers and are therefore extremely solid, while the felt material provides bulk and texture. The soft pile of fabrics is heat-pressed and the flax and PLA are melted into a rigid chair.

Figure 8. Flax chair Imagery. Retrieved from, https://christienmeindertsma.com/Flax-Chair [6].

Meindertsma's ambition was to make a locally made product affordable, scalable, environmentally friendly while exploring new production processes. The chair is made from a sheet of 60 x 100 cm, with very little waste. The outcome is completely biodegradable due to its materiality. The chair is in the collection of the Vitra Design Museum, National Gallery of Victoria, and Boijmans van Beuningen.

3.5. Beleaf Chair 2017, Designer: Šimon Kern

The Beleaf chair of Slovak designer Šimon Kern is made from a mixture of recycled/fallen leaves which would otherwise be taken as waste and bio-resin to bind them together. The prototype chair, made while Kern was studying at the University of Jan Evangelista Purkyně, in Ústí nad Labem, is designed to make the most of natural waste. The seat lies on a framework of tubular steel – designed to last for hundreds of years – and is made of a combination of leaves and bio-resin extracted from the remaining cooking oil. The material is pressed into a mould and sanded and fastened to the frame once it is set.

"I wanted to use a strong structure to work as a 'trunk and branches for leaves, There are also a lot of curves in the frame, so I decided that tubular steel had the best mechanical features for my purpose. If it gets damaged we just put it under the tree, where it disappears into the soil and fertilizes a tree, Then we pick the fallen leaves once again, and make a new seat."

- Kern, Emma Tucker (2017, February 26), Šimon Kern makes chair from recycled fallen leaves. Retrieved from

https://www.dezeen.com/2017/02/26/simon-kern-design-chair-recycled-fallen-leaves-bioplastic-chair-furniture/ [11].

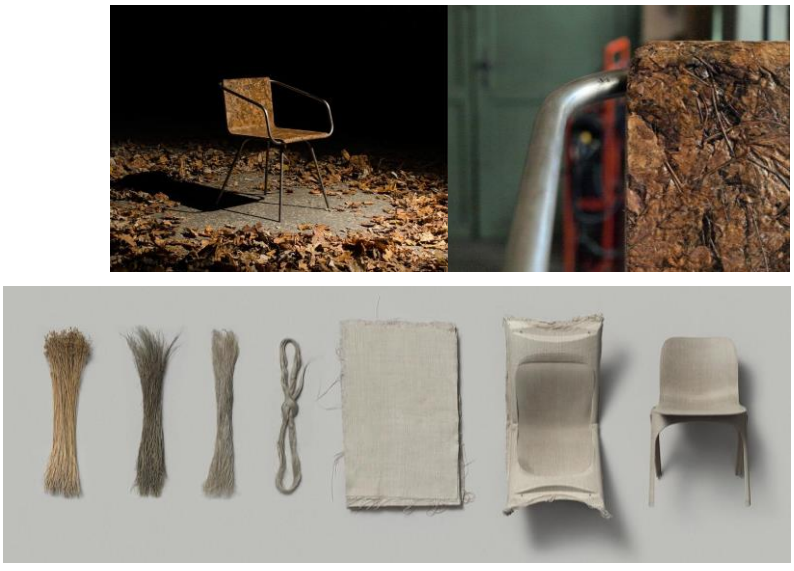

Figure 9. Beleaf Chair, Imagery, Emma Tucker (2017, February 26)
Šimon Kern makes chair from recycled fallen leaves. Retrieved from
https://www.dezeen.com/2017/02/26/simon-kern-design-chair-recycled-fallen-leaves-bioplastic-chair-furniture/
[11].

Kern is still perfecting the process, designing more ergonomic and biodegradable versions of the seat. He also plans to experiment with using the leaf material for lighting. Another biodegradable furniture has been made

using everything from flax fibers, a combination of seaweed and paper, and hand-woven yarn from seaweed fibers.

Figure 10. Process of pressing dried leaves with resin into the mould. Retrieved from, http://simonkern.sk/object/beleaf-chair-16.html [12].

4. ANALYSIS - RESULTS AND DISCUSSION

There are interesting outcomes from the study of the above-mentioned case studies.

4.1. Yamanaka Chair

Mycelium and fungi have been the starting point for the interest and research in biomaterials. But an in-depth study as part of furniture design would let us know more about the design as a whole and not just the materiality aspect.

Pros: Edible, Completely Biodegradable, No much energy involved in the manufacturing process. It can be homemade and involves less labor, the Harmonious process of using nature for production. Designs and moulds can be changed as the degradation time is approaching hence making up a cycle, comparatively easier process to be thought for mass manufacturing and a lot of companies are looking forward to this kind of biomaterial and manufacturing already.

Cons: However, the design does not make up for the comfort, ergonomics and the purpose to be solved. Degradation of the material is also faster, and cannot be used as outdoor furniture due to the effect of moisture and harsh sun on the material. It definitely does not look pleasing aesthetically to appeal over the existing range of furniture. Some reviews also suggest that it is overpriced as of now.

4.2. Zostera Stool

Designing from wastes that go to landfills and is also abundant in nature is a plus point that would make way for the production.

Pros: Biodegradable, No much energy involved in the manufacturing process. The lab is needed and can be manufactured under supervision. The intent is on the design of furniture and its reach ergonomically to people. Colour shades are available for now only in earthy brown tones which is a direct result of the shades of grass available. It can be used outdoors. The thickness of 1cm to bear the weight is showing a lot of promise.

Cons: Still it is only the seat which has been achieved and not a system of interaction with the furniture, More like an experiment of the material prototype phase. Legs and the definition of seating which can be changed through mycelium is a lack in the current alternative. The design of stool in itself is very similar to existing market varieties. Attempt to replace rather than to inform the design.

4.3. Potato Stool

This is an interesting case study as it is completely manufactured at home by a student with no meticulous effort.

Pros: Biodegradable, No much energy involved in the manufacturing process. Everything needed is done at home. The model to manufacture is like Ingredients for a recipe. The ease of availability of products and effort makes the material and the process available to the public. Avoids extra costs incurred and promotes design at home by the individual.

Cons: Similar to the Zostera stool, here also wooden legs are attached to the seating element. The system is broken into sub-components. Apart from this, no major cons can be observed. Since it was experimental and it was for a competition, no further improvisations have been seen to talk further.

4.4. Flax Chair 2015

Pros: By far the most promising method of manufacturing that many other designers have also adopted. Since Flax is combined with PLA 3d printing of components is also a possible method that can be adopted. It started as an experiment and showcased at museums. Made completely out of one material which is completely biodegradable.

Cons: The definition and language of seating still remain the same, the chair is still in the same language perhaps because of the emphasis on the material and experimentation to develop material more than the design that is being impacted.

4.5. Beleaf Chair 2017

Not many would have thought of such ideas of using fallen leaves. Another prototype from a student that is being tested for betterment.

Pros: Abundance of material, accessibility to the public, Ease of production, Replaceability and can be disposed of as manure to the tree when it is weathered. Mass manufacturing possibilities.

Cons: Steel frame and seating element, Crude in terms of thought though it is effective. Durability is a concern as one would not be replacing furniture often. Needs more thought into making a system of furniture.

5. CONCLUSIONS

Biomanufacturing 's benefit is undeniable: it provides a growing amount of viable alternatives to an industry accustomed to using synthetic content. As things stand, because of their environmental impact, the latter has no future so they need to be revisited and replaced. In addition, the interest of the designers and companies in biomaterials also offers positive signals from a qualitative perspective.

History, however, teaches us to be cautious. Inadequate for industrial production, synthetic materials were developed as an alternative to natural materials. Today, in a world where nature provides the alternatives, we can not ignore the fact that if these types of materials take hold on a much larger scale, nobody knows exactly what will happen.

Material cultivation requires us, at least, to question whether a mass transition to biobased products will really not only allow industry and society to restore but, most importantly, preserve a new environmental balance that can meet future requirements.

Biomanufacturing is not necessarily helping increating a bioinformed design world around us. Sustainable ecology can only be created with caution and more experiments. It can be said that the thought of the use of materials changing the ecological values and design definitions has to be really thought upon from bottom to top approach and taken forward with utmost care. Replacing is not a permanent solution and so we are still in a phase of work in progress.

Development of ideas and the thoughts of using Biomaterials and alternative materials have to be inculcated from the student level so that the next generation is not afraid to nurture, experiment, and play with the materials they create.

ACKNOWLEDGMENT

I am very grateful to Instr. Dr. L.N. Ece Ariburun Kirca, whose support and encouragement led to this study and has helped me throughout to pursue my field of interest.

REFERENCES

[1]. N. Oxman, Age of Entanglement. Journal of Design and Science. https://doi.org/10.21428/7e0583ad, 2016
[2]. B. Konarzewska, 'Smart materials in architecture: Useful tools with practical applications or fascinating inventions for experimental design?', IOP Conference: Materials Science and Engineering, 2017
[3]. A. Aksamija, Integrating Innovation in Architecture: Design, Methods, and Technology for Progressive Practice and Research, John Wiley and Sons Ltd, 1998.
[4]. A. Ritter, Smart materials in architecture, interior architecture and design, Birkhauser, 2007
[5]. CK. Khoo, 'Sensory morphing skins', Proceedings of eCAADe, 2012
[6]. E. Tucker (2016, November 14), Christien Meindertsma designs fully biodegradable chair using flax. Retrieved from https://www.dezeen.com/2016/11/14/christien-meindertsma-flax-chair-furniture-design-biodegradable-dutch-design-week-2016-awards/
[7]. F. Doveil, (2020, April 6). The future belongs to biomaterials. How designers are taking up the challenge. Retrieved from https://www.lifegate.com/biomaterials-design-future (2012)
[8]. (2012) This is alive website. [online], http://thisisalive.com/yamanaka-furniture/
[9]. C. Pertsch (2017, January 27). Material District website. [online], Zostera Stool: Sitting on washed-up seagrass,
[10]. Retrieved from https://materialdistrict.com/article/zostera-stool-sitting-washed-up-seagrass/
[11]. Potato Stool, FDA 2016, Finalist Entry https://www.facebook.com/SingaPlural/photos/a.620365121436059.1073741903.172127376259838/620365241436047
[12]. E. Tucker, (2017, February 26), Šimon Kern makes chair from recycled fallen leaves. Retrieved from https://www.dezeen.com/2017/02/26/simon-kern-design-chair-recycled-fallen-leaves-bioplastic-chair-furniture/
[13]. Simonkern website. [online], http://simonkern.sk/object/beleaf-chair-16.html

BIOGRAPHY

Teja Siva Srinivas Payapalle is currently pursuing his Masters at CEPT, Ahmedabad in International Masters in Interior Architectural Design under Faculty of Design. He has done his bachelors in Architecture from SPA, New Delhi. He is interested in future materials, sustainability and emergent technologies.

Ece Ariburun Kirca L.N, is a doctor and researcher at Istanbul Technical University, she is a Professor in Industrial Products in the Architecture Department. She is interested in studying design culture and the transition from traditional to future.

Micro-Structure Analysis of Ball Stud Fracture Surface with SEM and EDS Methods

Fatih Selman Eren[1], Engin Yildirim[2]

Abstract

Ball joint is the one of the main component of the suspension and steering systems of the vehicles. This component is responsible to connect two vehicle modules – control arm and steering knuckle – allowing rotation and oscillation movements in both suspension and steering systems of the vehicles. Ball joints have critical function in both systems and defined as a safety part. These components are exposed to different kind of loads during ride. That is why each sub-component of the ball joint must be durable enough. Unfortunately, the ball stud component of the ball joint has broken from the neck area – which is the narrowest spot – while riding and caused customer complaints. In this study, the reasons for fracture are investigated and chemical composition, micro-structure of fracture surface are also investigated with SEM (Scanning Electron Microscope) and EDS (Energy Dispersive X-Ray Spectroscopy) methods. After interpreting the analysis results, it has been seen that fracture caused because of fatigue.

Keywords: Ball Joint, Micro-Structure, SEM, EDS, Steering and Suspension

1. INTRODUCTION

Suspension ball joints are used to connect the control arms to the knuckle since they are the only joints which let rotational freedom. Ball joint is the one of the main component of the suspension and steering systems of the vehicles. This component is responsible to connect two vehicle modules allowing rotation and oscillation movements in both suspension and steering systems of the vehicles. Ball joints have critical function in both systems and defined as a safety part. These components are exposed to different kind of loads during ride and it has to be sure that the component is safe enough.

Figure 1 shows an assembly of ball joint in front suspension system. Suspension system consist of control arm, control arm bushing, steering knuckle and ball joint.

[1] *Corresponding author: Teknorot Automotive Product Industry, Research-Development Center, Duzce –Turkey.*
fatihselman.eren@teknorot.com

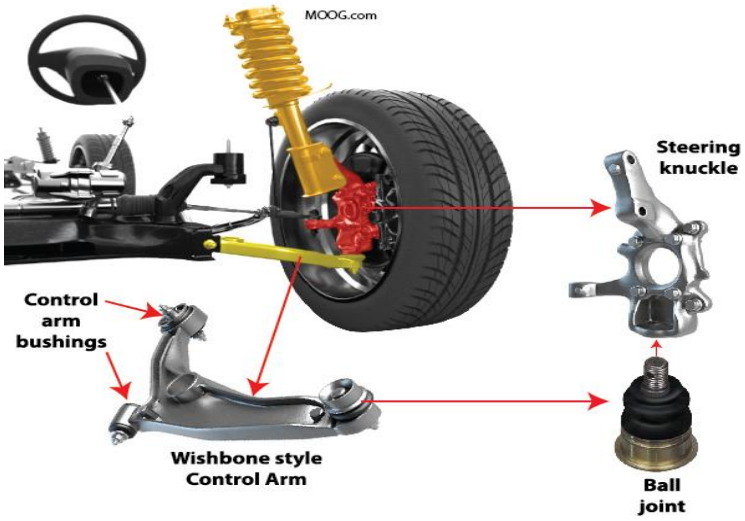

Figure 1. An assembly of ball joint in front suspension system

Ball joints consist various elements that their responsibilities, geometrical shapes and materials are different. The ball joints, one of the main components; ball stud provide a mechanical connection between the housing and with castle nut and cotter pin. The ball stud is subject to the highest forces in the ball joint.

Figure 2. Ball Stud Geometries

2. MACRO ANALYSIS

The damage surfaces of the broken ball stud part are given in Figure 3. It is clear from the pictures that the failure is typical fatigue failure. The presence of the line extending in the east-west direction in the middle of the fractured surfaces indicates that the piece was broken by working under bending loads. The fact that this line is not symmetrical indicates that the bending loads are more dominant in one direction. The part was broken due to fatigue as a result of vibration bending. The middle line is the final fracture zone and has a rough fracture surface. The crack started at two marked points on the upper part of the fracture surfaces. Due to the progress of the crack with time, the fracture surfaces both rubbed against each other during operation and partially mechanically damaged after rupture.

Figure 3. Broken surfaces of ball stud part. Typical bending fatigue failure image.

3. MICROSCOPIC ANALYSIS

3.1. Optical Microscope Analysis

The optical microscope image of the piece is given in Figure 4 and the microstructure of the piece is tempered martensite.

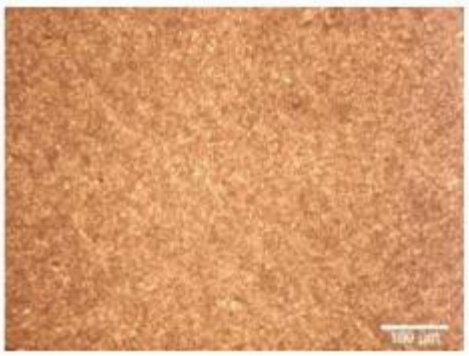

Figure 4. Optical micrography of the broken ball stud. 3% Nital. The structure is tempered martensite.

3.2. Scanning Electron Microscope Analysis

Broken Surface Adjacent to Mill Part

Scanning electron microscope (SEM) images of the fractured surface of the mill part of the ball stud are given in Figure 5. The image shows fracture surfaces starting from the south of the surface to the north.

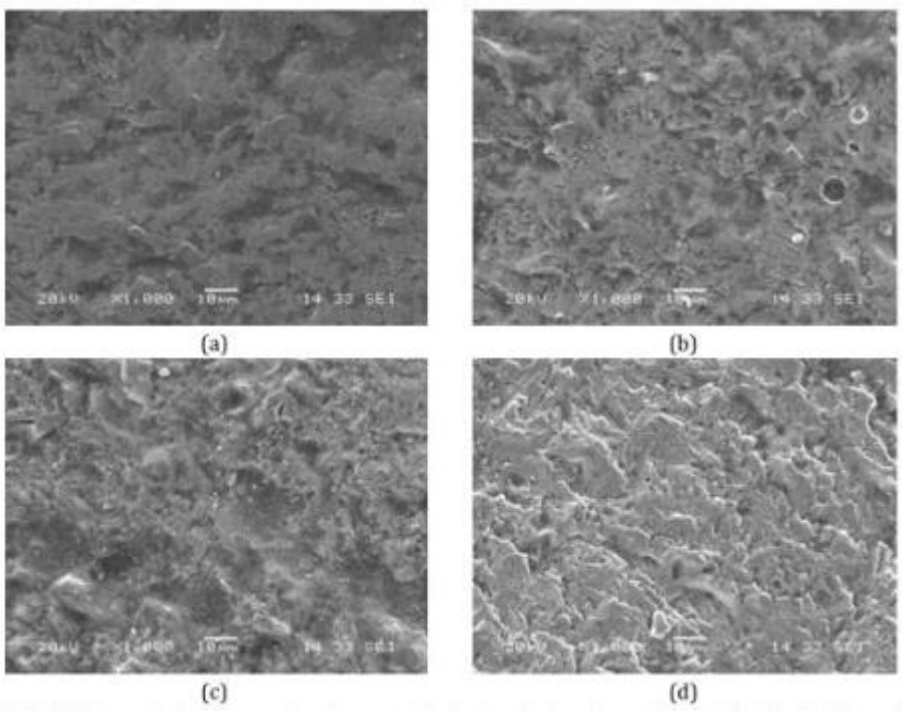

Figure 5. SEM images taken from the fracture surface of the ball stud close to the mill. (a) - (c) south zone, (d) - (e) midline (final break line), (f) - (h) north zone.

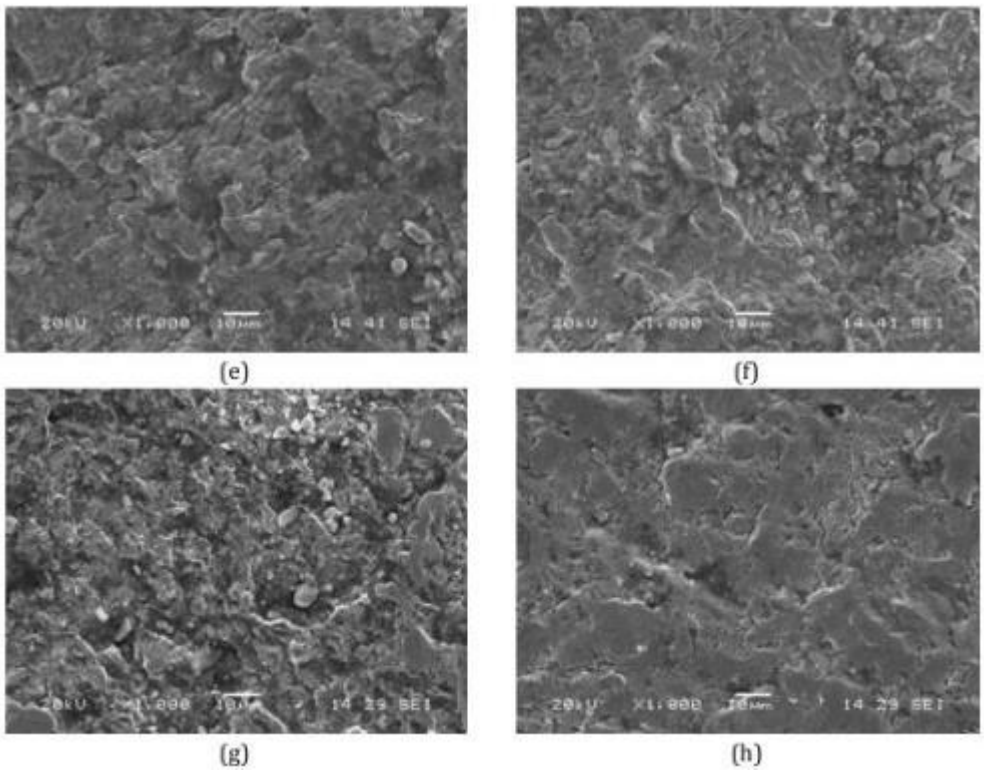

Figure 5 (continued). SEM images taken from the fracture surface of the ball stud close to the mill. (a) - (c) south zone, (d) - (e) midline (final break line), (f) - (h) north zone.

SEM images of fatigue lines on the fracture surface are given in Figure 6, and SEM images of discontinuities on the outer wall are given in Figure 7.

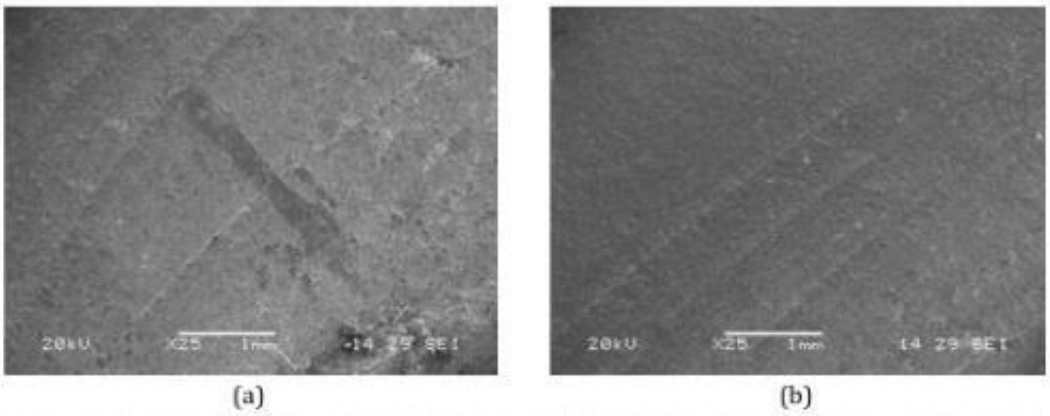

Figure 6. Fatigue lines on the fracture surface.

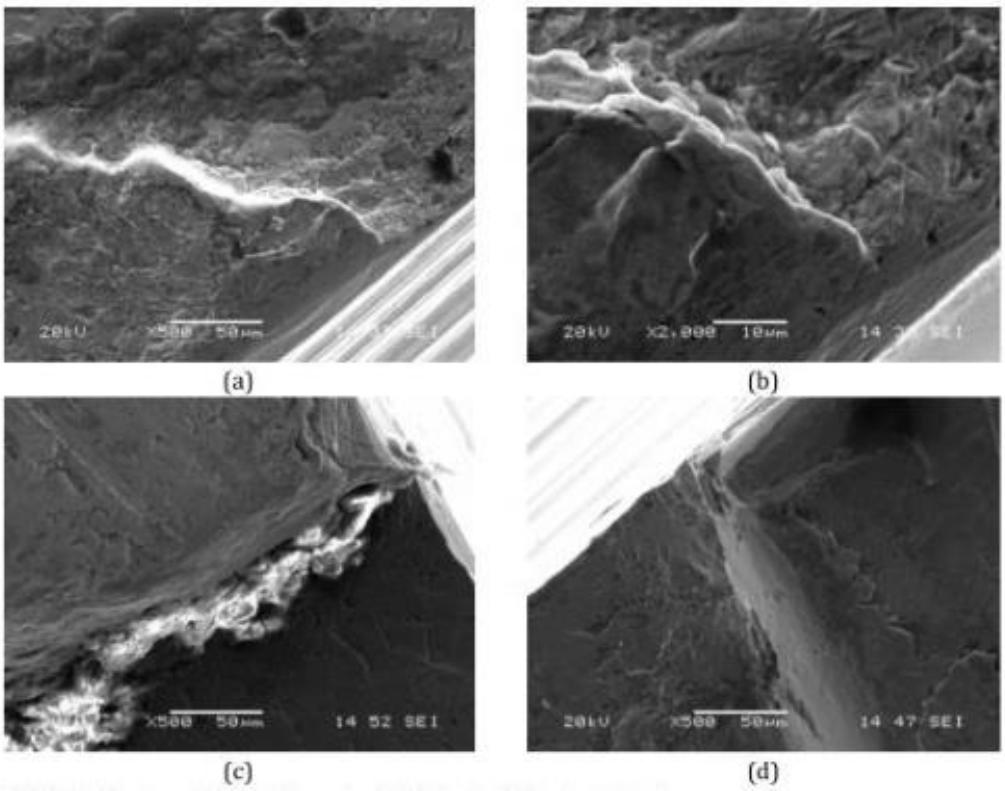

Figure 7. SEM image of discontinuities seen on fracture surface

Opposite Surface (Adjacent to Sphere Section)

Scanning electron microscope analysis of the fracture surface of the sphere section of the part are shown in Figure 8.

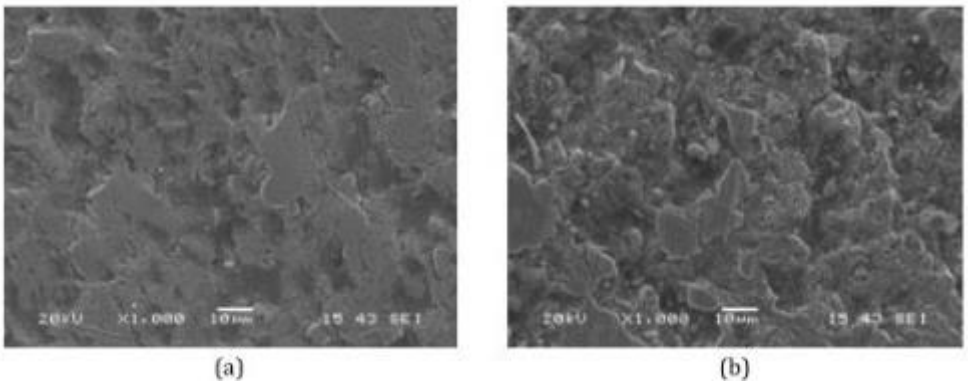

Figure 8. SEM images of the fracture surface adjacent to the sphere part of the ball stud. Mutual friction effect (pictures a, b and e) and some particles (c, d pictures) are seen in some parts of the fracture surfaces.

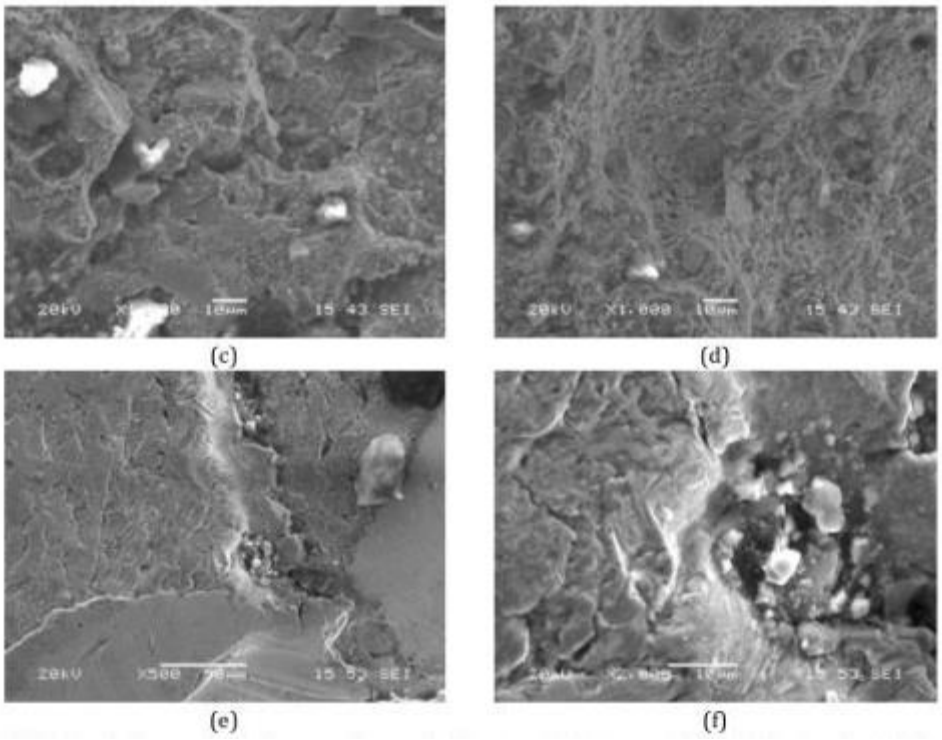

Figure 8 (continued). SEM images of the fracture surface adjacent to the sphere part of the ball stud. Mutual friction effect (pictures a, b and e) and some particles (c, d pictures) are seen in some parts of the fracture surfaces.

Polished Surface

SEM images of the polished and etched surface taken from the side surface of the broken ball stud part are given in Figure 9.

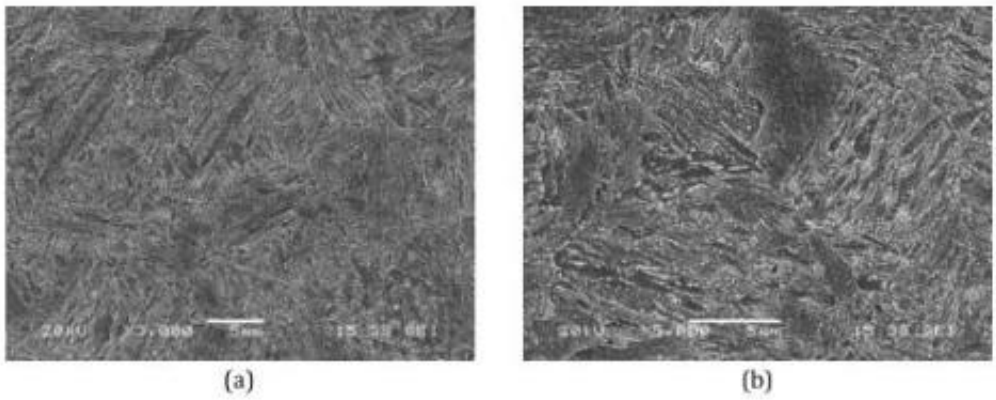

Figure 9. Polished and etched surface SEM images. The structure is typically tempered martensite. There is no obvious material defect.

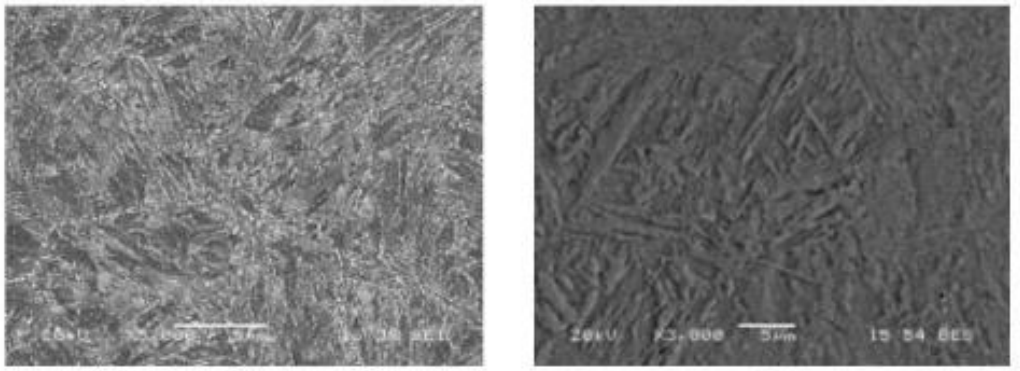

Figure 9 (continued). Polished and etched surface SEM images. The structure is typically tempered martensite. There is no obvious material defect.

3.3. Ball Stud Fracture Surface - SEM EDS Analysis

The results of SEM-EDS that performed in areas with critical fracture surfaces are given in Figure 10-14.

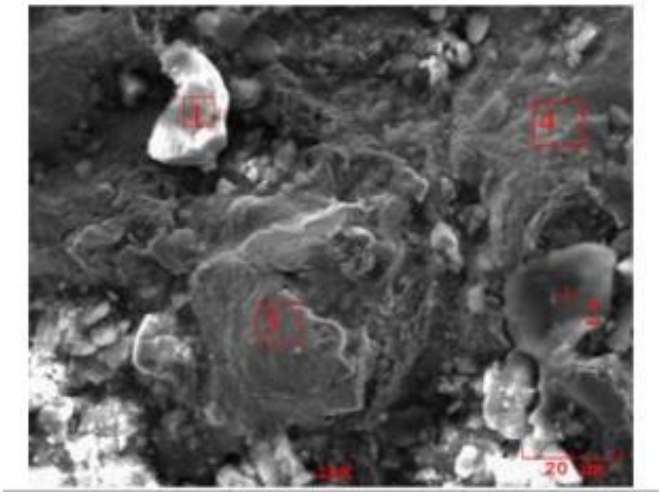

Bölge	C	O	Na	Mg	Al	Si	K	Ti	Ca	Mn	Fe
1		37,44	5,34		14,79	36,58			4,04		1,81
2		39,98		2,36	16,65	27,74	8,41	0,36			4,50
3	3,20	3,84								0,44	91,84
4	9,19	8,85			1,34	1,57			1,05	0,41	76,79

Figure 10. SEM-EDS analysis taken from the last fracture zone of the fracture surface close to the body. Al, Si and O are seen in the analysis of regions 1 and 2. It could possibly be aluminum silicate (complex oxide-silicate). Analyzes 3 and 4 contain Fe and O and are likely to be iron oxides.

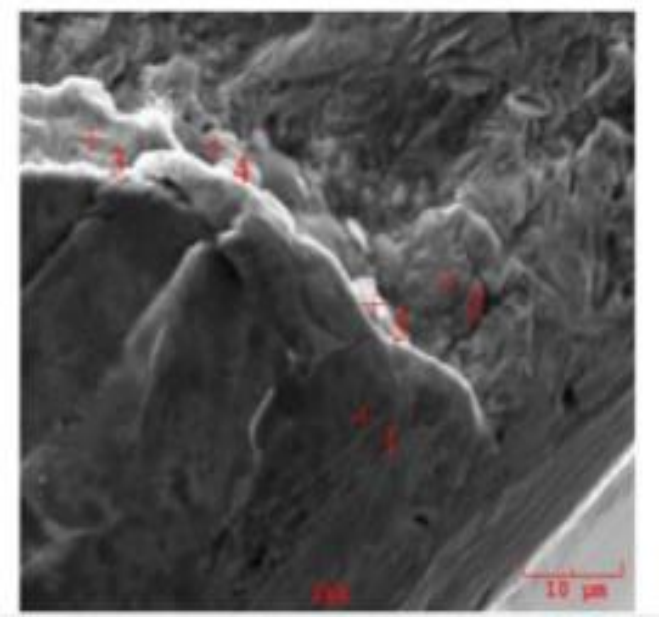

Bölge	C	O	Na	Mg	Al	Si	P	S	Ca	Cr	Mn	Fe
1	16,34	0,17								0,60	0,60	82,29
2	9,74	1,65								0,58	0,28	87,75
3	17,79	8,13								0,56	0,19	73,33
4	18,78	20,66			2,39				3,99	0,85	0,00	53,33
5	18,55	10,69				1,61			0,33	0,57	0,22	68,04

Figure 11. SEM-EDS analysis results taken from discontinuity points on the surface. The lower right part of the image (where the magnifying bar is) is the machined surface. Analysis numbered 1 and 2 were taken from regions at different heights, analyzes numbered 3, 4 and 5 were taken from the slope (side surface). Analyzes 1 and 2 mainly refer to the material of the ball stud piece (carbon remained after surface cleaning). Iron oxide is seen in the analyzes numbered 3, 4 and 5.

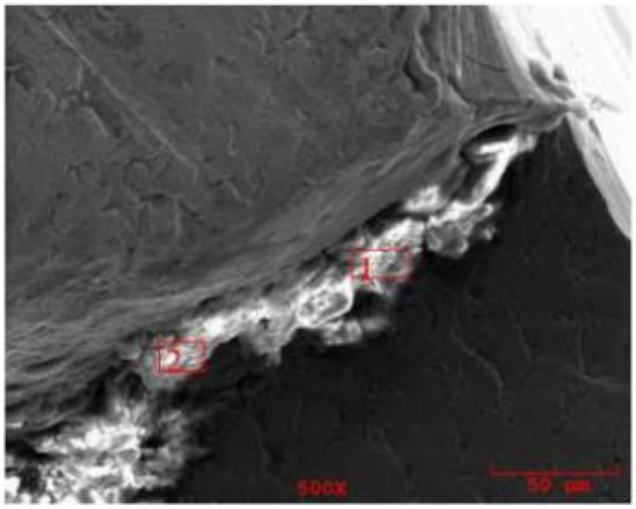

Bölge	C	O	Na	Mg	Al	Si	K	Ti	Ca	Cr	Mn	Fe
1	11,63	38,29			1,25	0,99		21,78	17,43	0,00	0,66	7,96
2	15,14	38,45		0,81	3,46	13,31	1,33		14,76	0,37	0,27	12,09

Figure 12. SEM-EDS analyzes taken from the other point of discontinuity. Analyzes 1 and 2 are taken from the slope regions and show that mixed oxides are present.

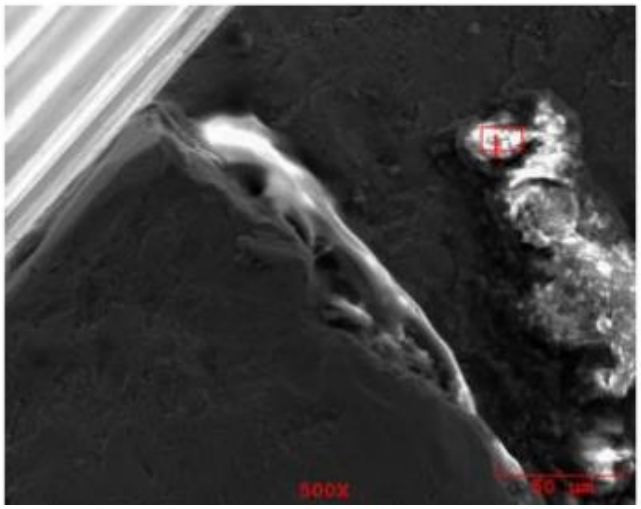

Bölge	C	O	Na	Mg	Al	Si	S	Cl	K	Ca	Cr	Mn	Fe
1	19,00	47,00	1,58	0,90	3,35	6,61	0,80	0,83	1,13	8,39	0,19	0,26	9,96

Figure 13. SEM-EDS analysis. Mixed oxides are present at the point of analysis.

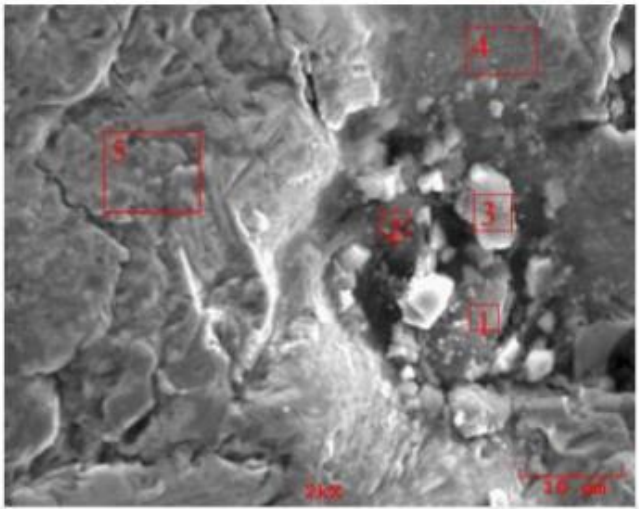

Bölge	C	O	Na	Mg	Al	Si	P	S	Ca	Cr	Mn	Fe
1	8,96	39,73	6,64		9,76	28,20			2,19	0,19	0,07	4,26
2	25,92	26,36	1,71	1,01	1,49	3,86	0,70	0,84	4,19	0,54	0,27	33,09
3	15,63	34,99				2,17			0,95	0,16	0,26	45,85
4	2,08	4,25								0,96	0,65	92,07
5		0,84								0,96	0,62	97,59

Figure 14. EDS analyzes taken from the fracture surface of the ball stud close to the sphere region. Analysis numbers 1, 2 and 3 indicate complex oxides. Analysis number 5 reflects the matrix of the steel. There is chrome in the material.

The hardness of the ball stud was 332 HV from the part close to the fracture surface.

4. CONCLUSIONS

1. The damage occurred in the form of fatigue with vibration bending. The fatigue lines are clearly visible. It is a definite fatigue damage.
2. The line seen in the middle of the fracture surface is the final fracture zone and has a rough fracture surface.
3. The part (near spherical cross section) is heat treated and has a tempered martensite structure.
4. Hardness measured as 332 HV.
5. No obvious material defects were found in cross-sectional inspection.
6. The broken surface diameter of the damaged part is about 13 mm
7. There are some discontinuities at the edges of the fracture surface. In these discontinuities, elements such as Al, Si, Ca along with O and Fe are also present (Figure 11-12). The presence of these elements (oxides) shows why the crack starts from discontinuities.
8. The damage to the ball stud was caused by fatigue cracks that started in discontinuities containing some oxides and silicates. The fact that the fatigue lines cover a large area indicates that the applied stress on the part is low.

ACKNOWLEDGMENT

This study was supported by Teknorot Automotive A.S R&D Center. We thank our colleagues from R&D Center who provided insight and expertise of this paper. Also, we appreciate to Prof. Dr. Sakin ZEYTIN, R&D Director

Mr. Murat ARSLANOGLU, R&D Manager Mr. Gokhan AKGUL, R&D Project Manager Mr. Fatih CAGIRANKAYA for their technical support.

REFERENCES

[1]. S. Swapp, Scanning Electron Microscope (SEM), University of Wyoming
[2]. https://en.wikipedia.org/wiki/Energy-dispersive_X-ray_spectroscopy
[3]. https://en.wikipedia.org/wiki/Scanning_electron_microscope
[4]. A. Rutci, F.S. Eren, Investigation of Suspension Ball Joint Pull Out Force Based on FEA Method and Experimental Study. 6th International Symposium on Innovative Technologies in Engineering and Science, 2018.
[5]. A. Rutci, F.S. Eren, Response Surface Method for Optimization of Suspension Ball Joint Pull Out Force by Using Ansys, III. International Conference on Engineering Technology and Innovation, 2019.
[6]. Prof. Dr. A. H. Demirci, Muhendislik Malzemeleri, Endustriyel Malzemeler ve Isil Islemleri, 2004
[7]. Teknorot Automotive R&D Center Design Guide

Cerebral Palsy Treatment Assistant

Seda Postalcioglu[1]***, Ilayda Ilter***[2]***, Zeynep Kocaturk***[3]

Abstract

Cerebral Palsy is a neurological disease. People with this disease have difficulty in doing daily movements such as walking, speaking, and comprehension. This neurological disease is tried to be treated with rehabilitation techniques. In this study, an exercise game is designed for cerebral palsy patients. The aim is to develop a system in which children with cerebral palsy can perform daily exercises that they need amused and the treatment can be followed. The kinect sensor is used to detect the position in the study, the Unity 3D game engine is used to feedback the accuracy of the movement. In the designed system, the avatar and the patient's exercise are matched. The game avatar verbally informs the patient whether he/she is doing it correctly or not. Scoring is done according to whether the move is made right or wrong. Thus, exercises that are mandatory for pediatric patients and other age groups are turned into a fun activity regardless of location and time. With the development of such a system, the crowd in physical therapy centers will decrease, and patients will be able to continue their treatment under all conditions, such as pandemics.

Keywords: Cerebral Palsy, Kinect camera, Unity 3D Game

1. INTRODUCTION

Today, rehabilitation centers have been developed with different virtual applications for diseases. For example, Virtual Rehab is one of the applications designed for rehabilitation patients using Kinect [1]. Another project for rehabilitation patients with Kinect is Jintronix [2]. Jintronix is a system that combines the virtual reality game system and treatment systems, making rehabilitation movements fun and effective [2,8].

This study has differences from similar studies. The system designed primarily is a game for patients with cerebral palsy. Joint angles are constantly checked during the patient's exercises. In case of wrong action, the avatar gives voice feedback and states that he/she made the action wrong. It is in constant communication with the patient. Also, in similar studies, one person goes across the camera and exercises. However, the patient needs help in cerebral palsy exercises. With this application, even if there is more than one person in front of the camera, the camera can only focus on the patient's data. Another difference is that patients generally exercise while standing, whereas, in the treatment of cerebral palsy, there are also exercises in the lying position.

Cerebral Palsy (CP) is a neurodevelopmental disorder that results in functional motor impairment and disability in children [3]. The main cause of Cerebral Palsy is a group of permanent movement limitations and postural disorders due to damage that may occur in the developing fetus or the baby's brain, causing restrictions in movements. To slow the progression of this disease, daily exercises are required to be applied. These exercises given to the patient are practiced by physical therapy centers. With the created cerebral palsy treatment assistant, patients will be able to practice their exercises at home.

At the same time, by giving audible feedback about the correctness of the exercises, the patients or their parents who help them do the exercises will make sure that the movements are done correctly. Thus, in environments where patients feel comfortable and safe, they will have the opportunity to perform their exercises correctly at any time. Besides, it will be very convenient for the parent who helps to do the exercise. Also, the fact that the treatment was not interrupted even when we closed the houses and had to live in

[1] *Corresponding author: Bolu Abant Izzet Baysal University, Department of Computer Engineering, Bolu, TURKEY.*
postalcioglu_s@ibu.edu.tr

isolation due to the pandemic, which we faced as a global problem, is one of the prominent features of the study.

Applications that are made by force or squeezing can be made more fun with an exercise program in a game format. Body movements have become the data that can be used in games with the increase of equipment that helps to perceive person movements. One of the hardware used is Kinect. Kinect equipment is used for rehabilitation at homes and clinics [8].

In this study, using Kinect camera, an assistant is designed for cerebral palsy patients, which can be used for exercise purposes, especially entertain children while exercising, and make them feel good. The difficulties experienced by the patient and his/her parent due to the density in the physical treatment centers and the difficulties in making appointments have been eliminated.

Patients will be able to perform their exercises comfortably and fun in any place without time restrictions by using the program written with Kinect camera they will buy instead of going to rehabilitation centers. This will both increase the motivation of the patient and provide convenience to the patient's relatives. At the same time, the crowded will decrease in physical therapy centers and other patients who have to go to the center will be able to make appointments more easily and perform their treatment more efficiently.

2. MATERIAL AND METHOD

Movements have been introduced to the system so that cerebral palsy patients can exercise correctly at home. In the designed application, the patient is audibly informed whether he/she is doing the exercise correctly. Exercises have been made more fun with animation by using the Unity 3D game engine.

The study consists of two basic parts: hardware and software. The hardware part of the study consists of Kinect Sensor, Kinect PC Adapter, and a mid-level computer, which can detect the movements of the human skeleton. Figure 1 and Figure 2 show the Kinect sensor and Kinect PC Adapter.

Figure 1. Kinect camera

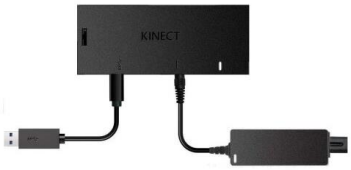

Figure 2. Kinect PC Adapter

Although Kinect is launched as part of the game consoles, it is also used in different fields such as biomedical, robotics, military, education, and security systems. The Kinect sensor consists of 4 parts: a 3D depth sensor, an RGB camera, a microphone group and a motor [4]. With the help of Kinect's depth sensor, the coordinate points of the joint points in the body of the users are obtained in three-dimensional space. In this study, instead of using only the position information of the joints in the game, the angle values of x, y and z are used.

Kinect, used with Microsoft's game console XBOX 360, can be used in Windows applications with Kinect V2 SDK. Kinect, powered by 5V power from an external source and plugged into USB, is detected by the computer and the environment is prepared for it to operate [5,6]. Minimum hardware requirements are for Kinect to run efficiently on a computer; Windows 7 (x86 or x64) and above operating system, dual-Core 2.66 GHz or higher processor, at least 2GB ram and Kinect PC connection cable [7].

The software part consists of the Unity3D game engine on C # programming language in the Visual Studio development environment. The Kinect sensor works as an interface between the Windows SDK Kinect device and our application. When we need to access the sensor, the application sends an API call to the driver and the Kinect driver controls access to the sensor data.

Unity is a game engine that supports 2D and 3D graphics, scripting with C #, and allows games to be played without being installed on the computer. The games performed can be run in environments such as Windows, Android, iOS, Linux, Xbox [7].

3. RESULTS

Patients with advanced cerebral palsy cannot perform movements alone. Movements can be done with help by someone. For this reason, first of all, it is necessary to detect only the sick person and not everyone within the field of view of the Kinect camera and to get the coordinate data of his/her joint points. For this reason, the Kinect V2 MS-SDK's Max Tracked Users component is limited to 1 in the Kinect Manager class. In this way, after the patient introduces himself/herself to the camera, only the angle values of the patient's joint points are taken. The diagram of the designed system is shown in Figure 3.

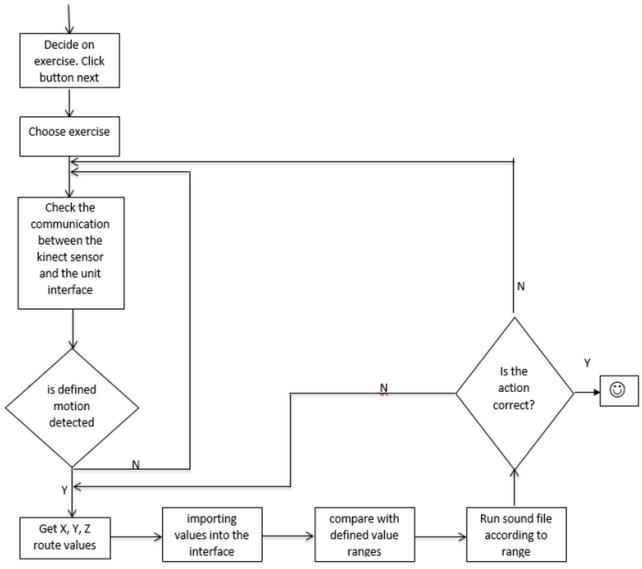

Figure 3. The designed system block diagram

With the Unity 3D game engine, a three-dimensional avatar is programmed, which the patient must see on the screen. The joints of the avatar are given to the program by giving the angle intervals of the exercises that the patient should do. When the user starts the game, the login screen appears first. In this screen, you can see the exercises defined in the program in a video. Figure 4 shows the cerebral palsy treatment assistant login screen.

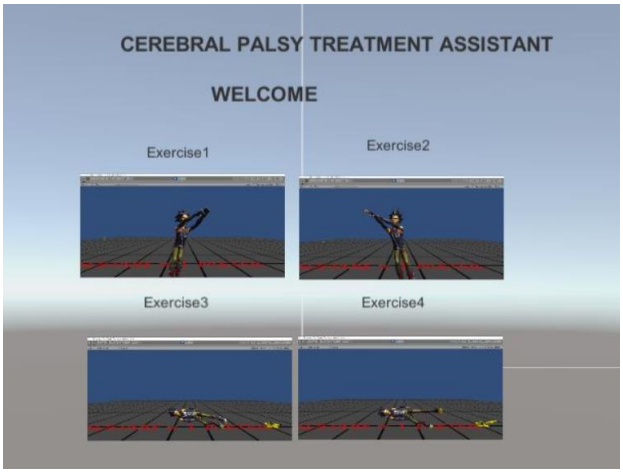

Figure 4: The cerebral palsy treatment assistant login screen

After deciding on the desired exercise, the exercise screen of the game is entered. In this screen, the desired exercise button is pressed and the patient is introduced to the camera. The patient will be able to do the exercises after introducing himself/herself to the camera. The avatar used on the screen performs the movements simultaneously while the patient exercises. While the patient is doing the exercises, monitoring himself through the avatar enables him/her to make the movements more carefully. When starting to exercise, the first move is reduced to -5 points if the first action is wrong. The avatar gives verbal feedback in case the patient does the exercise wrong. The avatar tells the exercise was done wrong and tells how it should be done. Figure 5 shows the part of the code sample. In the code sample shown below, the code lines that print the angle values of the joint points on the screen while the patient is moving, add 10 points in the correct angle intervals and decrease 5 points in the wrong angle range.

```
if (debugText)
{
    Vector3 vRotAngles = qRotObject.eulerAngles;
    debugText.text = string.Format("{0} - R({1:000}, {2:000}, {3:000})", trackedJoint,
                                   vRotAngles.x, vRotAngles.y, vRotAngles.z);
    if (65 < vRotAngles.x && vRotAngles.x < 80)
    {

        if (Ses1.isPlaying != true)
        {
            if (!alreadyplayed)
            {
                Ses1.PlayOneShot(SesKlip1);
                ScoreScript.scoreValue += 10;
            }
        }
        debugText.text = string.Format("{0} - R({1:000}, {2:000}, {3:000} )", trackedJoint, vRotAngles.x, vRotAngles.y, vRotAngles.z);
        Image2.SetActive(true);

        Text2.SetActive(true);
    }

    if (80 < vRotAngles.x && vRotAngles.x < 360)
    {

        if (Ses1.isPlaying != true)
        {
            if (!alreadyplayed)
            {
                Ses1.PlayOneShot(SesKlip2);
                ScoreScript.scoreValue -= 5;
            }
        }
    }
```

Figure 5. The part of the code sample

Figure 6 shows the synchronization of the patient and the avatar. The yellow skeleton in the lower right corner is the image of the patient taken from the Kinect camera. In the middle of the screen is our avatar.

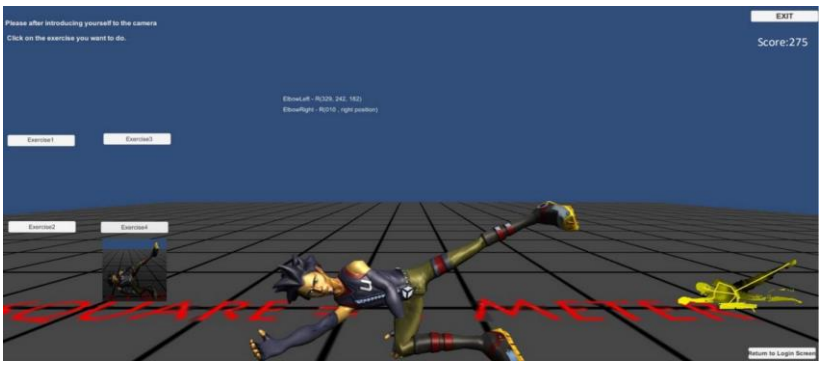

Figure 6. The synchronization of the patient and the avatar

Figure 7 shows the synchronization of the patient and the avatar. When the patient moves correctly, +10 points are added and the score value becomes 5. The patient is entitled to do the next exercise and the exercise is displayed.

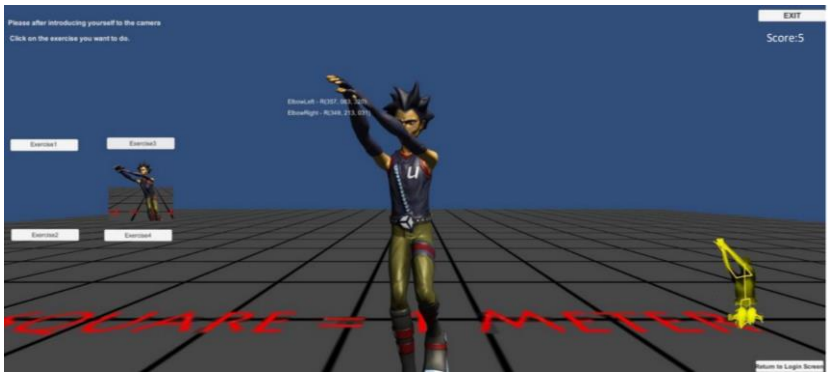

Figure 7. The synchronization of the patient and the avatar

4. CONCLUSIONS

In previous studies conducted with augmented reality and simulation systems, it was observed that the patients maintained the exercises and obtained more efficiency. However, this form of treatment is used in physical therapy centers. In general, patients have limited access to this treatment method. Cerebral Palsy Treatment Assistant will be a form of treatment that people can easily reach. This study aims to encourage of cerebral palsy patients for rehabilitation therapy earlier. Patients will be able to have a more accurate and efficient treatment process with the warnings they receive during the exercises from Avatar. In diseases where physical exercises are required during the treatment, continuity to the exercises is important. With this study, it is thought that continuity in exercises will be provided and results can be obtained faster. With the development of such studies, the difficulties faced by the patient and the parent due to the crowd in the physical treatment centers and difficulties in making an appointment will be eliminated. Instead of going to the rehabilitation center, the patient will be able to do their exercises in a comfortable and fun way without any time restrictions. This will increase the patient's motivation and provide convenience to the parent of the patient. At the same time, the crowd in the physical treatment centers will decrease and patients who have to go to the center will be able to make appointments more easily and perform their treatment more efficiently.

REFERENCES

[1]. Virtual Rehab, Virtual Rehabilitation Systems, http://www.virtualrehab.info/, accessed date: 20.06.2020.
[2]. Jintronix, Kinect Rehabilitation Software, http://www.jintronix.com/ accessed date: 20.06.2020.
[3]. C. A. Chaze, G. McIlvain, D. R. Smith, G. M. Villermaux, P. L. Delgorio, H. G. Wright, K. J. Rogers, F. Miller, J. R. Crenshaw, and C. L. Johnson, "Altered brain tissue viscoelasticity in pediatric cerebral palsy measured by magnetic resonance elastography," Neuroimage Clin, vol. 22, pp.1-7, Mar. 2019.
[4]. Fidan , U. , Ozkan , N. (2018), "Norolojik Rehabilitasyon icin Kinect Sensorlu Olcum ve Egzersiz Sisteminin Tasarimi ve Gerceklestirilmesi" , Afyon Kocatepe Universitesi Fen ve Muhendislik Bilimleri Dergisi, pp. 727-733.
[5]. A. P. L. Bó, M. Hayashibe, and P. Poignet, "Joint angle estimation in rehabilitation with inertial sensors and its integration with Kinect," 2011 Annual International Conference of the IEEE Engineering in Medicine and Biology Society, Boston, MA, 2011, pp. 3479-3483, DOI: 10.1109/IEMBS.2011.6090940.
[6]. Kinect, Kinect for Windows Runtime, https://support.xbox.com/help/hardware-network/kinect/kinect-for-windows-v2-setup-with-adapter. accessed date: 20.06.2020.
[7]. Ozturk , E. (2017) , "Sanal Fizik Tedavi Platformu" , Firat Universitesi , Fen Bilimleri Enstitusu , Bilgisayar Muhendisligi ,Yuksek Lisans Tezi , Elazig .
[8]. Erdogan, H., Ekenel H.K., (2015). Kinect Kullanarak Fizik Tedavi ve Rehabilitasyon Amacli Oyun Tasarimi, TIPTEKNO'15, PP:288-291.

Assessment of Durability of Inkjet Prints on Laboratory Paper Substrates with Wheat Pulp Based on Rub Resistance

Maja Rudolf [1], Katja Petric Maretić [2], Irena Bates [2], Ivana Plazonić [2], Valentina Radić Seleš [2]

Abstract

*Paper recycling is becoming increasingly important as the production of packaging and various printed products grows. As alternative to wood fiber that is the most common raw material in paper production this research examines the quality of paper which is made with addition of non-wood fibers derived from wheat straw. For this purpose, laboratory paper substrates were made by blending recycled newspaper pulp and wheat straw pulp in different proportions. In this study we analyse rub resistance of laboratory paper substrates with variable content of wheat pulp printed in full tone with black and yellow inks by digital ink jet printing technique. The main objective of this research is to determine whether this kind of print has necessary durability for carrying stable illustrations. One of the main characteristics of print quality is resistance to rubbing which is very important for packaging during transport, storage and the end use. Rub resistance test was executed according to BS 3110 standard. The print durability was assessed through the Euclidean color difference and the individual CIE L*a*b* differences before and after the rub tests. The analysis showed that the increase of wheat pulp content in paper substrates has affected the increase of color difference. Greater rub resistance was observed on substrates with lower share of wheat pulp. Samples printed with yellow ink showed overall greater durability than samples printed with black ink. In further analysis we observed that for the black prints the difference in lightness (ΔL') of the CIE L*a*b* color space was most affected as the prints became lighter with the number of rubbing cycles. In samples printed with yellow ink most affected was the color difference on yellow-blue axis (Δb') meaning that the yellowness of the prints was degrading with the number of rubbing cycles.*

Keywords: durability, inkjet printing, paper substrate, rub resistance, wheat pulp

1. INTRODUCTION

Rapid rise in the production of paper products leads the paper industry to the search for alternative fiber sources that would reduce or replace wood as a main source of virgin fiber in papermaking processes. So far, the alternative sources of the virgin fibers can be categorized as: agricultural crop residues such as cereal or straw residues, natural growing plants such as miscanthus, reeds or other grasses and non-wood crops that include textile crops such as cotton or flax [1]. Agricultural crops residues are interesting for their abundance and low cost but also for the shorter growing cycle than wood [2]. As the most available crop that is grown in Croatia is wheat [3], this research was focused on examining the quality and durability of laboratory paper substrates produced with different ratios of wheat straw fibers. The wheat straw was collected after harvesting, cut and converted to wheat pulp according to soda method where fibers are separated from plant tissue [4]. Wheat pulp was blended with wood pulp from recycled newsprint paper in different ratios to improve the characteristics of shortened recycled wood fibers [5]. The previous research has led to the conclusion that the addition of wheat pulp up to 30% provide good quality of the prints on such laboratory paper substrates [6-8].

[1] *Corresponding author: University of Zagreb, Faculty of Graphic Arts, Zagreb, Croatia. maja.rudolf@grf.unizg.hr*

[2] *University of Zagreb, Faculty of Graphic Arts, Zagreb, Croatia: katja.petric.maretic@grf.unizg.hr, irena.bates@grf.unizg.hr, ivana.plazonic@grf.unizg.hr, valentina.radic.seles@grf.unizg.hr*

Rub resistance is defined as the ability to resist damage during the friction of two surfaces in contact [9]. It is very important feature of the printed material, especially packaging, because it must endure the process of shipment, storage, and handling from production phase to the end use. It can be evaluated visually or by calculating Euclidean color differences (ΔE_{00}) of printed materials in the CIE L*a*b* color space [10].

2. MATERIALS AND METHODS

The research was divided into four phases: production of laboratory paper substrates, printing, rub resistance testing and spectrophotometric measurements of colorimetric values before and after the rub resistance testing to determine the changes in print coloration.

2.1. Production of laboratory paper substrates

Four types of paper substrates were produced with different weight ratios of recycled newsprint pulp and wheat pulp:

- N – reference paper substrate – with 100% recycled newsprint pulp,
- 1NW – with 90% recycled newsprint pulp and 10% wheat straw pulp,
- 2NW – with 80% recycled newsprint pulp and 20% wheat straw pulp,
- 3NW – with 70% recycled newsprint pulp and 30% wheat straw pulp.

Paper substrates were formed on the device Rapid Kothen (FRANK PTI) sheet former with the grammage of 42.5 g/m^2 according to standard ISO 5259-2:2001.

2.2. Printing

In the second phase laboratory paper substrates were printed using inkjet printing technique on EFI Rastek H652 digital printer. UV curable black and yellow inks were printed in full tone over the paper substrates. Settings of the printer were adjusted to "high quality" printing mode, with 8 passes in 600 dpi resolution and the printing speed of 12.1 m^2/h.

2.3. Rub resistance testing

Printed paper substrates were cut to smaller round samples with the diameter of 5 cm. The rub resistance test was performed on a tribometer Hanatek T4 Rub and Abrasion Tester according to the BS 3110:1959 standard under the constant pressure of 0.23 kg (0.5 lb) with rotational motions of 20, 40 and 60 cycles at the speed of 1 revolutions per second.

2.4. Spectrophotometric measurement of colorimetric values

Before the paper substrates were subjected to rub resistance tests the spectrophotometric measurements were made to determine the CIE L*a*b* colorimetric values of each printed sample. After the rub resistance tests had been made, the measurements were repeated and the Euclidean color difference ΔE_{00} was calculated according to CIEDE2000 formula (1). Device used for the spectrophotometric measurements was SpectroEye with illuminant D50 and 2° observer angle.

$$\Delta E_{00} = \sqrt{\left(\frac{\Delta L'}{k_L S_L}\right)^2 + \left(\frac{\Delta C'}{k_c S_c}\right)^2 + \left(\frac{\Delta H'}{k_H S_H}\right)^2 + R_T \left(\frac{\Delta C'}{k_C S_C}\right)\left(\frac{\Delta H'}{k_C S_H}\right)} \quad (1)$$

where: $\Delta L'$ is representing the difference in lightness between printed samples before and after the rub resistance test, $\Delta C'$ is the chroma difference between printed samples before and after the rub resistance test and $\Delta H'$ is the hue difference between printed samples before and after the rub resistance test. R_T is the rotation function, while k_L, k_C, k_H are the parametric factors for variation in the experimental conditions and S_L, S_C, S_H are the weighting functions [11].

In addition to the ΔE_{00} calculations, the difference of individual components of the CIE L*a*b* color space $\Delta L'$, $\Delta a'$ and $\Delta b'$ was calculated according to the formulas (2), (3) and (4) where the value marked with index 1 represents the value measured before the rub resistance test and the value marked with index 2 represents the value measured after the test.

$$\Delta L' = L_1^* - L_2^* \quad (2)$$

$$\Delta a' = a_1^* - b_2^* \quad (3)$$

$$\Delta b' = b_1^* - b_2^* \quad (4)$$

Durability is considered acceptable or print quality is good if the value of the Euclidean color difference is less than 1 and can be tolerated up to 2. The untrained eye of the observer does not notice a difference in color change for those values of ΔE_{00} [12].

3. RESULTS AND DISCUSSION

Euclidean color difference (ΔE_{00}) was measured before and after the rub resistance test on 30 samples, and average value was calculated. Table 1. shows values of ΔE_{00} for four types of paper substrates (N, 1NW, 2NW and 3NW) printed in full tone black and yellow after the rub resistance test with 20, 40 and 60 rubbing cycles. Prints on paper substrates with added wheat pulp showed slightly increased color difference compared to the prints on the reference paper substrates without added wheat pulp.

For the black prints, calculated color difference on samples marked N was 0.55 for 20 cycles, and 0.75 for 40 and 60 cycles, meaning that the color difference can't be perceived with the untrained eye and that the black prints are stable to rubbing. Black prints on papers with added wheat pulp show lesser durability and more fluctuation in rub resistance tests, regardless of the number of cycles and wheat content, with increased value of Euclidean color difference ranging from 0.77 to 1.2.

The Euclidean color difference for the yellow prints is less pronounced as indicated by the low ΔE_{00} values ranging from 0.39 to 0.51 on reference substrates marked N. Substrates with added wheat pulp showed a slight increase in Euclidean color difference values from 0.43 to 0.86 that predictably rise with the number of rub test cycles.

Table 1. Average ΔE_{00} values of black and yellow prints made on four paper substrates N, 1NW, 2NW and 3NW after the rub resistance test with 20, 40 and 60 rubbing cycles

Paper substrate type	N			1NW			2NW			3NW		
No. of rubbing cycles	20	40	60	20	40	60	20	40	60	20	40	60
	Average ΔE_{00}											
Black prints	0.55	0.75	0.75	0.98	0.83	0.91	0.8	0.82	1.2	0.77	0.79	0.98
Yellow prints	0.42	0.39	0.51	0.43	0.62	0.69	0.55	0.72	0.66	0.62	0.62	0.86

Further calculations have examined the difference of individual components of the CIE L*a*b* color space ($\Delta L'$, $\Delta a'$ and $\Delta b'$) with purpose to determine which of them were most affected by rub tests in respect of 20, 40 and 60 rubbing cycles. As predicted, the paper substrates printed with black ink had most significant change in L^* component which suggests that the rubbing test had most impact on lightness. Figure 1. shows the charts with the difference of $\Delta L'$, $\Delta a'$ and $\Delta b'$ for each type of the tested paper substrates. The reference substrate marked N showed gradual increase in $\Delta L'$ values with the increased number of rubbing cycles (Figure 1.a). The negative values indicating that the black color tone becomes lighter. Change on a^* (green/red) and b^* (blue/yellow) axis was slightly rising in the positive direction (< 0.2), although the changes cannot be perceived with the human eye. With the addition of wheat pulp, color durability showed greater fluctuations compared to reference paper substrate, with unpredictable results of $\Delta L'$ in relation to the number of rubbing cycles.

However, Figure 1. b), c) and d) shows that all calculated Δ*L'* values were measured in the acceptable range < 1.2. In the paper substrates with added wheat pulp, the Δ*a'* values did not change significantly and the Δ*b'* values had slight increase with the number of rubbing cycles, although the difference was insignificant (< 0.4). The amount of wheat pulp in the paper substrate had no significant impact on the measured values.

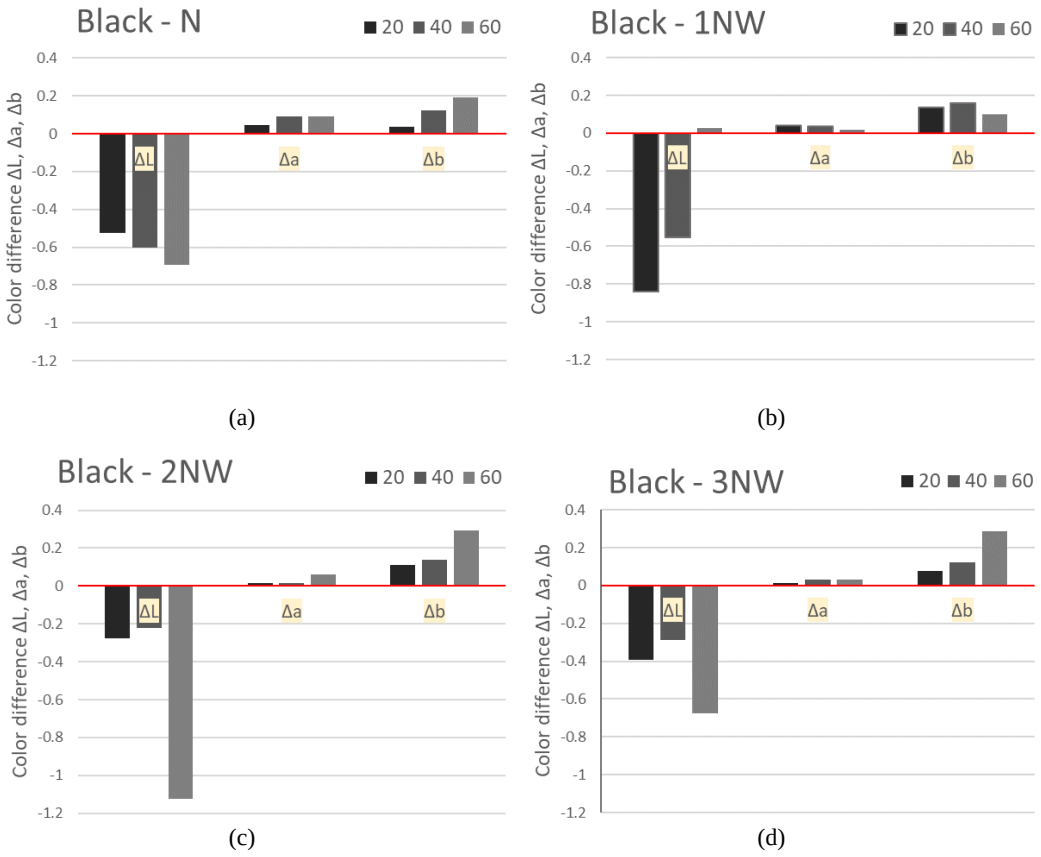

*Figure 1. Color difference of Δ*L'*, Δ*a'* and Δ*b'* for black prints on four paper substrates N, 1NW, 2NW and 3NW calculated from measurements before and after the rub resistance test with 20, 40 and 60 cycles*

The greatest differences in *b** component of the CIE L*a*b* color space – the blue/yellow axis, was observed on prints with yellow ink. The reference sample (Figure 2.a) shows increase in Δ*L'* values in the acceptable range < 0.5 and shows good durability throughout 20, 40 and 60 rubbing cycles. The color difference in the component *a** – the red/green axis – had shown insignificant increase < 0.2, after the rub resistance testing. As expected, the greatest difference was observed for the Δ*b'* with the increased values in the positive range < 1.5, indicating that the yellow color after the rubbing test has slightly decreased yellowness. Figure 2. b), c) and d) show calculated values of Δ*L'*, Δ*a'* and Δ*b'* for yellow prints on paper substrates with added wheat pulp. The change in lightness indicated with Δ*L'* has insignificantly increased compared to the reference substrate, measuring < 0.73 given the highest number of rubbing cycles. Differences Δ*a'* have not changed significantly in respect to the rubbing cycles and increase of wheat amount in the paper substrate (< 0.5). In the *b** axis changes were more pronounced after 40 and 60 rubbing cycles compared to the reference paper substrate, resulting with Δ*b'* of ~1 with 20 rubbing cycles regardless of wheat content, from 1.3 to 1.5 for 40 rubbing cycles and from 1.8 to 2 for 60 rubbing cycles. These results can still be categorized as acceptable with the very small color difference.

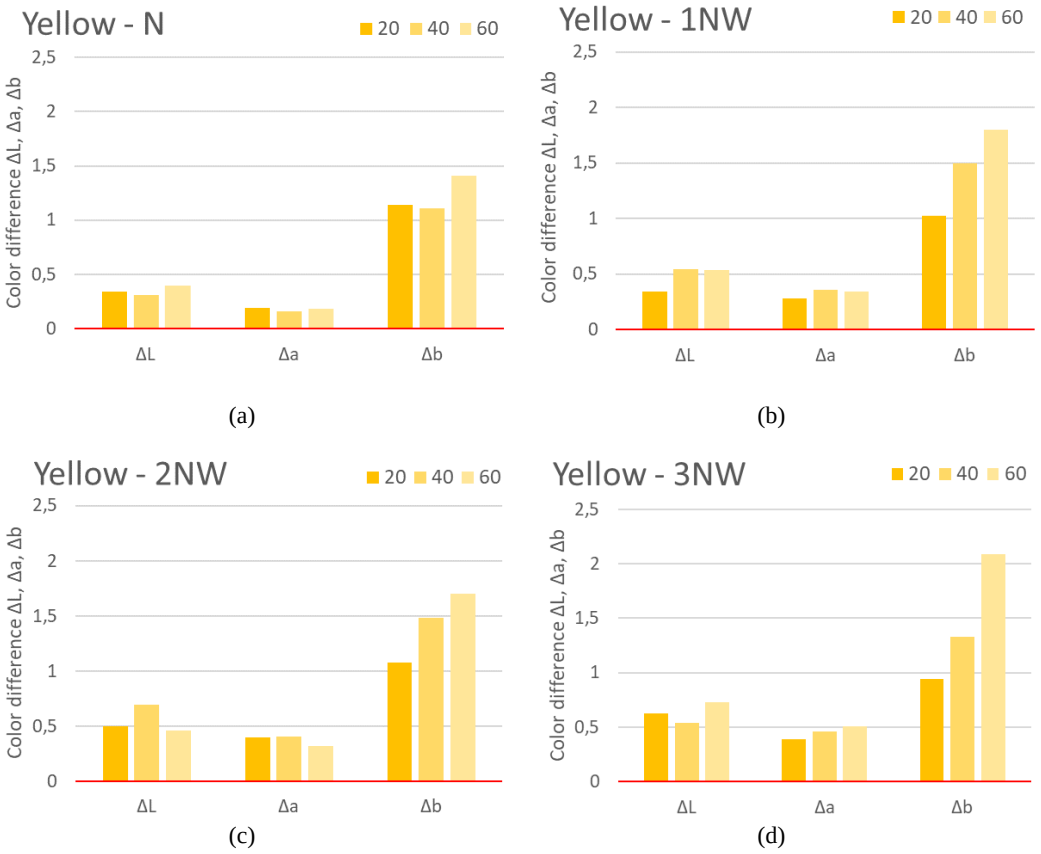

Figure 2. Color difference of ΔL', Δa' and Δb' for yellow prints on four paper substrates N, 1NW, 2NW and 3NW calculated from measurements before and after rub resistance test with 20, 40 and 60 cycles

4. CONCLUSION

In this paper the durability of black and yellow prints made on the paper substrates with added wheat pulp was assessed based on the rub resistance testing. The calculated Euclidean color difference and the color difference of separate components of the CIE L*a*b* color space values showed the satisfactory level of print durability for the black and yellow prints. Lesser rub durability of prints was determined on the paper substrates with added wheat pulp than on the reference substrate without wheat pulp, but the results were still in the acceptable ranges. The prints in full tone black ink showed overall the greater Euclidean color difference than the prints made with full tone yellow ink which indicated that the yellow prints were more durable in comparison with black ones. Black samples on paper substrates with added wheat pulp showed slightly unpredictable results in the Δ*L'* calculations regardless of the percentage of added wheat pulp or the number of rubbing cycles in the resistance testing. All results were within acceptable ranges. Yellow prints on paper substrates with added wheat pulp showed the greatest increase in Δ*b'* component with respect of the rubbing cycles increase, meaning there was a slight loss of yellowness in the color, but also in the acceptable range. The amount of wheat pulp in the substrate had not significantly affected results. It can be concluded that laboratory paper substrates with added wheat pulp up to 30% has provided satisfactory durability of digital inkjet prints in the rub resistance tests and can be recommended for further development in creating paper for packaging and other purposes.

ACKNOWLEDGMENT

This work has been supported in part by Croatian Science Foundation under the project "Printability, quality and utilization of substrates with non-wood fibers" (UIP-2017-05-2573) and by the University of Zagreb.

REFERENCES

[1]. E. S. Abd El-Sayed, M.E. l-Sakhawy, and M. El-Sakhawy, "Non-wood fibers as raw material for pulp and paper industry", *Nordic Pulp & Paper Research Journal* vol. 35(2), pp. 215-230, 2020.
[2]. G. Fang, and K. Shen, "Wheat Straw Pulping for Paper and Paperboard Production", Chapter 12 in Global Wheat Production, Intech Open, Edited by Shah Fahad, pp. 223-239, 2018.
[3]. "Agriculture, Hunting, Forestry and Fishing: Crop production" Croatian Bureau of Statistics, Available: http://www.dzs.hr/PXWeb/sq/f89a3233-db53-4c01-a514-f8e59e54bd81
[4]. I. Plazonić, I. Bates, and Ž. Barbarić-Mikočević, "The Effect of Straw Fibers in Printing Papers on Dot Reproduction Attributes, as Realized by UV Inkjet Technology", *BioResources*, vol. 11(2), pp. 5033-5049, 2016.
[5]. I. Plazonić, Ž. Barbarić-Mikočević, V. Džimbeg-Malčić, and I. Bates, "The rub resistance of printed papers with variable content of wheat pulp", *Proceedings of Natural resources, green technology and sustainable development/2*, 2016. pp. 76-79
[6]. I. Plazonić; I. Bates; Ž. Barbarić-Mikočević, and B Lajić, "Chemical degradation of prints made on papers with wheat pulp", *Proceedings of International Conference on Innovative Technologies IN-TECH 2017*, 2017. pp. 117-120
[7]. I. Bates, I. Plazonić, V. Džimbeg-Malčić, and D. Banić, "Influence of straw pulp in printing substrate on stability of digital prints", *Proceedings of International Conference on Innovative Technologies IN-TECH 2017*, 2017. pp. 113-116
[8]. M. Rudolf, I. Plazonić, K. Petric Maretić, I. Bates, and V. Radić Seleš, "Rub resistance of ink jet prints on laboratory substrates with wheat pulp" *Proceedings of Printing&Design 2020.*, 2020, pp. 126-131
[9]. J. Vališ, B. Jašurek, and T. Syrovy, "Methodology of evaluation of print abrasion resistance", *Proceedings in Wood, Pulp & Paper Polygrafia Academica*, 2014, pp. 107-110
[10]. S. Jamnicki Hanzer, R. Kulčar, M. Vukoje, and P. Širol, "Mechanical and chemical resistance of thermochromic packaging prints", *Proceedings - The Tenth International Symposium GRID 2020*, 2020, pp. 109-118
[11]. G. Sharma, W. Wu, and E. N. Dalal, "The CIEDE2000 color-difference formula: implementation notes, supplementary test data, and mathematical observations", *ColorResearch and Application*, vol. 30, pp. 21–30, 2005.
[12]. I. Zjakić, *Upravljanje kvalitetom ofsetnog tiska*, Zagreb, Croatia: Hrvatska sveučilišna naklada, 2007.

Comparison of Optical Stability of Papers Containing Wheat Pulp Printed with Digital and Flexographic Printing Technique after Accelerated Ageing

Valentina Radić Seleš[1], Irena Bates [2], Maja Rudolf [2], Ivana Plazonić [2], Katja Petric Maretić [2]

Abstract

Flexographic and digital printing are currently the fastest growing branches in the printing industry. The selection of printing substrates for these printing techniques is large, but paper substrates are the most widely used. Paper manufacturing is based mainly on the use of renewable fibers, and the dominant fiber resource for the pulp and paper industry is wood which is accounting for 90% of the world's fiber utilization. As woods consumption for paper production is still high, there are various possibilities to reduce it. One way is by reducing the proportion of wood pulp in paper by adding straw pulp of various cereals such as wheat. Wheat straw has numerous advantages and can be used in pulp form as a source of primary fibers for paper production. As paper as a multi-component material, besides fibers composed of cellulose, hemicellulose and lignin also includes additives, minerals and synthetic polymers. Due to its complex nature it is prone to deterioration when exposed to elevated temperature, humidity and light. Paper ageing is irreversible change and is the best indicator of paper optical permanence. Objective of this study was to determine the optical stability of prints after undergoing aging treatment with elevated temperature and UV light for 48 and 96 hours. Laboratory papers containing wheat pulp were printed by two printing techniques with cyan and yellow inks to compare better optical stability: UV inkjet and flexographic technique. The optical stability of all prints was observed based on the difference in the reflection spectra (ΔR). The results indicated that all laboratory papers printed with cyan ink with flexographic technique show better optical stability than the ones printed with digital technique. Laboratory papers printed with yellow ink by both techniques show good optical stability.

Keywords: accelerated ageing, digital, flexographic, optical stability, prints, wheat pulp

1. INTRODUCTION

Flexography printing is a method of direct printing, that uses resilient relief image plates of rubber or photopolymer material. The plates are inked by a cell-structured, ink-metering „anilox“ roll carrying a fast-drying fluid ink to plates which achieve high quality printed reproduction of text and images on any substrate, absorbent or nonabsorbent. Flexographic printing is an efficient, cost-effective and versatile printing method. Flexography printing uses low-viscosity inks which dry very quickly beetwen the printing units of a printing machine. Solvent-based, water-based and ultraviolet-curable inks are used in flexographic printing and the appropriate ink for each substrate must be very careful choosen. Adhesion, block resistance, rub resistance, heat resistance and lightfastness can be satisfactory on one substrate but terrible on another. Different ink systems require different control and different conditions [1]. Recently developed digital printing technique differs from traditional, analog printing methods because digital printing machines do not require any printing plates. Instead of using printing plates to transfer an printing image, digital printing machines print the ink

[1]*Corresponding author: University of Zagreb, Faculty of Graphic Arts, Zagreb, Croatia.valentina.radic.seles@grf.unizg.hr*

[2]*University of Zagreb, Faculty of Graphic Arts, Zagreb, Croatia. irena.bates@grf.unizg.hr,maja.rudolf@grf.unizg.hr, , ivana.plazonic@grf.unizg.hr, kpetric@grf.hr*

directly onto the printing substrate. Ink jet printing is a technique where inkjet heads deposit droplets of ink on the paper as the printing substrate and the image is produced by means of a dot matrix that creates the letter or graphic image [2]. Digital production print technology is evolving quickly, and its output quality is improving continuously [3]. It is predicted that digital printing technique will grow dramatically as press become cheaper with improvements in the print quality [2]. Flexographic and digital printing, both with their advantages and disadvantages can print on all kinds of substrates from paper, board, polymer materials (foil and film) to thick cardstock, heavyweight papers, folding cartons and fabric. [1,3]. Since paper is the most widely used printing substrate all over the world and wood is currently dominant raw material for paper manufacture, it would be sensible and commercially viable to replace it as much as possible with other plant biomasses by utilization of non-wood fiber materials to produce cellulose pulps [4,5]. The non-wood fibers have some features that are superior to those of wood fiber and others that represent clear disadvantages, such as fiber storage issues. Nonetheless, it is possible to manufacture high-quality paper from these fibers. The cellulose content of wheat straw is very similar to that of wood. The hemicellulose content tends to be higher, but the lignin content is considerably lower. The lower lignin content is an advantage in papermaking [4]. Several studies have shown that straw fibers from certain cereals like wheat show suitable characteristics required for pulp and paper production.

The quality and appearance of graphic product are crucial when end users consider buying products [6]. Therefore, optical stability is amongst most important factors when it comes to product appearance. Paper is constantly exposed to numerous endogenous and exogenous factors that affect its stability. Due to factors such as heat, light and moisture, paper ageing processes cause change in chemical and mechanical properties of paper elements and ink components during the ageing process [7]. Artificial ageing speeds the natural ageing process of paper by subjecting it to extreme conditions for certain period of time, and is used to determine the lifespan or permanence of paper or even to predict the long term effects of conservation treatments [8]. In researches several methods of simulation of the natural ageing process are used, since the process of natural ageing is impractical because of the involved period of time [9]. In this research, the optical stability of flexography and digital prints made on substrates with wheat pulp will be observed trough difference in reflectance spectra where deterioration will be visible after accelerated ageing process.

2. MATERIALS AND METHODS

2.1. Laboratory Papers

Wheat straw was converted into semi-chemical pulp according to soda method [10]. Pulping conditions are presented in Table 1.

Table 1. Pulping conditions

Type of straw	Pulping method	Extraction conditions
Wheat	Soda pulping	Temperature of 120°C, alkali level of 16% for 60 min, and a 10:1 liquid biomass ratio

Obtained unbleached wheat pulp was mixed with recycled wood pulp in different weight ratios, 10%, 20% and 30%. A laboratory paper containing only recycled wood pulp was used as a reference paper in the process of comparing quality of optical properties of laboratory papers containing wheat pulp. Laboratory papers weighed approximately 42.5 gm^{-2} were formed by a Rapid Kothen sheet former ((FRANK- PTI GmbH, Birkenau Germany) according to EN ISO 526 9-2:2001 standard [11]. In total, 4 types of laboratory papers were formed. Abbreviations used in marking all samples are listed in Table 2.

Table 2. Abbreviations used in marking samples

100R	laboratory paper with 100 % recycled pulp (reference)
90R10W	laboratory paper with 90% recycled pulp and 10% wheat pulp
80R20W	laboratory paper with 80% recycled pulp and 20% wheat pulp
70R30W	laboratory paper with 70% recycled pulp and 30% wheat pulp
48h	accelerated aged for 48 hours
96h	accelerated aged for 96 hours

2.2. Printing of Laboratory Papers by Flexographic Technique

All laboratory papers were printed in full tone with cyan and yellow ink by flexographic laboratory device Esiproof RK Printcoat Instruments with water based flexographic inks. Printing was performed with anilox roll with total volume of 39.1 cm^3/m^{-2} and engraved with line screen of 40 $lincm^{-1}$ at a temperature of 23° C and a relative humidity of 50%. An engraving angle for anilox roll was 60 degree angle, respectively the hexagonal cell that offers higher quantity of cells that indicates increasing in the ink transfer, as well as homogeneity.

2.3. Printing of Laboratory papers by Digital Technique

Each laboratory paper was also printed in full tone with cyan and yellow ink by digital EFI Rastek H652 UV curable inkjet printer with the resolution of 600 x 600 dots per inch (dpi) (respectively with high quality mode 8 pass) and printing speed of 12.10 m^2/hr.

2.4. Accelerated Ageing

Laboratory papers printed with both techniques were exposed to accelerated ageing treatment in the test equipment SunTEST XSL+ according to standard ASTM D 6789-02 [12] under conditions summarized in Table 3.

Table 3. Conditions used during artificial ageing

Conditions	
Wavelength (nm)	290 - 800
Irradiance (Wm^{-2})	765 ± 50
Test equipment	SunTEST XSL+, Id.No. 196 Rotronic Hygrolog, Id.No. 180/2
Duration process (h)	48 96
Ambient condition	24.8°C 54.7 % RH
Filter	daylight

2.5. Optical properties

For assessment the quality and permanence of the prints obtained on laboratory papers with added wheat pulp after artificial ageing, optical stability was observed trough color degradation. Color degradation was estimated through the difference in reflectance spectra between unaged and aged prints (ΔR), calculated according to the equation 1. Prints reflectance spectra measurements were processed using X-rite spectrophotometer with standard illuminate D50 and 2° observer, in the interval of the wavelengths from 400 nm to 700 nm for every 10 nm. Reflectance values (R) were measured for all printed paper samples before and after ageing. Optical measurements were repeated 25 times on each sample.

$$\Delta R = R_{unaged} - R_{aged} \quad (1)$$

3. RESULTS AND DISCUSSION

Figures 1-4 present the experimental results of reflectance measurements presented as ΔR, before and after accelerated ageing in the visible part of electromagnetic spectrum for all analyzed papers printed with digital and flexographic technique.

Following graph in Figure 1 shows the difference in reflectance values on laboratory papers printed by flexographic printing technique with cyan water based printing ink. The highest reflectance difference is visible on paper made from 100% recycled pulp after 48 hours of artificial ageing. It also shows the highest difference after 96 hours of accelerated ageing compared to other papers printed with cyan flexographic ink. The highest optical stability is visible on laboratory paper made with the addition of 10% wood pulp after 48 hours of accelerated ageing.

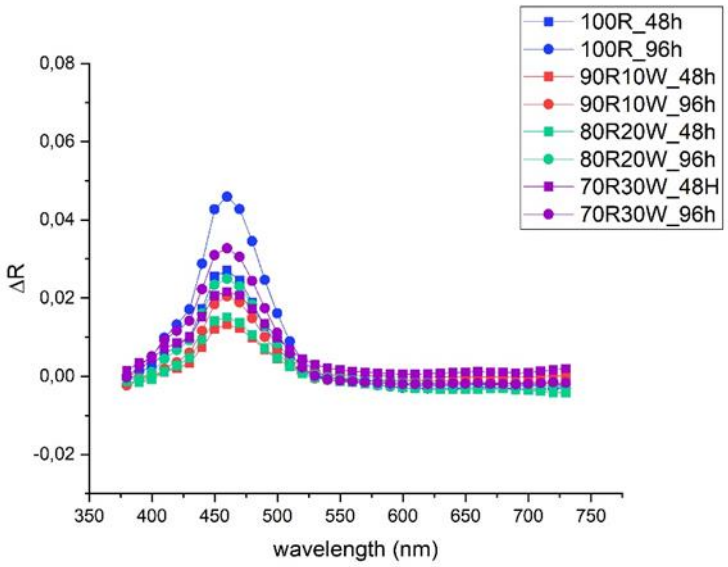

Figure 1. The influence of ageing time on reflectance spectra of cyan prints made by flexographicprinting technique on laboratory papers without (100R) and with wheat pulp (90R10W, 80R20W, 70R30W)

Figure 2 shows the difference in reflectance values between unaged and aged laboratory papers printed by flexographic printing technique with yellow water based printing ink. It is visible that the highest degradation occurs on paper made from 100% recycled pulp after the first 48 hours of accelerated ageing. The best optical stability of prints provides papers made with addition of wheat pulp of 20% and 30%.

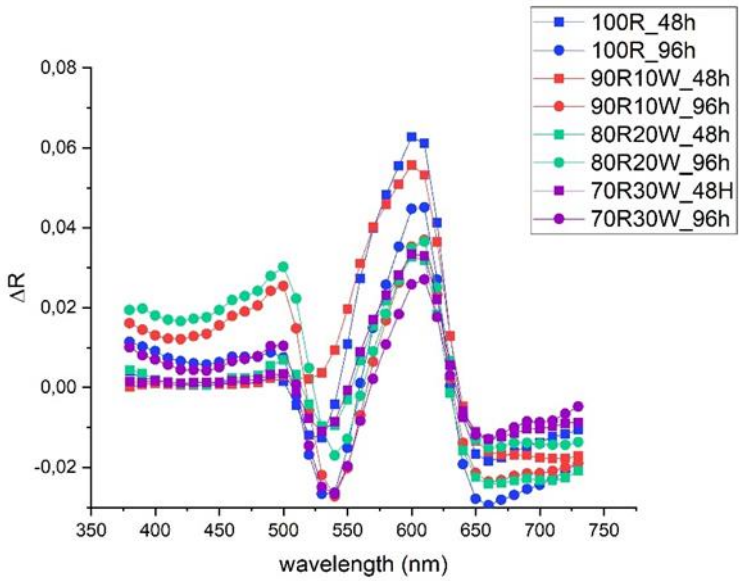

Figure 2. The influence of ageing time on reflectance spectra of yellow prints made by flexographic printing technique on laboratory papers without (100R) and with wheat pulp (90R10W, 80R20W, 70R30W)

In Figure 3, cyan prints on all laboratory papers obtained by digital printing technique present expected reflectance curves. The highest degradation of all cyan prints occurs after first 48 hours of accelerated ageing on laboratory paper 100R, paper without wheat pulp. After additional 48 hours of accelerated ageing, degradation is still visible but significantly lower. Others cyan prints obtained on laboratory papers with wheat pulp addition show similar behavior. However, cyan prints made on papers with 30% of wheat pulp exhibit the lowest reflectance differences, so they are the most stable ones. It is clearly visible that reflectance values of all cyan prints drop with addition of wheat pulp into papers.

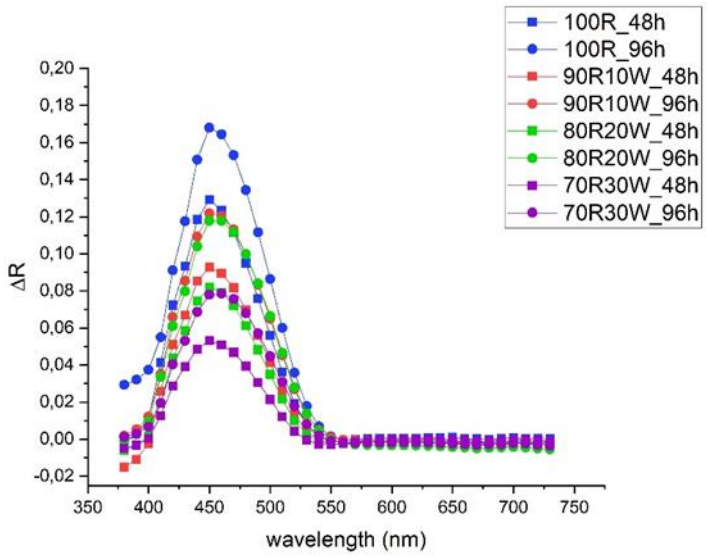

Figure 3. The influence of ageing time on reflectance spectra of cyan prints made by digital printing technique on laboratory papers without (100R) and with wheat pulp (90R10W, 80R20W, 70R30W)

Figure 4 represents the difference in reflectance values for laboratory papers printed by digital technique with yellow ink. The same trend is also visible here as on previous graph for cyan prints. The highest degradation occurs within the first 48 hours of accelerated ageing, and stability is better with each additional increase in shere of wheat pulp in printing substrate. The best optical stability was noticed on prints obtained on paper with addition of 30% wheat pulp. Yellow prints show better optical stability than cyan prints.

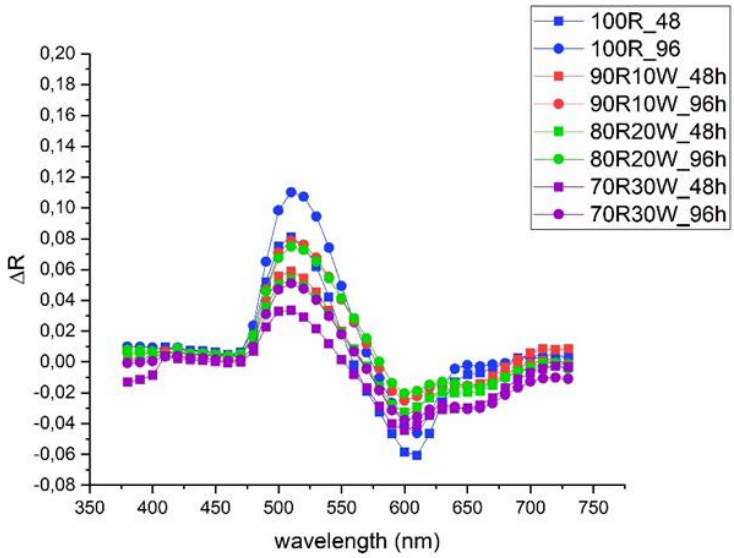

Figure 4. The influence of ageing time on reflectance spectra of yellow prints made by digital printing technique on laboratory papers without (100R) and with wheat pulp (90R10W, 80R20W, 70R30W)

4. CONCLUSION

The aim of this research was to point out the influence of printing technique and printing substrate with wheat pulp on optical stability of prints. Considering all obtained results, the following can be concluded:

- The highest color degradation of cyan and yellow prints occurs in the first 48 hours of accelerated ageing on all papers printed with both techniques,
- Cyan ink printed with flexographic printing technique provides better optical stability than the one printed with digital technique,
- Yellow ink provides prints with higher optical stability of prints on all printing substrates than cyan ink for both printing techniques,
- Addition of wheat pulp into paper substrate positively influences optical stability of all analyzed prints

The results in this research suggest that the optical stability of prints on papers formed with addition of wheat pulp is satisfactory and could be additionally improved if papers would be formed in industrial production.

ACKNOWLEDGMENT

This work has been supported in part by Croatian Science Foundation under the project „Printability, quality and utilization of substrates with non-wood fibres“ (UIP-2017-05-2573) and by the University of Zagreb.

REFERENCES

[1]. G. Cusdin, Flexography: *Principles & Practices. 5th edition, Volume 1*. Foundation of Flexographic Tehnical Association.Inc. USA, 1999.
[2]. D. Bann, *„The all new print production Handbook"*, Watson-Guptill Publications, New York 2007.
[3]. Digital Printing & Types of Digital Printing – Xerox, [Online] Available: https://www.xerox.com/en-ng/digital-printing/insights/what-is-digital-printing
[4]. V. Radić Seleš, I. Bates, I. Plazonić, I. Majnarić, *„Analysis of optical properties of laboratory papers with straw pulp coated with titanium dioxide white ink"*, Cellulose chemistry and technology, 54 (5-6), 473-483, 2020. doi:10.35812/CelluloseChemTechnol.2020.54.48.
[5]. R. Shmulsky and P.D. Jones, *„Pulp and Paper Map"* 2014. The Forestry Chronicle
[6]. N. Pauler, *"Paper Optics-Optical and colour science related to the pulp and paper industry"*, AB Lorentzen & Wettre. Sweden, 2012
[7]. V. Radić Seleš, I. Bates, I. Plazonić, M. Rudolf, K. Petric Maretić, V. Džimbeg-Malčić, *„Optical stability of laboratory papers with wheat pulp printed by digital technique after artificial ageing"* U: Oktav, M., Akgul, A., Oguz, M., Ozdemir, L., Ozomay, Z. & Sesli, Y. (ur.)Proceedings of 3rd International printing technologies symposium Istanbul Turkey, 2019.
[8]. S. Soleymani, T. Ireland, D. McNevin, *„Influence of acidity on the mechanical stability of retouched Japanese tissue papers during the course of artificial ageing"* AICCM Bulletin, 38:1, 3-14, 2017. DOI: 10.1080/10344233.2017.1337324
[9]. B. Thompson, *„Printing Materials: Science and Technology"*, Pira International, Leatherhead, Surrey, United Kingdom (2004).
[10]. I. Plazonic, I. Bates, Z. Barbaric-Mikocevic, *„The Effect of Straw Fibers in Printing Papers on Dot Reproduction Attributes, as Realized by UV Inkjet Technology"* BioResources, 11(2), pp. 5033-5049, 2016.
[11]. M. Vukoje, I. Bates, I. Plazonić, *„Optical stability of papers with wheat fibers after accelerated ageing"*, International Conference MATRIB 2015 Materials, Wear, Recycling Proceedings, pp. 362-369, 2015.
[12]. ASTM D 6789-02, *Test Method for Accelerated Light Aging of Printing and Writing Paper* by Xenon-Arc Exposure Apparatus, 2002.

ICETI

4TH INTERNATIONAL CONFERENCE ON ENGINEERING TECHNOLOGY AND INNOVATION

www.iceti.org

Western Michigan University

National University of Public Service

International University of Sarajevo IUS

University of Cincinnati

Turkish Airlines

CNR Group